ABSTRACT

COX, WILLIAM CHARLES JR. A 1 Mbps Underwater Communication System Using a 405 nm Laser Diode and Photomultiplier Tube. (Under the direction of John Muth.)

Radio frequency communications in seawater are impractical due to high conductivity of seawater limiting the propagation of electromagnetic waves. Current methods, such as acoustic communication, are limited in bandwidth, and the use of cables, such as fiber optic, are expensive and not practical for autonomous vehicles. Underwater tethered communication systems are also very costly to repair if damaged. Optical wireless communications that exploit the blue/green transparency window of seawater potentially offer high bandwidth, although short range, communications.

The goal of this Masters thesis was to build sufficient infrastructure to experimentally validate the performance of underwater optical communication systems under laboratory, but hopefully realistic, water conditions.

An optical transmitter based on a 405nm blue laser diode was constructed. The transmitter is capable of sourcing 200mA of current to a blue laser diode at speeds of up to 200MHz. The receiver was based on a photomultiplier tube. The high gain and blue/green sensitivity of a photomultiplier tube make it ideal for underwater optical communications. Finally, a 1,200 gallon water tank was constructed that allows the water conditions to be appropriately controlled to simulate an ocean environment

Experiments were conducted to validate the design and construction of the receiver, transmitter and water tank. An underwater optical data link was demonstrated that was capable of transmitting data at 500kpbs in return-to-zero format, or 1Mpbs in non-return-to-zero format. The transmitted signal could then be optically detected, digitized and stored on a PC for later signal processing.

A 1 Mbps Underwater Communication System Using a 405 nm Laser Diode and Photomultiplier Tube

by
William Charles Cox Jr.

A thesis submitted to the Graduate Faculty of
North Carolina State University
In partial fulfillment of the
Requirements for the degree of
Master of Science

Electrical Engineering

Raleigh, North Carolina

2007

APPROVED BY:

_____	_____
Dr. Brian Hughes	Dr. Robert Kolbas

_____
Dr. John Muth
(Chair of Advisory Committee)

DEDICATION

This work is dedicated to my father,

Charles Cox

1953 - 2006

You ran the race well.

I miss you.

BIOGRAPHY

William Cox was born and raised in Raleigh, NC, where he was home-educated all the way through High School. This enabled him to fuel his love of electronics and robotics, and to spend long hours in his shop crafting robotic inventions. During his senior year of High School, William constructed a robot to compete in the Trinity College Robotic Firefighting Competition. With high hopes of winning, William traveled to Connecticut where, at the critical moment, his creation completely failed to work. For some strange reason, William decided that this all-too-familiar story to most engineers was how he wanted to spend the rest of his life. Armed with a vendetta against creations that refuse to comply with their creator's wishes, William attended NC State University in the Fall of 2002. In 2006, he earned a degree in Electrical Engineering. During his undergraduate career William was involved in several student groups and organizations devoted to robotics, one of which was the NCSU Underwater Robotics Club. Through his work in this group, William came in contact with Dr. John Muth, who had a research interest in the field of underwater optical communications. Based on this contact, William decided to pursue a Master's degree to study this topic under the advisement of Dr. Muth.

ACKNOWLEDGMENTS

I would like to acknowledge the support of Dr. John Muth through this research.

Thank you to all my friends at NCSU, especially Mike Faircloth.

Special thanks to Jim Simpson, my research partner. Two heads are often better than one.

Thanks to my family for their love.

Thank you to my wife, Jamie. You are my princess. I couldn't have made it without you.

Finally, I acknowledge my humble gratitude to the Risen Savior.

Soli Deo Gloria.

TABLE OF CONTENTS

LIST OF TABLES

LIST OF FIGURES

1. Introduction

A major challenge facing ocean exploration and surveillance is how to quickly and accurately communicate the data obtained by the sensors or unmanned system to a surface ship or shore-based station. The primary reason for this challenge is that radio frequency waves do propagate well underwater. The solution to this has traditionally been to use an acoustic modem or a communications tether to the surface ship or shore station. However, with the increase of mobile unmanned systems underwater, this is not feasible, as it would require the vehicle to surface or dock to download its data.

Figure 1-1 shows that radio frequency waves, which are predominately used for high-speed wireless systems above water, suffer attenuation which allows them to propagate only a few feet under water. Infrared wavelengths, which are typically used in fiber optic systems, suffer even greater attenuation, leaving only visible wavelengths between 400nm (violet) and 730nm (red) as a useful source for communication. Due to attenuation from other environmental affects, such as chlorophyll or gelbstoff (dissolved organic compounds), blue/green wavelengths are best suited for aquatic environments.

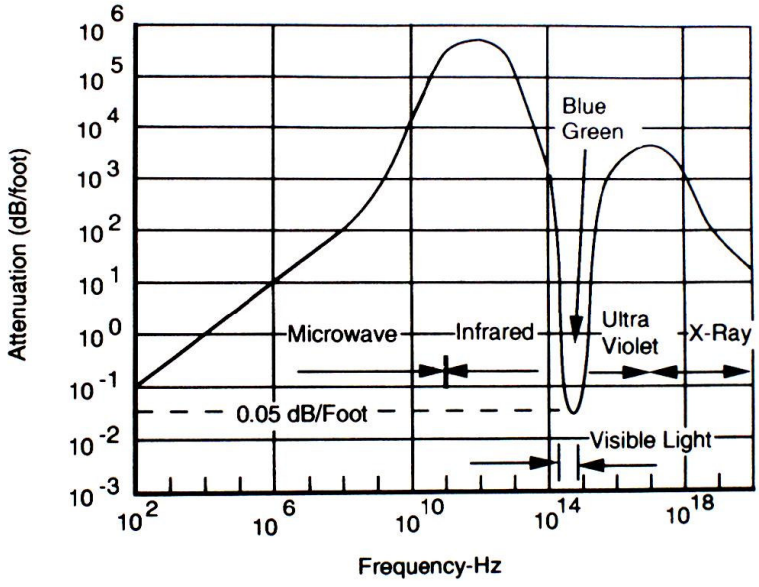

Figure 1-1 – Attenuation of electromagnetic radiation from 100 Hz to the 10 ^{19} Hz [1]

As the amount of undersea exploration and exploitation of undersea resources increases, aquatic freespace optical communication links are potentially very useful in several situations, including:

- Underwater observatories
- Underwater vehicle to surface ship links
- UAV to moored or floating Buoys equipped with RF links.
- AUV to AUV communications
- Diver to diver or diver to ship communications.

Underwater observatories like in [2] are stationary installations that monitor interesting seafloor features like hydrothermal vents or coral reefs. Such installations may be permanently fixed to the seafloor and passively collect data over time. Once the local storage space has been filled, or when data is needed by scientists, a small AUV or surface ship could communicate with the observatory via an optical link to extract its data.

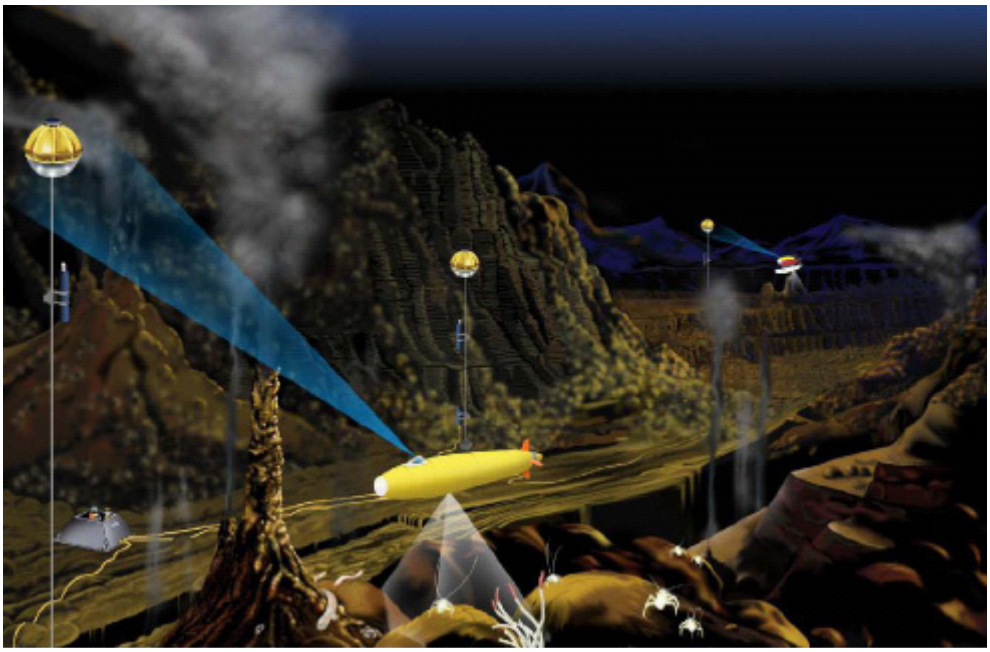

Figure 1-2 – AUV communicating to underwater observatory via optical modem [2]

Underwater vehicle to ship or buoy links enable the data to be transferred to a storage system for later analysis or to be transferred to shore or satellite by radio. In both cases, current acoustic technologies available in the commercial sector limit the channel bandwidth to a few tens of kilobits per second [3]. An optical link would allow large amounts of data to be transferred quickly and reliably between the surface and aquatic environment.

Mobile networks of AUVs would also be possible with optical links. A high bandwidth link between the vehicles would allow for sophisticated collaborative path planning and observation. Such a system could be employed for military uses, such as locating and disarming underwater mines or for finding enemy submarines. In addition, a similar system was demonstrated in [4] to gather ocean data.

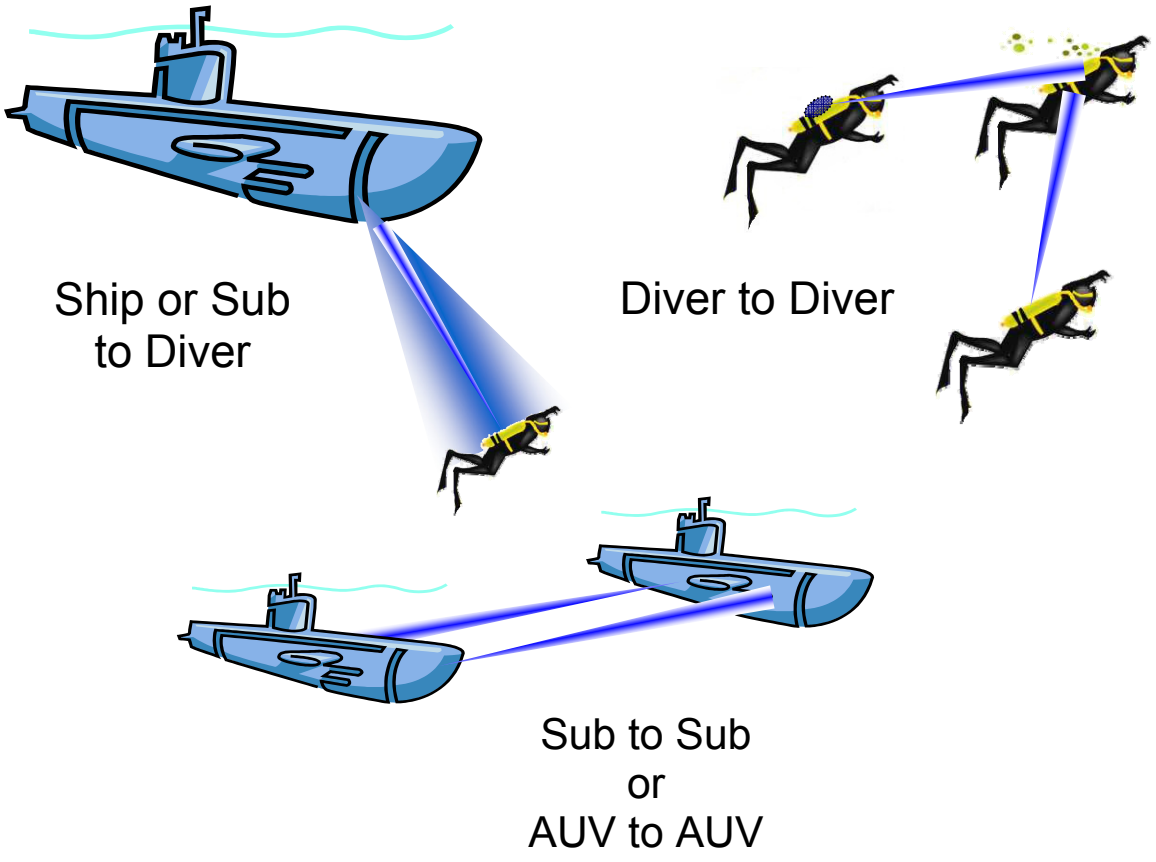

Figure 1-3 – Examples of situations where underwater optical communication links are useful

Diver-to-diver and diver-to-ship communications could be significantly improved via an optical communication link. One of the reasons that diving is a dangerous activity is due to the lack of communication with the surface or with other dive partners. An optical link would allow for high fidelity communications between divers and also allow the transfer of data, such as navigation information, between divers. Diver-to-ship communications would have similar benefits and allow the surface ship, for example, to download path planning and mission objectives to a heads-up-display (HUD) mounted in the diver's face mask. However, human factors and engineering difficulties, including integration into the dive suit and the line of sight nature of light make this a challenging engineering task.

In general these goals may be achievable using other methods, such as tethered electrical wires, acoustic modems, fiber optic communication, or RF communications. Table 1-1 summarizes their respective advantages and disadvantages.

Table 1-1 - Advantages and disadvantages of different underwater communications channels.

Method	Advantages	Disadvantages
Tethered electrical	Simple	Tethered, voltage drop over long distances. Susceptible to corrosion, environmental degradation including being eaten by marine life.
Fiber optic	High bandwidth, Secure, Reliable	Tethered, expensive Vulnerable to marine life.
RF	Inexpensive Wireless	Doesn't propagate underwater
Acoustic modem	Status quo, Omnidirectional low attenuation in water	High power, multipath interference, low bandwidth

Recently our group has investigated the possibility of high bandwidth underwater freespace optical communications and calculated link budgets showing that these systems should be feasible for ranges up to about 100m [5].

Figure 1-4 shows the performance of optical fiber, measured data points from a variety of acoustic systems and distinguishes between dispersion limited and attenuation limited optical systems. Examining the graph we see that that for short ranges, optical systems can be expected to significantly outperform acoustic systems.

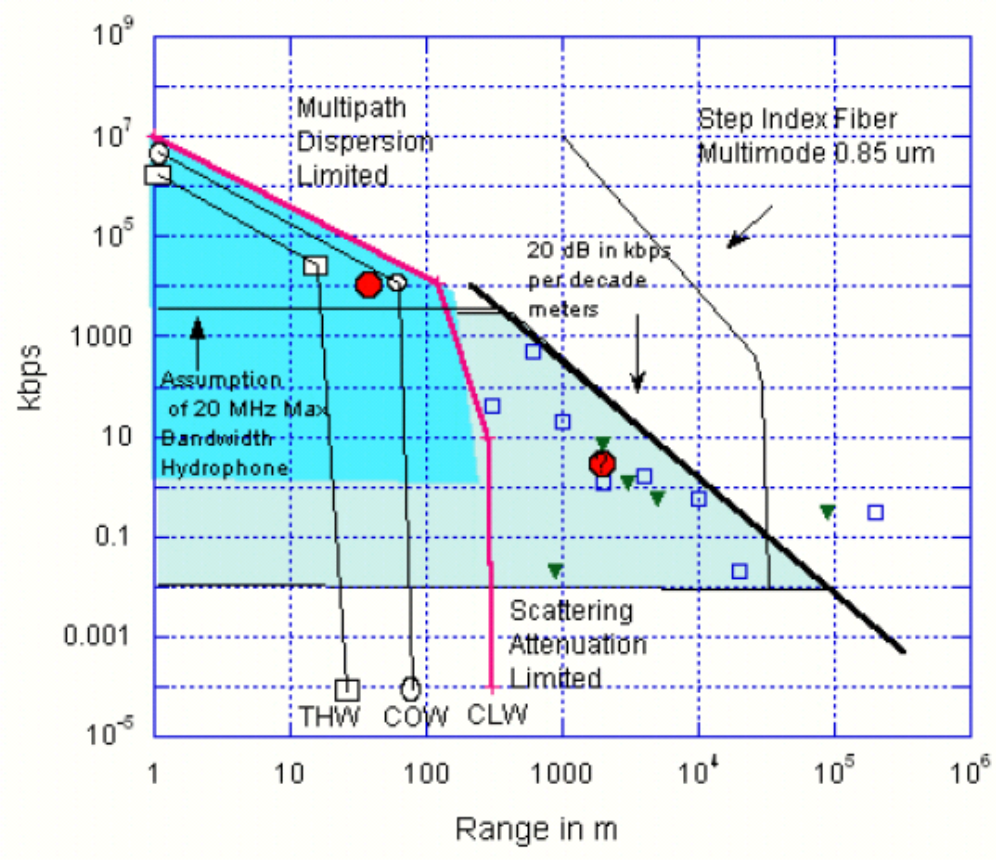

Figure 1-4 - Small blue squares represent Acoustic systems operating in deep water, green triangles represent acoustic systems operating in shallow water. The red line represents a laser based system, operating in clear ocean water (CLW) environment. The attenuated range is approximately 300 meters. Similar plots are also constructed for Turbid Harbor Water (THW), and Coastal Ocean Water (COW) with correspondingly shorter ranges. The light green region represents area where acoustic systems could be expected to be successful. The light blue region represents where optical communications can be expected to compete. For example the red circle at 10 Mbps, with a range of 40 m is an LED based system that has been successfully tested. Note that above 10 Mbps, or for distances below 100 meters, it appears that optical systems can be expected to out perform acoustic systems on the basis of just having a faster bit rate. With current generation lasers, and detectors ~100 Mbps could realistically anticipated for 10-30 meters in a variety of water conditions [5].

As Muth and Chancy [5] point out, practical underwater communication systems are constrained in size, weight, and power. There are also additional operational constraints such as minimum speeds at which the platform can maintain neutral buoyancy

and heading especially in the presence of a current. This can be an important issue when pointing stability between the transmitter and receiver is required. These factors can be expected to degrade the range of operation unless careful attention is paid to the engineering of the system. In this project we are most concerned with building the infrastructure of transmitters and receivers and understanding the effects of water conditions on the underwater channel.

The principle goal of this Masters thesis was to build sufficient infrastructure to experimentally validate the performance of underwater optical communication systems under laboratory, but hopefully realistic, water conditions. This required three major objectives to be met.

1. Construction of optical transmitters and receivers
    a. Transmitter based on blue laser diodes.
    b. Receiver based on a photomultiplier tube.
2. Construction of a water tank where the water conditions can be appropriately controlled. e.g. changing the amount of scattering by addition of particulate
3. Measurement of communications performance as a function of water conditions.

Chapter 2 will examine the existing literature and consider the propagation of light through water from the perspective of an underwater communications system.

Chapter 3 will describe the experimental apparatus, and describe the construction of the tank, transmitter and receiver

Chapter 4 will describe experimental procedures and results performed using the tank, transmitter and receiver with the focus on bit error rate, and attenuation measurements.

Chapter 5 will describe the experimental results and summarize the conclusions of our investigations.

The **Appendices** include documentation and schematics that should allow future students, or interested people to reproduce the circuits and experiments

References

[1] M. Katzman, *Laser Satellite Communications.* Englewood Cliffs, NJ: Prentice-Hall, 1987, pp. 239.

[2] N. Farr, A. D. Chave, L. Freitag, J. Preisig, S. N. White, D. Yoerger and F. Sonnichsen, "Optical modem technology for seafloor observatories," in *OCEANS 2006,* 2006, pp. 1-6.

[3] I. F. Akyildiz, D. Pompili and T. Melodia, "Underwater acoustic sensor networks: Research challenges. *Ad Hoc Networks 3(3),* pp. 257, 2005. Available: http://www.ece.stevens-tech.edu/iNetS/infolibrary/underwaternetpapers/underwater.pdf

[4] I. Vasilescu, C. Detweiler and D. Rus, "AquaNodes: an underwater sensor network," pp. 85-88, 2007.

[5] M. A. Chancey, "Short range underwater optical communication links," *North Carolina State University*, 2005.

2. Propagation of Light Underwater

There has been extensive work performed that requires an understanding of light propagating through water. Biologists have sought to understand how energy from the sun is captured by phytoplankton. Numerous underwater optical imaging and underwater laser ranging and imaging systems have been investigated. Similarly above the water there has been substantial work on freespace terrestrial laser communication systems. However, when examining the field of underwater optical communications systems there has been virtually no work performed in the open literature.

Table 2-1 – Considerations for freespace optical communication systems [1]

Solar Interference	Sunlight can be picked up by the detector adding white and shot noise.
Alignment	LOS beams are very narrow which causes issues with alignment. Tracking is required for moving links and even on some stationary links.
Scintillation & Turbulence	Variation of the refractive index along the propagation path caused by temperature and density variations lead to large variations in signal strength on the receiver photodetector.
Absorption	Loss of Light intensity due to wavelength dependent particle absorption in the medium.
Scattering	**Mie Scattering** – Light being redirected by particle roughly same size as the propagating wavelength. **Rayleigh Scattering** – Light being redirected by particles smaller than the wavelength.
Multi-Path Scattering & Dispersion	The path a photon takes is ideally a straight line, but due to scattering the photon may be redirect several times causing the light pulse to spread in time.
Physical obstructions	Living organisms blocking the beam path causing dropping of bit or total loss of connection.

Table 2-1 provides a good starting point for examining the effects taken into consideration for any freespace optical link, including those operating underwater.

For underwater light propagation, scattering and absorption are the predominant forces that may limit the transmission length [2]. This is a complicated function of geographic parameters and physical parameters which are summarized in Figure 2-1 from [1].

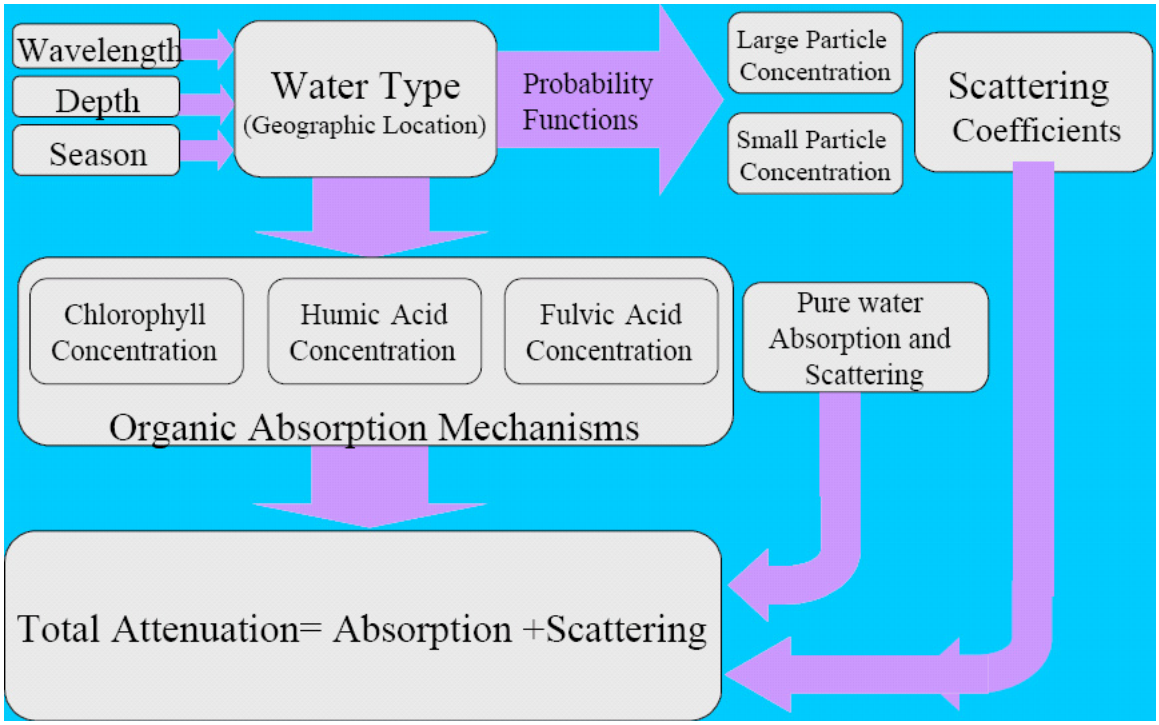

Figure 2-1 – Flow chart showing the total attenuation in seawater [1]

Water Types

The physical or geographic location of the optical link plays an important part in the total attenuation of the signal. Various types of ocean water are classified based on the Jerlov water types. Figure 2-2 shows Jerlov water types for various geographic locations. Jerlov water types are classified as either coastal or oceanic waters and are numbered I-III for oceanic waters and 1-9 coastal waters. These classifications give important general information about the amount of particulate and other dissolved materials in the water.

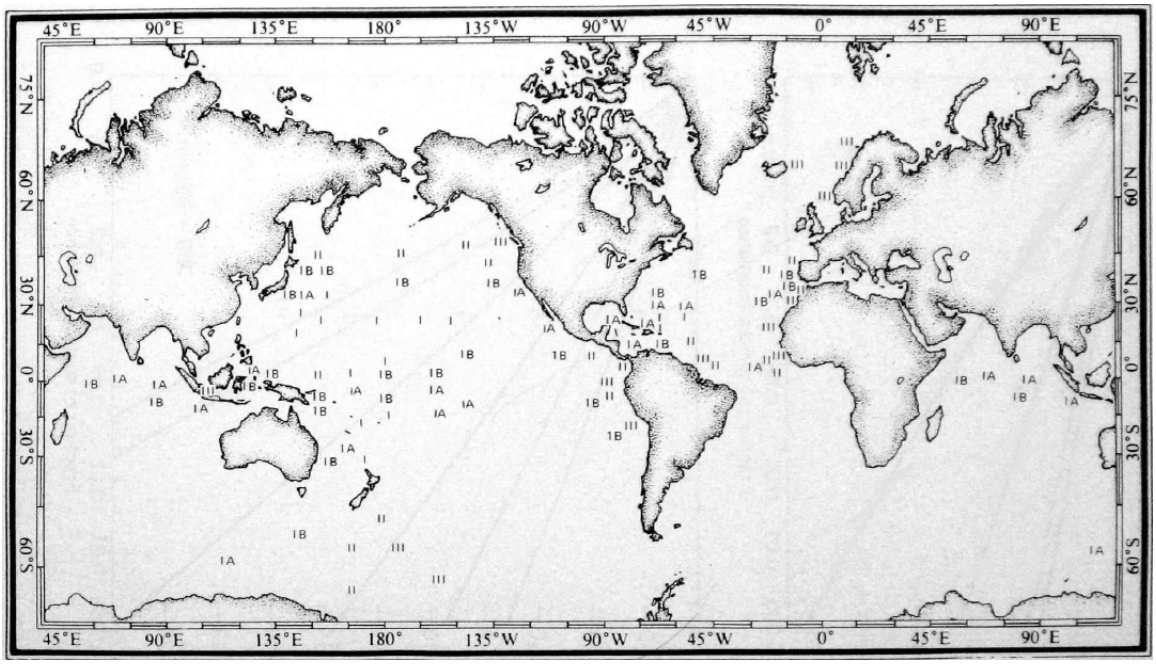

Figure 2-2 – Jerlov water types based on geographical location [3]

Absorption

Light absorption in an underwater optical link is due to four main areas:

- Pure seawater absorption
- Absorption due to chlorophylls in phytoplankton
- Color Dissolved Organic Material (CDOM), or "Gelbstoff"
- Other particulate matter

These factors all play a part in attenuating an optical signal at the receiver.

Given a beam of light passing through a layer of water of length r, the amount of absorbed energy in the beam of light is given by

$$d\Phi_a = -a \cdot \Phi_0 \cdot dr \qquad \textbf{Equation 2-1}$$

where Φ_a is the absorbed energy, a is the absorption coefficient, and Φ_0 is the original energy of the beam. Rearranging Equation 2-1 yields the following equation for a [4].

$$a = -\frac{d\Phi_a}{\Phi_0 \cdot dr} \qquad \textbf{Equation 2-2}$$

Where the units for *a* are given in m^{-1}. This leads to the common expression, in the form of Beer's Law, of

$$\Phi = \Phi_0 e^{-ar} \qquad \textbf{Equation 2-3}$$

where *a* is the absorption coefficient, and *r* is the path length of the light.

Absorption Due to Pure Seawater

Absorption due to pure seawater is comprised of absorption due to pure water, and the additional dissolved salts, like NaCl, $MgCl_2$, Na_2O_4, and KCl. Pure water absorbs heavily in the red and infrared regions, and the dissolved salts tend to have a greater affect in the UV region [4].

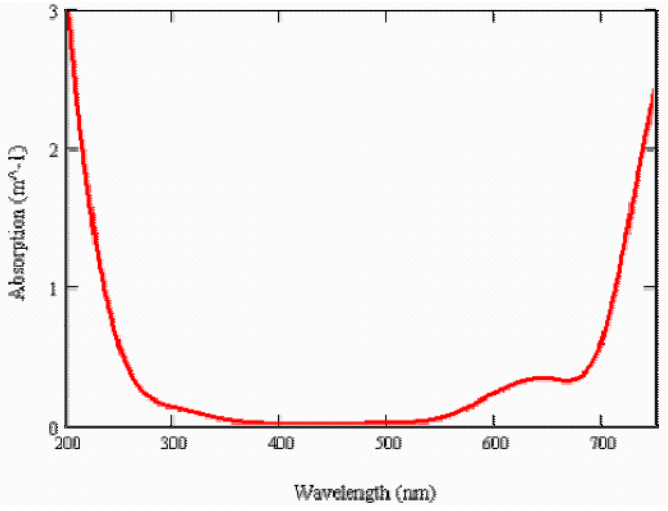

Figure 2-3 – Absorption coefficient for pure seawater based vs. wavelength [1]

Absorption coefficients equal to 1 m^{-1} indicate that approximately 33% of the light has been absorbed in one meter of pathlength. Figure 2-1 shows that pure ocean water is very transmissive for light in the 400nm (violet) to 550nm (green) region.

Absorption Due to Chlorophyll in Phytoplankton

Phytoplankton are a major source of absorption for light in ocean water. The chlorophyll-a that the phytoplankton use to produce energy, is very absorptive in the blue and red regions of the visible spectrum [4].

The concentration of chlorophyll, which is a function of the phytoplankton concentration in seawater, is highly dependant on geographic location, water type, and water depth. Data taken by the SEAWiFS project to study the color properties of ocean waters is illustrated in Figure 2-4. The different colors on the map illustrate different concentrations of chlorophyll.

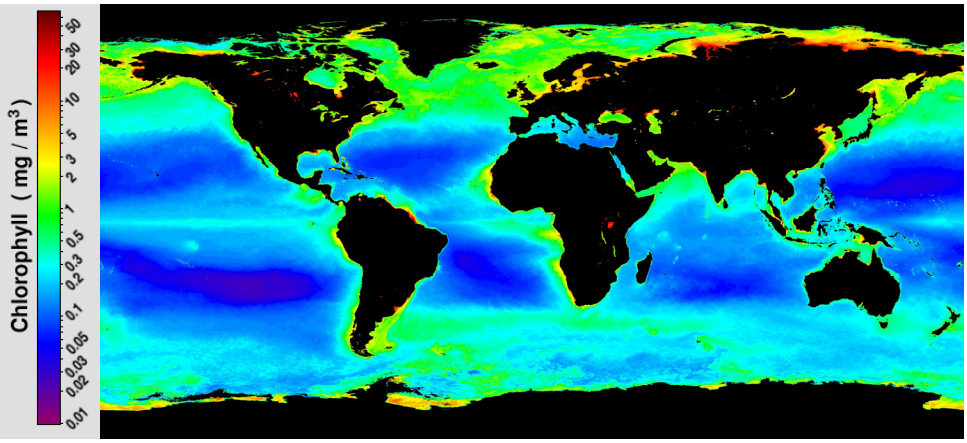

Figure 2-4 - Chlorophyll concentration in the World's oceans taken by SEAWiFS project [5]

Phytoplankton also is not evenly distributed through the water column, but instead takes on a Gaussian distribution which changes based on time of day, season, nutrients in the water, and temperature fluctuations. The distribution of phytoplankton also changes based on water type. For coastal waters, the phytoplankton is closely concentrated in the top levels of the water, with a much more gradual distribution for deep ocean waters [6].

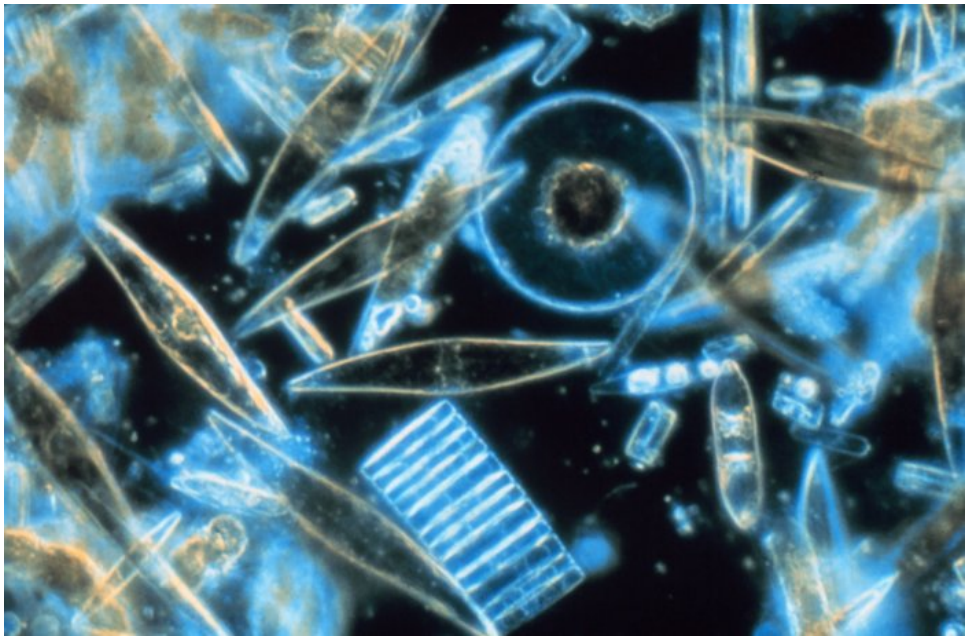

Figure 2-5 – Diatoms, a type of phytoplankton, as seen through a microscope [7]

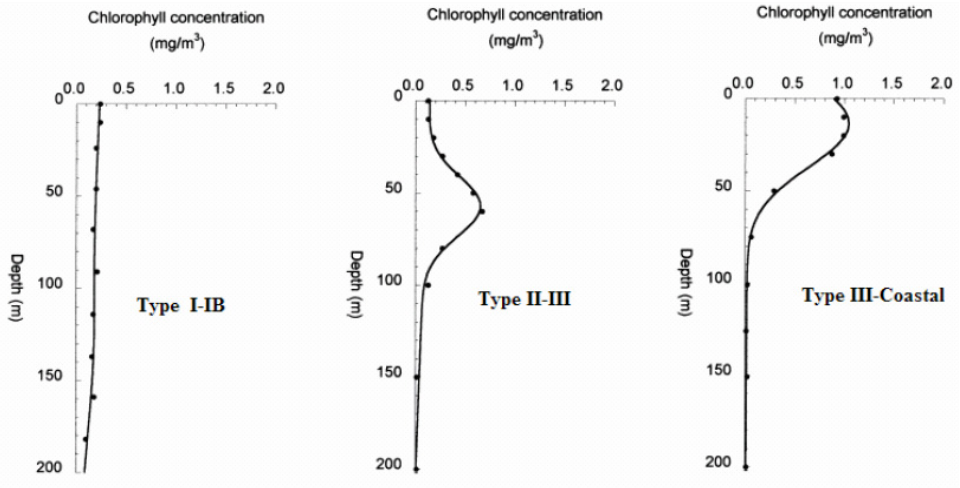

Figure 2-6 – Plankton distribution in water column for various water-types [6]

A summary of chlorophyll concentrations for various Jerlov water types is contained in Table 2-2.

Table 2-2 – Chlorophyll concentrations for various water-types [1]

Jerlov Water Types	Concentration of Chlorophyll mg/m^3
I	0.03
IA	0.1
IB	.4
II	1.25
III	3
Coastal Water 1	9
Coastal Water 2	12

Absorption Due to Gelbstoff

Colored Dissolved Organic Matter (CDOM), or gelbstoff, also plays a role in light absorption in seawater. Its properties make it absorb in the blue region of visible light leaving it with its characteristic yellow color. CDOM is primarily composed of decaying organic material which decomposes into various chemical compounds, and is more concentrated in coastal water areas [4].

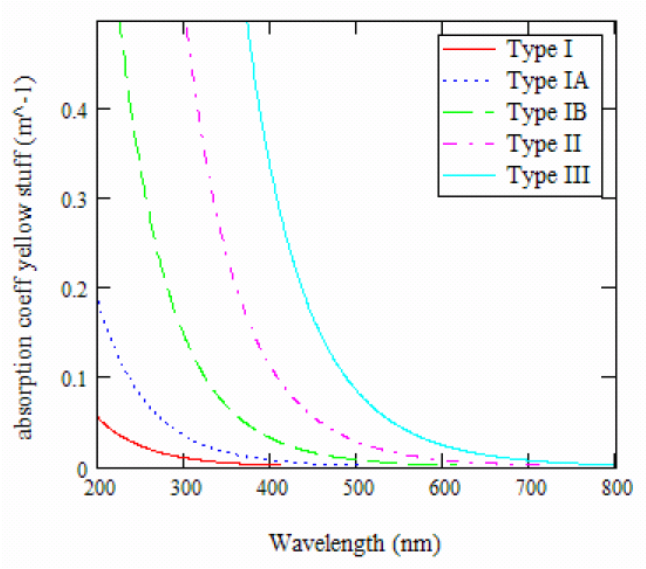

Figure 2-7 – Concentration of CDOM based on wavelength and Jerlov water type [1]

Figure 2-7 shows a graph from [1] which relates the absorption coefficient of CDOM to wavelength and Jerlov water type. It is clear that the effects of CDOM are more pronounced in coastal waters.

Scattering

Scattering results from the interaction of light with the molecules and atoms of the transmission medium. A scattering medium is one that redirects the trajectory of the photons. This scattering can be quantified using the volume scattering function which expresses the probability of a photon of wavelength λ diverting from its original path by angle Φ. Scattering is defined as being either Rayleigh or Mie, where Rayleigh scattering is produced by particles that are smaller in size than the wavelength of the light, and Mie scattering is produced by particles that are the same order of magnitude as the wavelength of the light [8].

Scattering Due to Pure Seawater

The scattering due to pure seawater is somewhat limited in magnitude. Figure 2-8 shows that the scatter is limited in nature for wavelengths above 400nm, and is much smaller than the absorption coefficient for the same wavelengths.

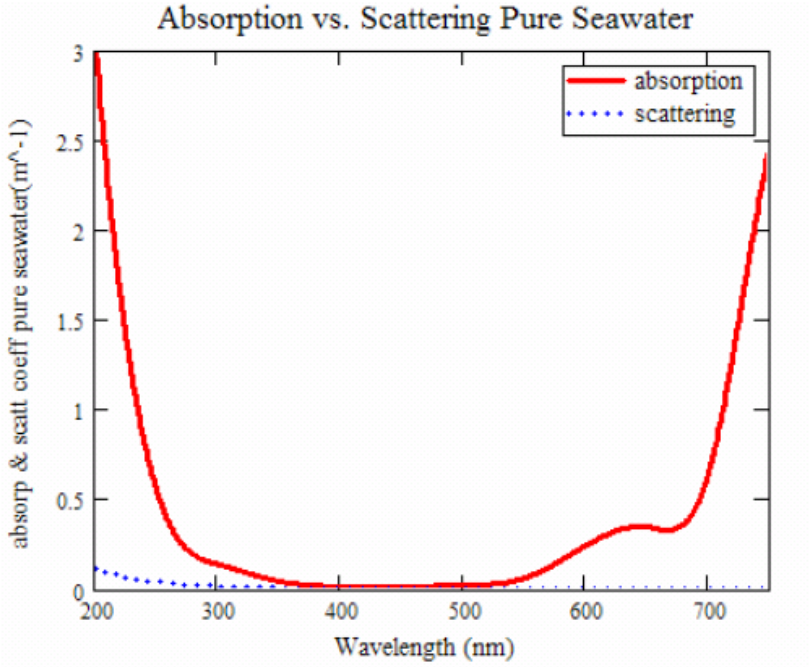

Figure 2-8 – Scattering coefficient compared to absorption coefficient of pure seawater vs. wavelength

Scattering Due to Particulate

Scattering due to suspended particulate in water is caused by inorganic and organic matter in the water column. These concentrations can be extrapolated based on work done in [9]. Figure 2-9 shows some example scattering coefficients based on $1 mg/m^3$ of chlorophyll concentration.

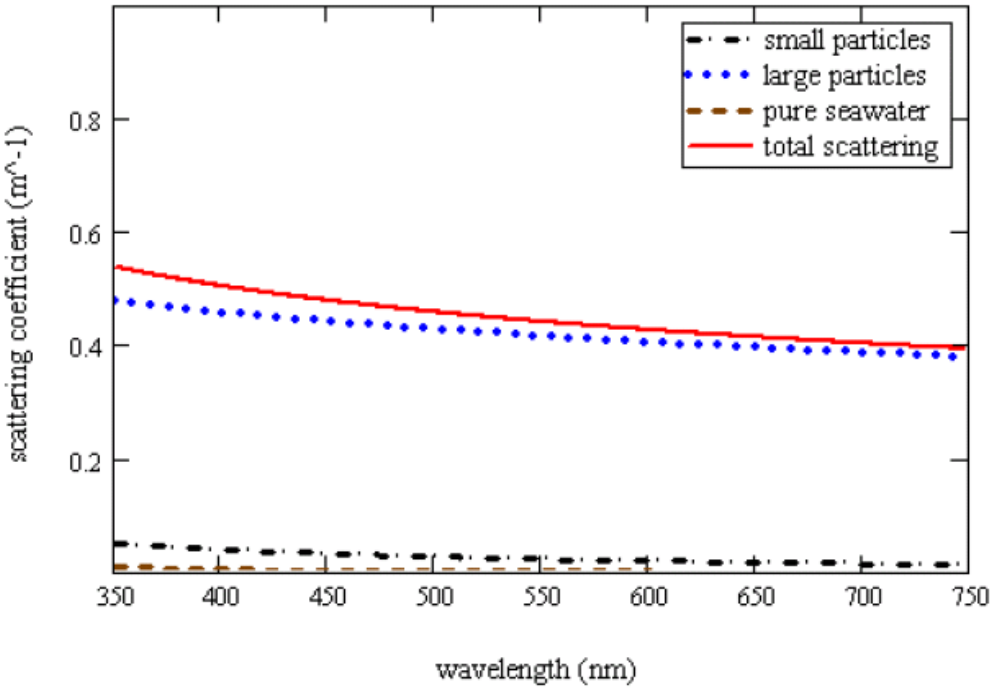

Figure 2-9 – Scattering coefficients based on 1mg/m3 of chlorophyll concentration [10].

Scattering and Absorption Summary

Table 2-3 summarizes and illustrates the effects that various water properties have on the absorption and scattering of light underwater. Phytoplankton is included under the "Particulate matter" category.

Table 2-3 – Summary of absorption and scattering characteristics [2]

	Absorption		Scattering	
	Character	λ-dependence	Character	λ-dependence
Water	Invariant at constant temp. and pressure	Strong	Invariant, small compared to absorption	λ^{-4}
Sea salts (inorganic)	Negligible in the visible, weak in the UV	Some increase towards short λ		
Gelbstoff	Variable	Increase towards short λ		
Particulate matter	Variable	Increase towards short λ	Variable	Usually dependant on λ

Typical values for many of the variables discussed above are expressed in Table 2-4. *a* is the absorption coefficient in m^{-1}, *b* is the scattering coefficient in m^{-1}, *c* is the sum of both *a* and *b*, called the attenuation coefficient, Λ is the photon survival probability, or $\frac{b}{c}$, and β(γ) is the volume scattering function which is dependant on γ, the scattering angle. For ocean water, the total attenuation is much higher than in atmosphere free-space optics, while the beam is less scattered [4].

Table 2-4 – Comparison of the optical properties of the ocean and the atmosphere based on typical values [4]

Medium	Coefficients (m^{-1})			Λ	Reduced volume scattering function $\beta(\gamma)/\beta(90^\circ)$				
	a	b	c		0	5	10	45	90
Ocean	0.07	0.16	0.23	0.7	10^4	10^3	250	8	1
Atmosphere	0	$2x10^{-4}$	$2x10^{-4}$	1.0	600	200	100	10	1

Other Considerations

Other possible sources of attenuation for a freespace laser beam includes scintillations due to turbulence, receiver and transmitter misalignment, interference from the sun and other light sources, multi-path interference, and physical obstructions. These factors are important considerations even if they are not as predominant as absorption or scattering.

Turbulence

The effects of atmospheric turbulence on freespace laser communication systems predominantly manifest themselves as localized refractive index fluctuations caused by temperature, humidity or pressure variations, and cause changes in beam quality, the beam size on target, and intensity on target [11].

Temperature, pressure and salinity changes also affect the refractive index of ocean water. Data from [10] shows that these fluctuations may change the refractive index of water by several thousandths. Future study is required to obtain a more accurate picture of the effects of turbulence on aquatic optical links.

Alignment

Due to scattering and beam diffraction, the receiver will only gather a fraction of the transmitted light. This can be expressed by [12]

$$Aff_{geometric} = S_d / S_{capture} = (d\theta)^2 \frac{\pi}{4} \Big/ S_{capture} \qquad \textbf{Equation 2-4}$$

with θ is the divergence of the beam, d is the distance from receiver to transmitter, $S_{capture}$ is the capture area of the receiver, and S_d is the are of the beam at distance d. Due to geometric loss, accurate pointing of the transmitter is critical.

Solar Interference

Solar interference must be taken into consideration for any optical link operating in the euphotic zone of the ocean. This zone ends where 99% of all of the incident sunlight is absorbed [1]. This zone, however, only accounts for 10% of the entire ocean environment [13]. Appropriate optical filters for the transmitted wavelengths would help reduce the affects of solar radiation.

Multi-Path Interference

Multi-path interference is caused when scattered photons are re-scattered back towards the receiver, thereby creating dispersion and spreading in the received signal. This phenomenon, which is routinely experience in RF communication schemes, is a relatively explored area of research in the field of optical communication, and the effects of such interference on underwater optical link is unknown.

Physical Obstructions

Physical obstructions such as fish or other marine animals will cause momentary loss of signal at the receiver. Appropriate error-checking and redundancy measures must be taken to assure that lost data is retransmitted.

In conclusion, it is difficult to simulate and understand all of theses factors and extremely expensive to test such systems in the open ocean. This suggests that laboratory experiments to validate underwater optical communications systems are important in learning how to best implement these systems.

References

[1] M. A. Chancey, “Short range underwater optical communication links,” *North Carolina State University*, 2005.

[2] N. G. Jerlov, "Optical oceanography," in , vol. 5, Anonymous New York: Elsevier Publishing Company, 1968, pp. Pg 15, 51-62, 118-126.

[3] J. R. Apel, "Principles of ocean physics," in *International Geophysics Series* Anonymous London: Academic, 1987, pp. 2-4, 63-66.

[4] K. S. Shifrin, "Physical optics of ocean water," in *AIP Translation Series* Anonymous New York: American Institute of Physics, 1988, pp. 2, 35-39, 66-70, 160-165.

[5] G. C. Feldman, *Background of the SeaWiFS project*. *2007(10/25),* 2007 Available: http://oceancolor.gsfc.nasa.gov/SeaWiFS/BACKGROUND/SEAWIFS_BACKGROUND.html

[6] Kameda, “Chlorophyll biomass off sanriku, northwestern pacific, estimated by ocean color and temperature scanner (OCTS) and a vertical distribution model,” *Journal of oceanography 55(1),* pp. 99, 1999

[7] N. Sullivan. Marine diatoms. *2007(10/30),* pp. 1. Available: http://www.photolib.noaa.gov/htmls/corp2365.htm

[8] O. Bouchet, *Free-Space Optics : Propagation and Communication.* London ; Newport Beach, CA: Iste, 2006, pp. 219.

[9] Haltrin, “Chlorophyll-based model of seawater optical properties,” *Applied optics 38(33),* 1999

[10] Y. J. Gawdi, “Underwater free space optics,” *North Carolina State University*, 2006

[11] J. Ricklin and A. Mujumdar, "SC656 fundamentals of free-space laser communications," the SPIE 49th Annual Meeting, Denver CO, Tech. Rep. SPIE Education Sevices Short Course Notes, 2004.

[12] D. L. Begley, "Free-space laser communications: A historical perspective," in *2002 IEEE/LEOS Annual Meeting Conference Proceedings: 15th Annual Meeting of the IEEE Lasers and Electro-Optics Society,* 2002, pp. 391-392.

[13] P. D. N. Hebert. 2002, Canada's aquatic environments: Ocean zonation. *2007(10/25),* Available: http://www.aquatic.uoguelph.ca/oceans/Introduction/Zonation/zonation.htm

3. Experimental Apparatus

In order to meet the goals of this research, three main areas needed to be addressed:

1. The creation of an effective test-bed for evaluating and studying the propagation of light underwater.
2. Construction of a blue/green laser transmitter capable of sending light pulses of varying speeds along with streams of data.
3. Construction of an optical receiver circuit.

First, the design and construction of a 12 ft long, 1,000 gallon, water tank with optical access to perform communications experiments is discussed. The windows of the tank permit optical links to be made and the performance to be measured as a function of attenuation due to absorption and scattering by particulate. The open access allows for the spread of the transmitter beam to be observed and measured. In addition, the design of a blue (405nm) laser diode transmitter capable of transmitting data in excess of 10 Mbps is discussed. The transmitter allows binary data to be sent from the computer via a USB link, to an FPGA which transmits the data using a 405nm blue laser diode. The flexible FPGA processing platform will allow for features such as arbitrary transmission schemes and error correction encoding. Finally, the design of a high-gain, high-dynamic range photomultiplier tube receiver board is discussed. The receiver uses a high-speed transimepdance amplifier which is capable of supplying a single-ended or differential output voltage.

Design and Construction of a Water Tank

The goal was to construct as large a tank as possible that would fit within the space constraints of the laboratory, while being properly supported by the floor. The tank also required at least two viewing ports, and a pumping and filtration system to be able to control the particulate levels in the water.

Figure 3-1 – Water tank with suspended particulate, prior to addition of 2nd viewport

Tank Design

The shape of the water tank was constrained by the physical size of the lab. This limited the overall size of the tank to a rectangular design, four feet wide by twelve feet long. In addition, the water in the tank needed to accessible both for observation and for adding particulate and other matter. In order to keep any particulate suspended in the water, adequate circulation was needed in addition to filtration to establish a base-line for any measurements. Transmission windows on either end of the tank were needed for transmission of light through the length of the tank. A secondary design consideration was the ability to test small underwater vehicles in the tank. This would allow practical implementation and testing of the communication systems.

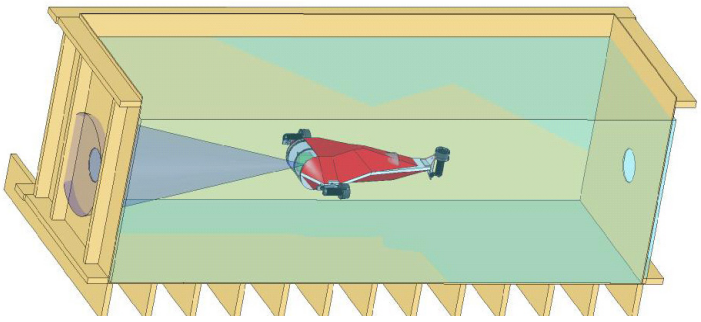

Figure 3-2 – Example of underwater robot in water tank communicating with an optical beam

Several commercial tanks were considered, but these did not meet the shape, size or cost constraints for the project. The lab space to contain the tank also had limited accessibility due to the construction of the building.

Figure 3-3 – Examples of tanks considered, but rejected due to cost, size, or accessibility

A custom designed tank built from concrete was considered, but rejected due to the weight of the materials. The laboratory to house the tank was also not on the ground floor of the building, so weight was a major concern and ultimately limited the depth of the tank to four feet. The weight of one cubic foot of water is approximately sixty-eight lbs, so for each additional inch added to the water depth, the total weight increased by over two hundred and seventy pounds.

A metal tank was also rejected due to the difficulty of working with the materials – including metal bending and complex welding.

The final solution was to construct the tank from standard lumber and to reinforce and seal it using fiberglass cloth and resin. A smaller prototype was first constructed to test the merits of the design. Having corrected various flaws, but ultimately proving the design to be sound, the full size tank was constructed over the period of several months.

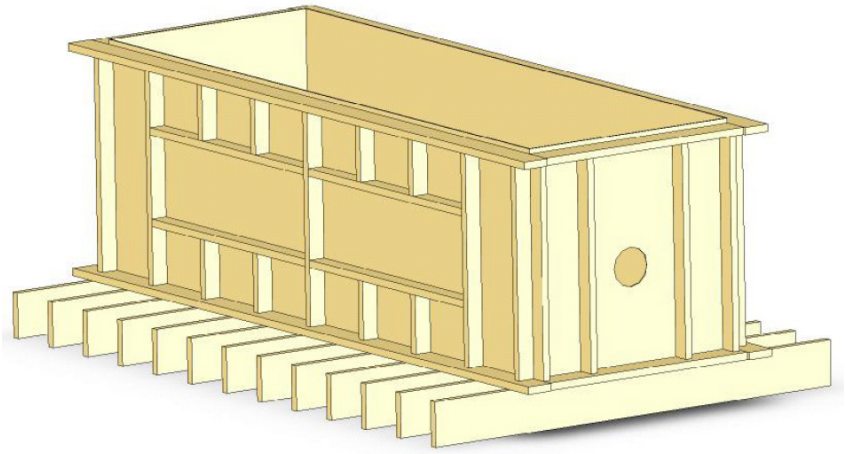

Figure 3-4 Final tank design pictures

The final design had an inner dimension of 4’ x 4’ x 12’ and could hold over 1,200 gallons of water, with a total water-weight of over 10,000 lbs. The tank rests on an 8’ x 12’ platform to distribute the weight of the water over the floor. This reduces the per-square-foot loading from a maximum of 240lbs/ft^2 to 120lbs/ft^2.

Plumbing and Filtering

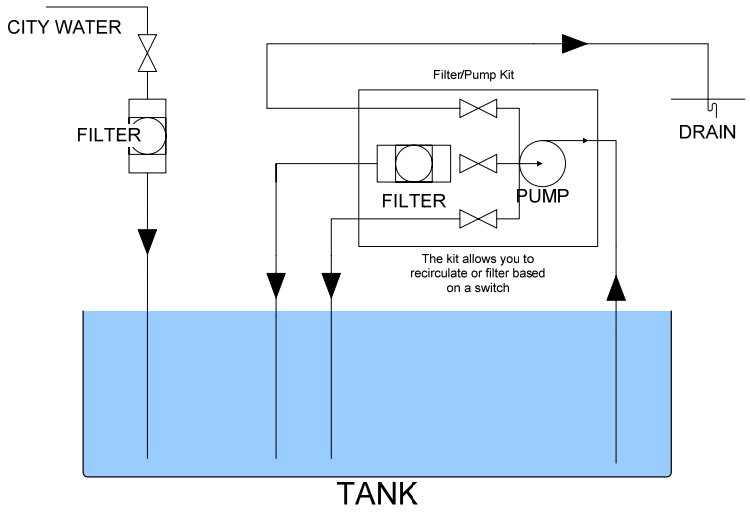

Figure 3-5 – The Plumbing diagram. City water passes through a cartridge filter to remove sediments. The pump/filter kit allows the water in the tank to be recirculated, filtered, or pumped to the drain.

In addition to holding water, the tank also needed to be filled and drained in a reasonable amount of time, along with being circulated and filtered.

Figure 3-6 - Picture of pump and pool filter. The pool filters particles as small as 3 um in diameter.

Several custom designs were considered for pumping and filtering, but ultimately a commercial pool pump and filter, the Hayward S180T model, was chosen. This model would allow the tank to be drained in about ten minutes, or be filtered or circulated at the rate of 80 gallons per minute (GPM).

Since Maalox® would be the primary particulate added to the water, an appropriate filter was needed to remove the particulate. According to [1], the particle size of Maalox is approximately 11μm, so a sand filter was chosen with a diatomaceous earth filtering compound. This type of filter can remove particles down to 3μm in size and was therefore adequate for the design requirements.

Underwater Observation

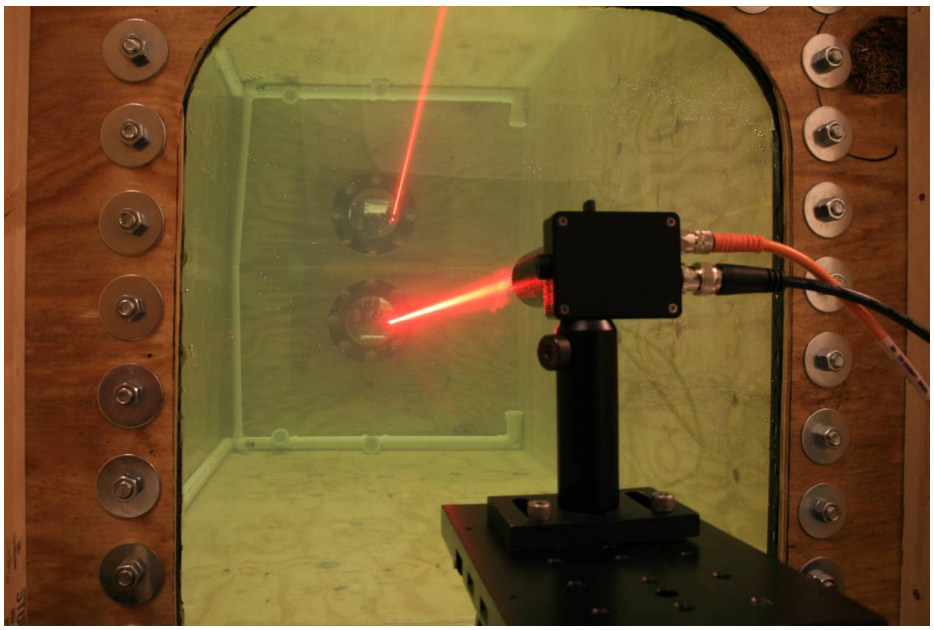

Figure 3-7 – Laser beam through water showing forward scattering. Note that the top red line and upper window is the reflection from the surface of the water.

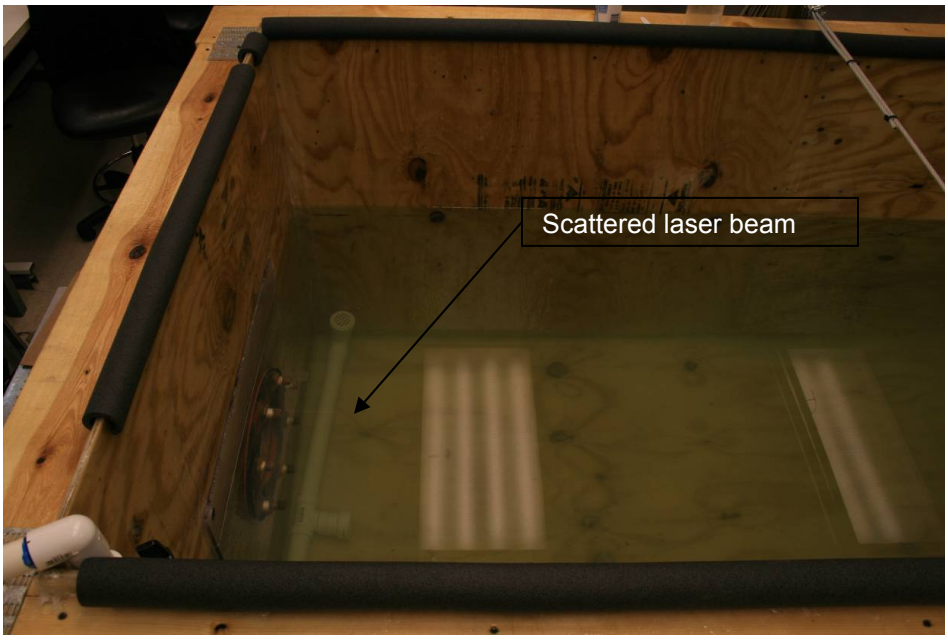

Figure 3-8 – Laser beam through water, showing very little scattering orthogonal to the beam path. The arrow points to the location of the beam through the water.

Initial tank requirements called for both transmission-windows on either end of the tank, and viewing-windows laterally along the length of the tank. However, based on visiting a tank used for underwater optical experiments at NSWC Patuxent Md., it was decided that lateral viewing windows were not necessary due to the predominately forward scattering nature of the light which was far greater than any orthogonally scattered light which could be observed along the length of the beam. The open top of the tank also allows the lateral spreading of the beam to be measured.

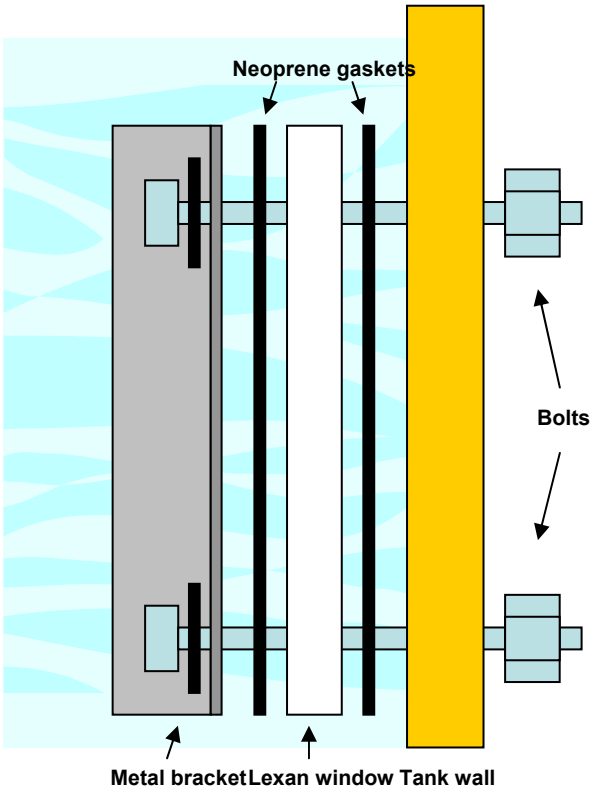

Figure 3-9 – Illustration showing the construction of the viewing windows

The initial transmission window design involved an 8” polycarbonate viewing window mounted in the end of the tank, and sealed with two flange gaskets and a metal flange. The bolt holes were sealed using rubber washers and duct-sealant. Polycarbonate was chosen based on it superior strength as compared to glass.

A later window design expanded upon the original design and included a window made from 1/4" polycarbonate sheeting, and was 21 inches by 15 inches. A similar neoprene flange gasket was used and a flange constructed from L-shaped metal stock. When the tank is completely filled, the window shows approximately 0.249" of outward flex at the center.

Future expansion for the water tank would include painting the inside of the tank with a flat black paint to prevent light from reflecting off the surface of the walls or floor of the tank. This would better simulate an open water situation and allow for more accurate measurements. Also, a more complex internal plumbing scheme would allow a more sophisticated flow of water inside the tank to better approximate varied water conditions in aquatic environments. In addition, glass windows with anti-reflection coatings could be used to reduce the light lost through reflection losses.

Design Considerations for Laser Transmitter

The initial goal was to gain some experience using laser diodes and to better understand the requirements for a diode driver and transmitter board. A red laser diode, and a driver circuit removed from an obsolete laser printer was first used as a transmitter system. While this wavelength is clearly a poor choice for underwater optical communications it was convenient and allowed a Labview and C++ based transmitter system to be constructed that would be suitable for sending data to future laser diode driver circuits. Based on previous discussion in Chapter 2, blue/green lasers are most advantageous for underwater communication systems. There are a variety of lasers that operate in this wavelength regime some of which are shown in Table 3-1 with advantages and disadvantages listed.

Based on power and size constraints, semiconductor diode lasers were selected as the best option for this project. The low power requirements and compact size are appropriate for the size of the water tank. The limitation to the semiconductor diode lasers is that available wavelengths are only ~400nm and ~550nm, with the later being DPSS.

Table 3-1 – Information on several types of lasers capable of operating in the blue/green spectrum [2], [3]

Type	Characteristics	Advantages	Disadvantages
Argon-ion Laser	Gas discharge laser	High output power. Tunable output in the 458nm to 514nm range.	Strict cooling requirements. Requires high power input.
Flashlamp Pumped Frequency Doubled Nd:Yag	Frequency doubled solid state laser	High Power	Hard to modulate
Doubled Ti : Sapphire	Frequency doubled solid state laser	Ultrafast output pulses, Frequency tunable	Expensive, sensitive to vibration
Diode pumped solid state doubled Nd:Yag	Frequency doubled solid state laser.	Highly efficient, long lifetime, compact	Higher cost-per-watt compared to lamp pump
Fiber lasers	Solid state laser, typically diode pumped.	Rugged, small, efficient, high output power	Expensive, may require external modulator
Semiconductor diode lasers	GaN diode laser outputs from 375nm to 473nm	Highly efficient. Compact. Low power consumption	Low power, usually <200mW. Difficult to couple or focus

The transmitter is primarily designed to communicate using on-off keying (OOK) of the light source due to the difficulties of obtaining a linear output response from a diode when using an amplitude modulation scheme. The ability to modify the transmission scheme (return-to-zero, non-return-to-zero, pulse position modulation) is also of importance.

Violet laser diodes

LEDs in wavelengths ranging from 400nm (violet) to 550nm (green) have been in existence for several years, but the most recent addition to the semiconductor light source arsenal has been the creation of the violet laser diode. The diodes, which emit at close to 400nm, are prized by the consumer electronics industry for their ability to be focused to a small spot size which increases the storage capacity optical storage mediums. This has helped in reducing the price for such diodes, but their costs still remains very high in comparison to red laser diodes and NIR diodes.

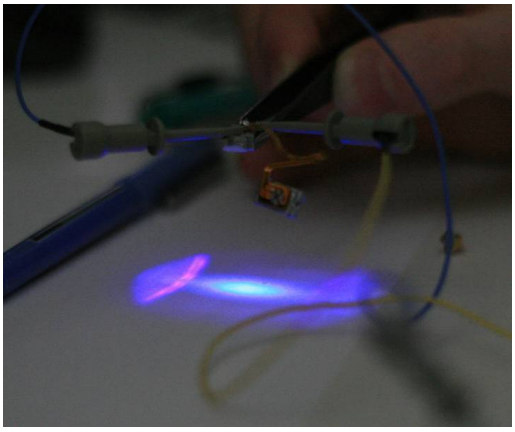

Figure 3-10 – PS3 Laser diode lasing. Note that in this particular laser package the widow was cracked which leads to the streak in the left hand side of the image.

Purchasing violet laser diode modules from optics suppliers was considered, but rejected due to their high costs. In response, several consumer electronic optical storage devices were purchased that used similar violet diodes. Competition between rival, next generation, optical storage standards, HD-DVD™, and BlueRay™, has pushed the hardware cost to consumers far below the price of individual laser diode modules. Compare the cost of the popular Microsoft Xbox 360 HD-DVD player, at $200 USD, to an individual 405nm laser diode which can cost between $1,800 at Thorlabs, Inc. and $6,000 USD at Edmund Optics, Inc.

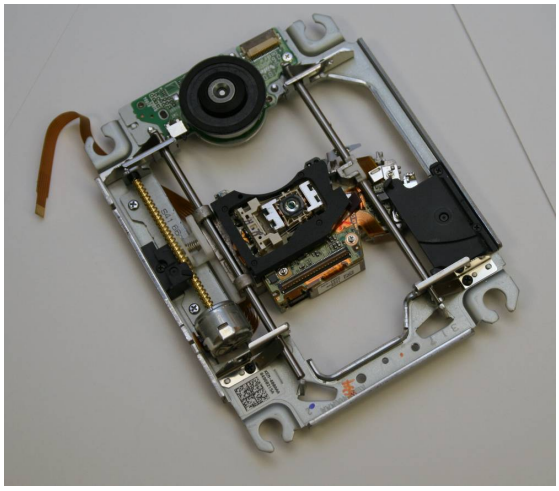

Figure 3-11 – PlayStation 3 optical assembly. The laser is below the lens that is in the center

Several 405nm violet laser diodes were extracted from both HD-DVD and BlueRay drives. Those diodes extracted from the BlueRay disk drives ultimately proved more accessible and cost effective.

The effective output power of the laser diode was calculated by focusing the output of the diode onto a Thorlabs PD100A photodetector. By varying the current to the laser diode and recording the output voltage from the PDA100A, a relationship was established which would allow the current input to the laser diode to be translated into received optical power at the PDA100A. By using these values and the conversion between voltage and radiant flux on the detector, the plot shown in Figure 3-12 was generated. The three separate lines show the minimum, maximum, and nominal values based upon a ±2% error in the PDA100A. At 40mA input current, the calculated output power is 17mW. For the scale of experiments to be done in the water tank, this is sufficient power. Initially, the laser diodes were treated very carefully. However, in the future it should be possible to pulse the laser diodes at significantly higher powers, especially if the laser are appropriately mounted in a heat sink.

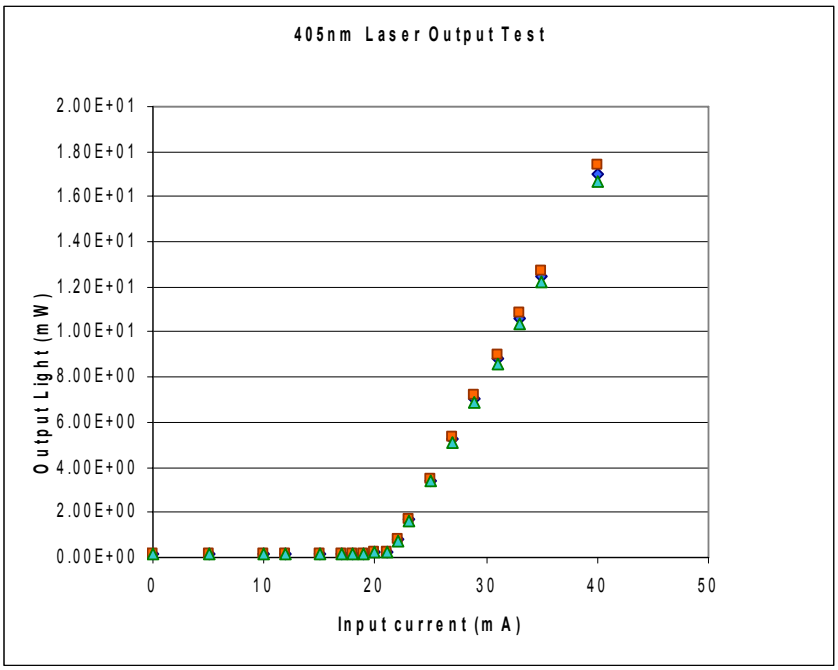

Figure 3-12 – Experimental results showing power output from 405nm laser diode

Laser Diode Driver

An appropriate diode driver needed to be built in order to drive the violet laser diodes at high data rates. Most current laser diode driver chips are not suitable for driving a GaN violet laser diode due to the large turn-on voltage.

The Maxim MAX3701 Blue Laser Driver chip was chosen to drive the diode due to its simplicity over designing a discrete diode driver circuit. The chip allows for a total drive current of 200mA and is capable of driving a diode at speeds of 400Mbps, with a rise/fall time of 0.9nS.

The chip was initially tested on a prototyping board shown in Figure 3-13. This board was able to drive the laser diode at rates exceeding 1Mpbs and demonstrated that the MAX3701 was an appropriate choice to meet the needs of the project.

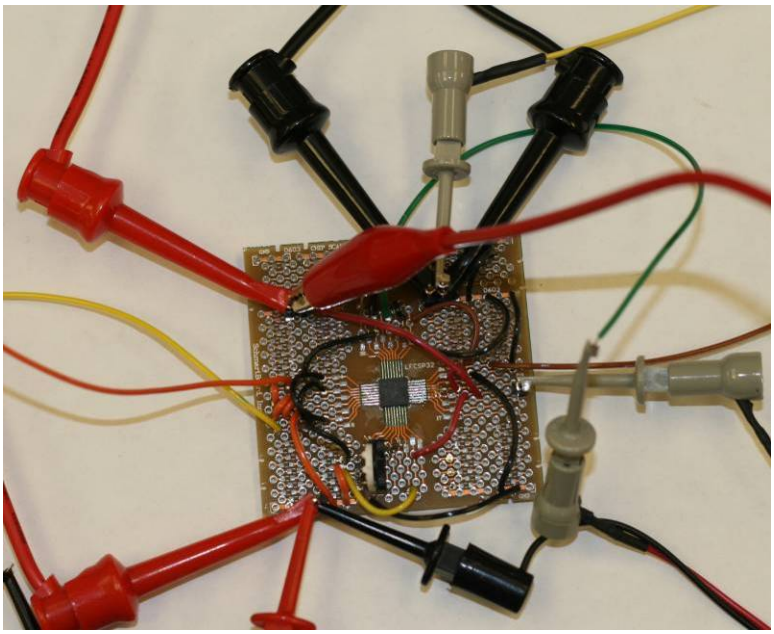

Figure 3-13 – Initial prototype of MAX3701 laser diode driver board

A PCB was created that would allow the MAX3701 to be controlled via an Alterra Cyclone II EP2C5 FPGA. The PCB also incorporated an Analog Devices AD7822 ADC to digitize the voltage from the internal transimpedance amplifier on the driver chip. This would allow the input power to be adjusted based on the internal feedback photodiode in the laser diode.

An onboard potentiometer is used to set the bias current for the diode, which is controlled via the V1 pin shown in Figure 3-15. A PWM signal is generated from the FPGA at 400MHz, and driven through a low-pass filter, to provide a voltage output to control the modulation current. The modulation current is set by the V2 pin on the MAX3701. A pin on the FPGA is used to control one of the current driver output enable pins on the MAX3701, to generate an on-off keying (OOK) output signal on the laser.

Figure 3-14 shows the block diagram for the system and Figure 3-16 shows a simplified schematic for the system. Figure 3-17 shows the final board design. In this image the ADC is unpopulated. Initial tests showed that the output is stable, given adequate heat-sinking, and the ADC feedback loop isn't necessary for short lengths of time.

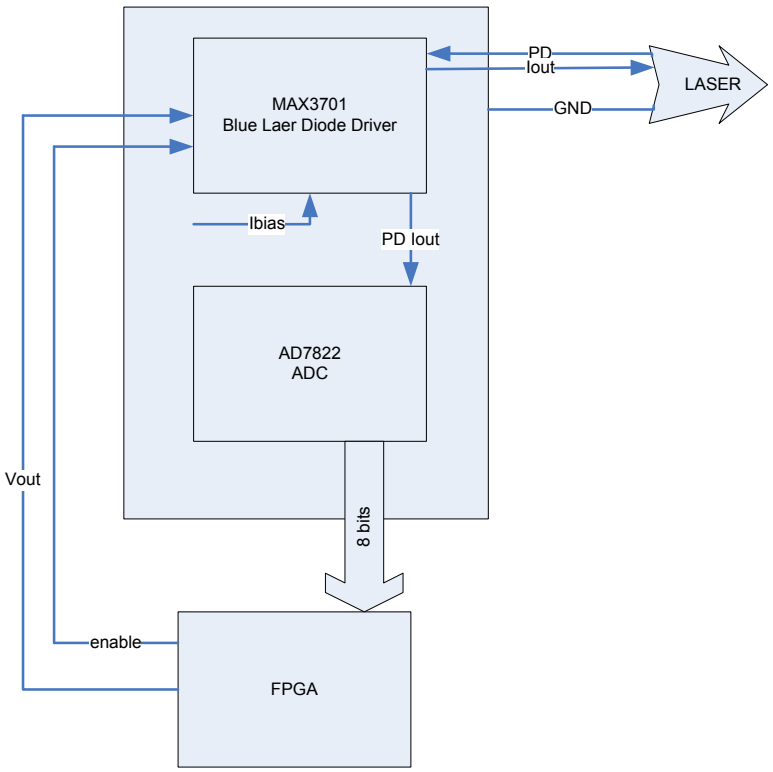

Figure 3-14 – Block diagram of the laser diode driver

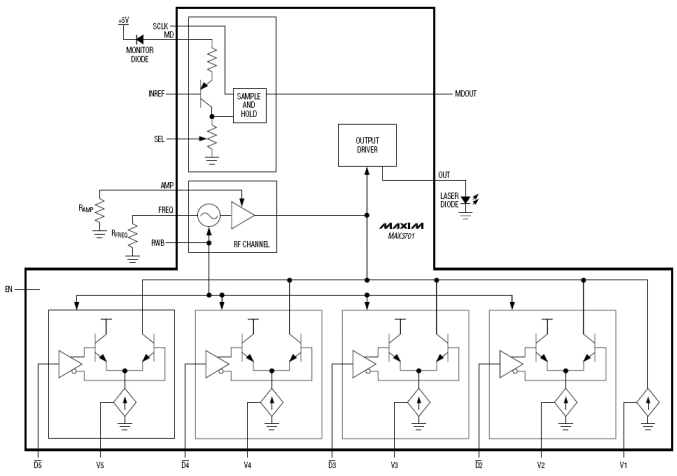

Figure 3-15 – Block diagram of MAX3701 blue laser diode driver [4]

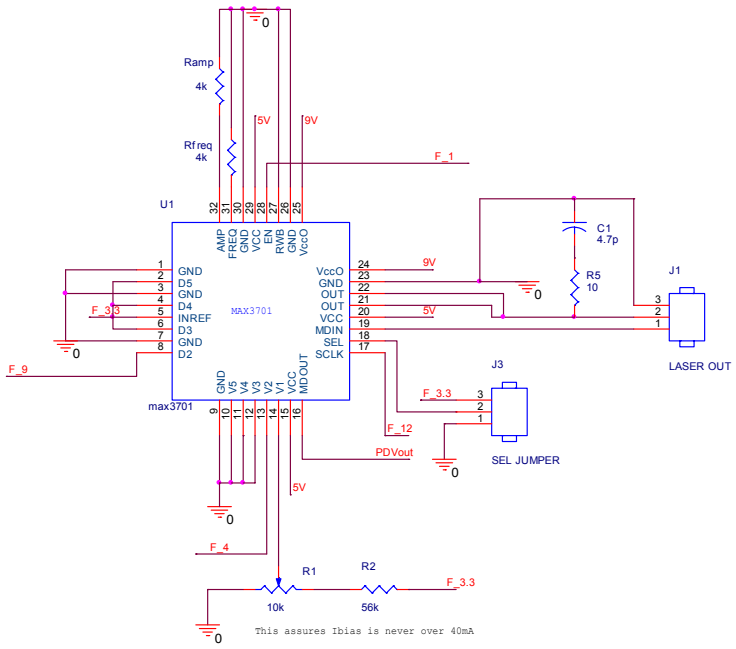

Figure 3-16 – Simplified schematic for MAX3701 violet laser diode driver board

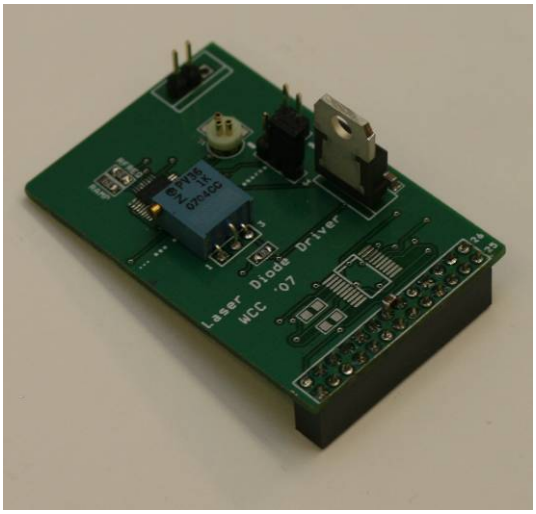

Figure 3-17 – The completed blue laser diode driver board

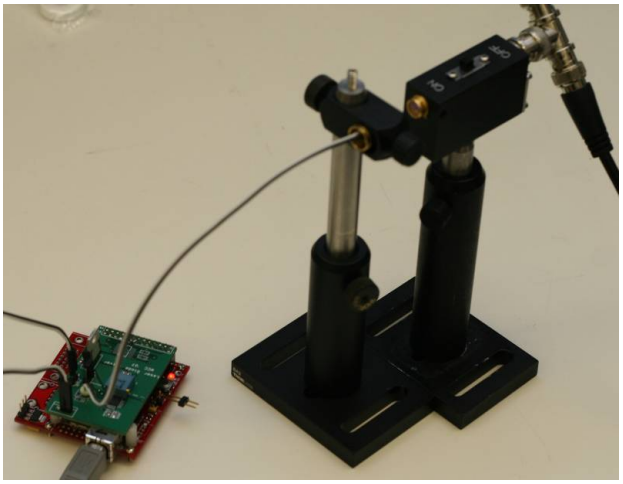

Figure 3-18 - Experimental setup to test 405nm laser diode and driver

Figure 3-19, Figure 3-20, and Figure 3-21 show the laser diode response to a 1Mbps input signal. The signal exhibits ringing on the rising and falling edge, however this could be damped with appropriate compensation impedance at the output.

Figure 3-19 – 405nm laser diode being driven at 1Mbps

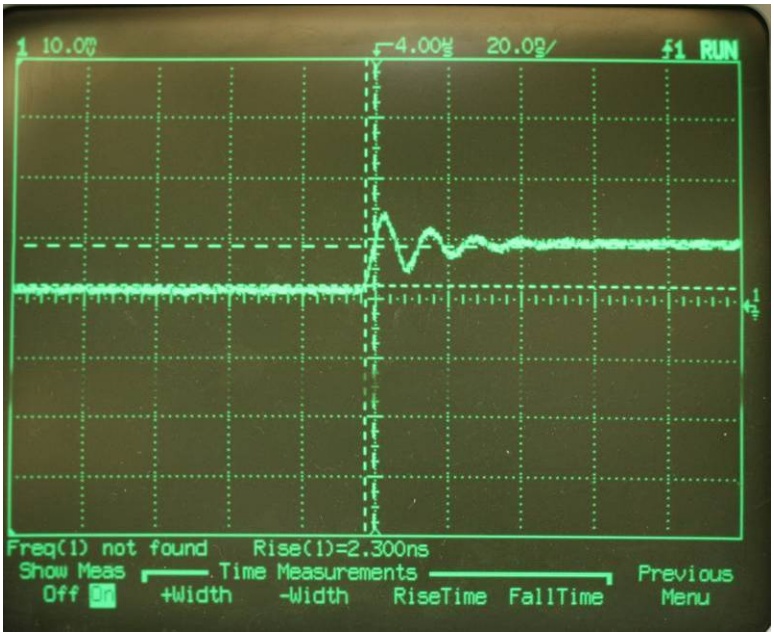

Figure 3-20 – 405nm laser diode rise time for 1Mpbs data

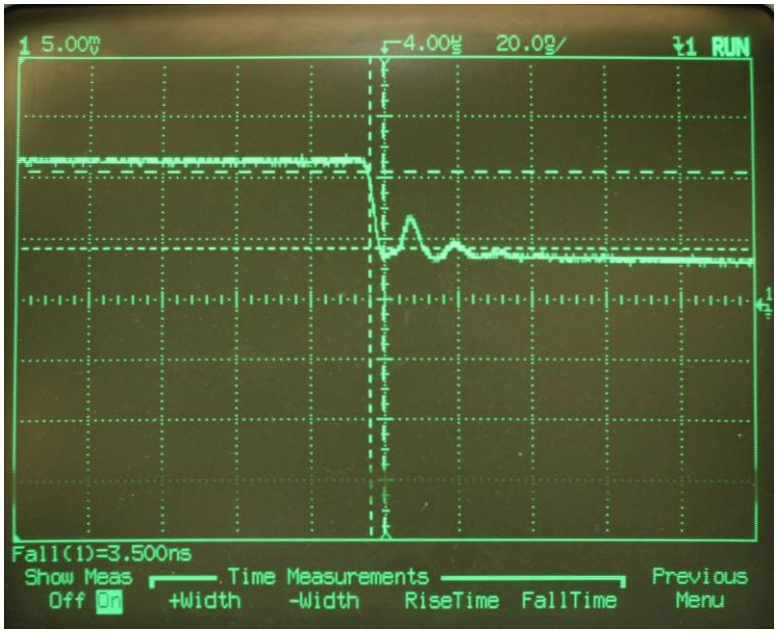

Figure 3-21 – 405nm laser diode fall time for 1Mpbs data

Figure 3-22 and Figure 3-23 show the laser diode response to a 10Mpbs signal. Again, the ringing on the rising and falling edges could be removed using compensation impedances on the output of the laser diode driver.

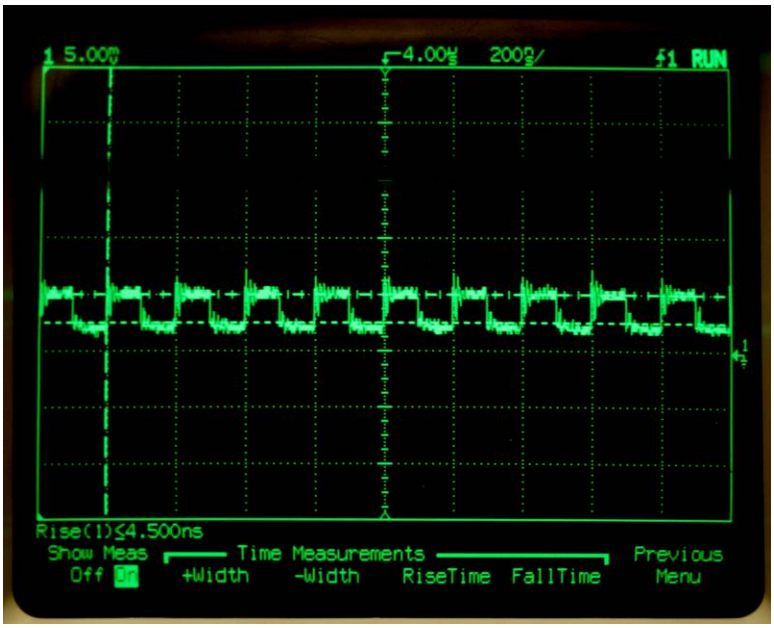

Figure 3-22 – 405nm laser being driven at 10Mbps

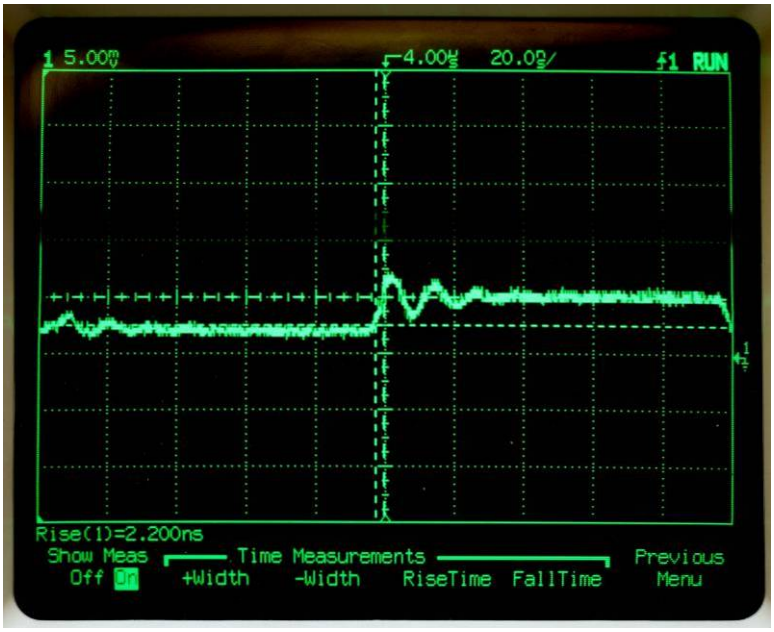

Figure 3-23 – Rise time and overshoot for 405nm laser at 10MBps

Computer to Laser Diode Driver Interface

In order to transmit useful data through the water tank, an interface between a computer and the laser diode driver board needed to be developed. A custom built system was chosen over commercially available DAQ systems due to cost constraints and the desire to have a compact modular system that could eventually be used for field tests. As mentioned previously, the system used to transmit the data using the laser diode driver board was an Alterra Cyclone II EP2C5 FPGA. The processor board, purchased from KNJN.com, comes with a USB interface chip which was chosen to interface with the computer. A program written in C++ is used to download a bitstream from the computer to the FPGA, where it is then transmitted using the laser diode driver board.

The use of the FPGA allows for powerful pre-processing of the data and exploration of alternative coding schemes, such as return-to-zero, non-return-to-zero, or pulse-position modulation. Pre-processing of the data stream using a forward error correction code, like Reed-Solomon a Hamming code will allow for a more robust optical link and usability in a larger variety of aquatic environments.

Transmitter Conclusions

In conclusion, the design requirements of a compact, low cost, laser transmitter capable of driving blue laser diodes were met. The transmitter is capable of driving a 405nm blue laser diode at speeds in excess of 10Mpbs using on-off keying (OOK), and at a current of up to 200mA. Additional control circuitry and a processing allow datastreams to be transferred from the PC to the transmitter. This system could easily be mounted to small underwater vehicle for field testing and further study.

Receiver Specifications

In order to develop a robust optical communication link, a receiver was needed that would be able to perform in a variety of water conditions and provide adequate signal-to-noise ratio. Three primary optical sensors were considered for the receiver:

- Si photodiode (PD)
- Avalanche photodiode (APD)
- Photo multiplier tube (PMT)

Initial work focused on creating a photodiode transimpedance amplifier circuit. This provided a quick path to making a simple receiver circuit that would be sufficient for data rates up to 10 Mbps and high light levels. However, photodiode sensitivity in the blue green region of the visible spectrum is limited. Avalanche Photodiodes are promising, and potentially offer a compact form factor and high sensitivity. Potentially GaN or GaP avalanche photodiodes, if developed, would be very attractive. Finally, it was decided to use a PMT due to their high gain and good blue green responsivity.

Noise, Dynamic Range, and Receiver Sensitivity

One of the important requirements for a receiver is a high dynamic range. This is due to the fact that light underwater can experience a wide range of attenuation based on the various water types, time of day, depth of operation, and other factors. In addition, the transmitter and receiver distance is not fixed, so a receiver operating 5m from the transmitter will experience a significantly higher amount of light than the receiver

operating 50m from the transmitter. Also, the scattering nature of seawater causes the signal strength to drop dramatically when the receiver is not properly aligned with the beam. Finally, sunlight and bioluminescence can add significant amounts of background light which is added to the received signal.

A receiver with high dynamic range is one that is able to detect light levels over many orders of magnitude. The range is usually expressed as a ratio between the highest observable signal and the noise floor of the system. This is determined both by the sensor of choice and the supporting circuitry. For photodiodes, which do not have built in gain, high gain external amplifiers are usually needed to extract a useful signal, high noise is usually a tradeoff for high gain, and the overall system's dynamic range is reduced. PMTs, on the other hand, can exhibit very high, low noise, gains within the sensor. These gains can be upwards of 10^6. For this reason, PMTs are often the choice for situations that require wide dynamic range [3].

Si photodiodes were initially chosen based on their low cost and the ease of integrating them into circuits. The downside to Si photodiodes is that they are not nearly as responsive to the 400nm – 550nm wavelength spectrum of visible light as they are to higher wavelengths which are unsuitable for aquatic applications.

A typical response curve for a Si photodiode is shown in Figure 3-24. Notice that the sensitivity at 400nm is $1/6^{th}$ of the sensitivity at 950nm. This is due to the intrinsic properties of Si and the construction of the photodiode.

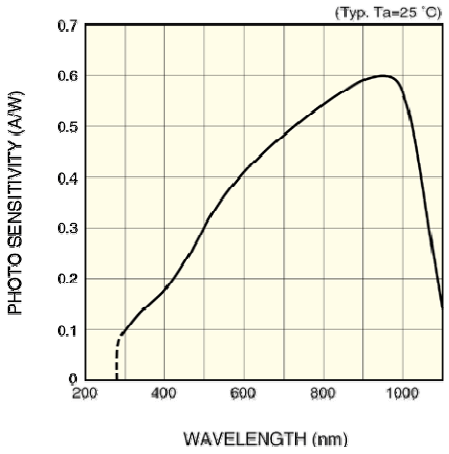

Figure 3-24 – Typical photodiode responsivity curve [5].

More blue/green responsive photodiodes can be found, like the Hamamatsu S5973-2 photodiode, but it still has no internal gain, unlike APDs or PMTs. Figure 3-25 shows the responsivity of this photodiode.

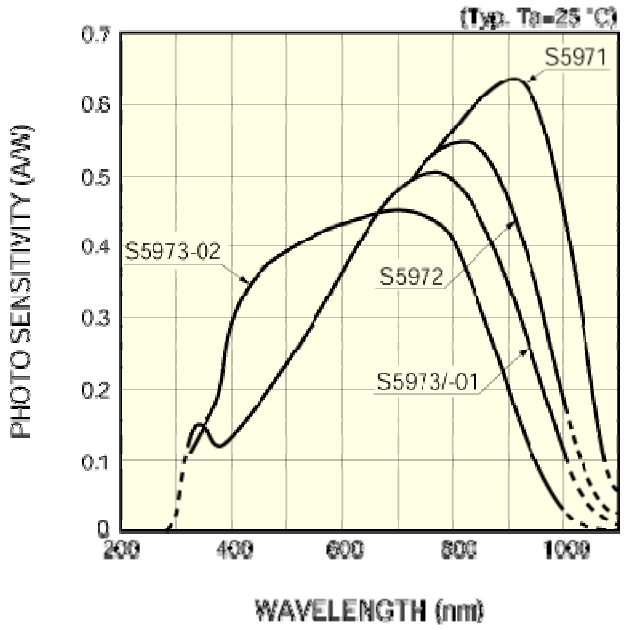

Figure 3-25 – Responsivity curve of the Hamamatsu S5973-2 photodiode [5]

In contrast, the responsivity of a PMT is largely dependant on the material its photocathode is constructed from. Figure 3-26 shows the sensitivity of the photocathode in the R7400 series PMTs. When compared to the sensitivity of the Si photodiode, the PMT is less, however the gain of the PMT overcomes this limitation. For underwater optical communications, the low response to wavelengths above 550nm is also useful.

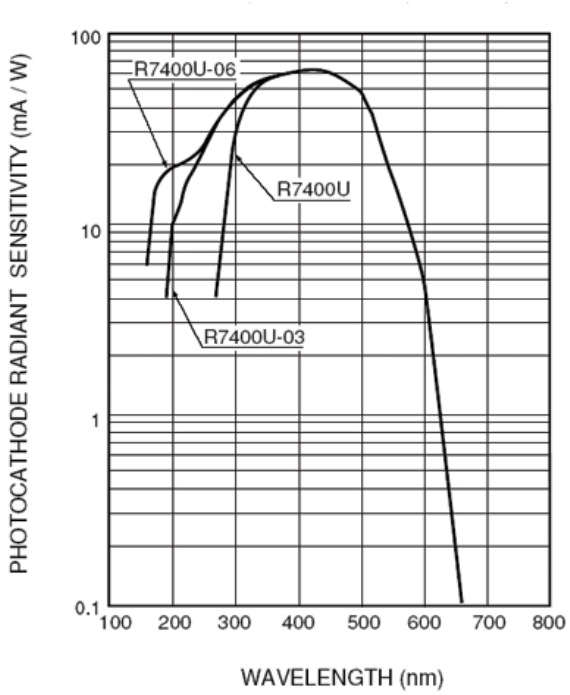

Figure 3-26 – Sensitivity of bialkali photocathode for R7400U PMT

PMT Theory

Photomultiplier tubes are devices which utilize the external photoelectric effect to convert incident photons into an amplified electrical signal.

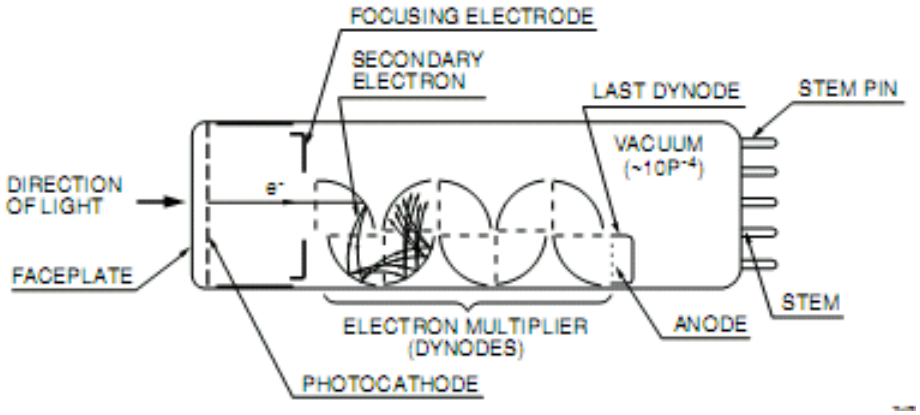

Figure 3-27 – Illustration showing basics of a photomultiplier tube [6]

A PMT is constructed using a series of dynodes which are biased at large negative voltage. Each successive dynode in the PMT is biased at a slightly higher potential and creates a "pathway" for electrons based on the electric field between successive dynodes.

Light first enters the faceplate of the PMT where it encounters the photocathode. The electrons in the valence band absorb the photo energy and move towards the photocathode surface. If the electron has sufficient energy to overcome the vacuum level barrier, an electron is ejected from the photocathode and is then directed to the first dynode in the series by the focusing electrode. Each dynode is constructed from a secondary emissive material that eject a certain number of electrons when an electron with a high enough initial energy level strikes the surface. This secondary emission process is repeated for each dynode in the PMT. At the end of the PMT, all of the emitted electrons are collected by the anode and exit the PMT as a current [6].

Since the photoelectric effect is based upon incident photon energy, PMTs are naturally more responsive to higher energy wavelengths of light – like blue, as opposed to red. The lower bound on the wavelength sensitivity is usually set by the window material on the device.

PMTs are also characterized by their radiant sensitivity and quantum efficiency. Radiant sensitivity is a relationship between the incident radiant flux and the photoelectric current from the photocathode. This number, just like a photodiode, is expressed in terms of amps per watt. The quantum efficiency of a PMT is the number of number of photoelectrons emitted from the photocathode divided by the number of incident photons on the photocathode.

All PMTs exhibit a dark current, which is current that flows out of the anode even in the total absence of light. This is caused by several factors including thermionic emission due to the low work function of the photocathode and dynode materials, leakage current through the anode, ionization of residual gasses inside the tube, and cosmic rays. The dark current can be expressed as a function of supply voltage and effectively limits the lowest level of light detection by the PMT [6].

PMT Receiver Circuit Design

The basic circuit components needed to utilize a PMT are

1. A high-voltage, stable power supply
2. A voltage divider circuit to distribute the voltage potential to the dynodes.
3. An output load or amplifier circuit.

In addition, care must be taken to prevent too much light from entering the PMT while it is powered, or possible damage may occur due to the high current on the anode.

Hamamatsu Photonics, one of the major suppliers of PMTs, has a wide array of PMTs with varying window and photocathode materials. For the application of underwater communication, the R7400U PMT unit was chosen, due to its small size, excellent sensitivity to blue/green light, high speed and low-cost.

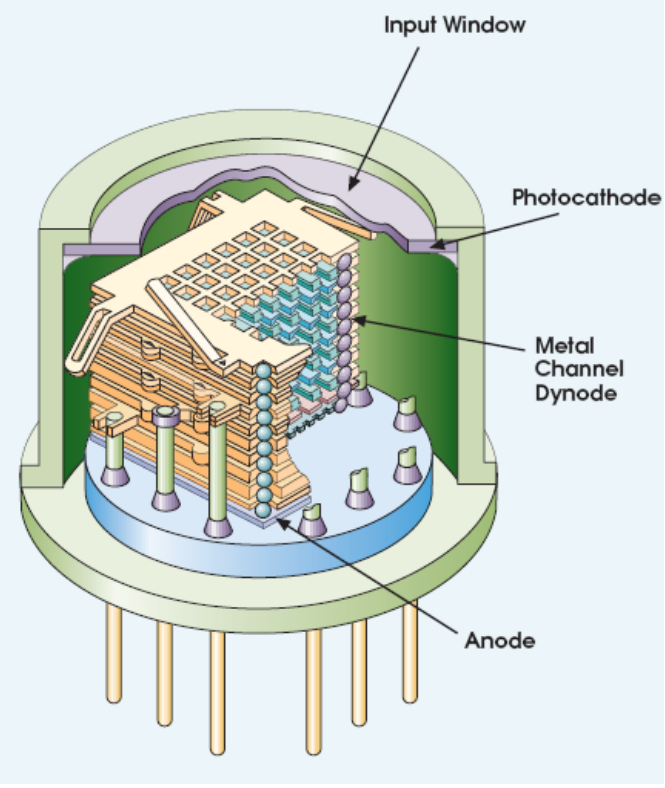

Figure 3-28 – Illustration showing metal channel PMT structure [3]

The R7400U PMT is a metal-channel type device (illustrated in Figure 3-28), which allows it to respond very quickly to incident photons due to its small size and precise machining. The R7400U also has peak sensitivity at 420nm, which is very close to the 405nm used in the laser diode driver. The maximum supply voltage for the R7400U is 1,000v and the absolute maximum average anode current is 100µA.

PMTs can also be used as single photon counting devices. Further work may explore using the single photon counting abilities for extremely low light situations. However, the photon counting mode is expected to only be practical in certain situations due to the high solar, and bioluminescent backgrounds that can be encountered. In this project, the PMT was treated as an ideal current source.

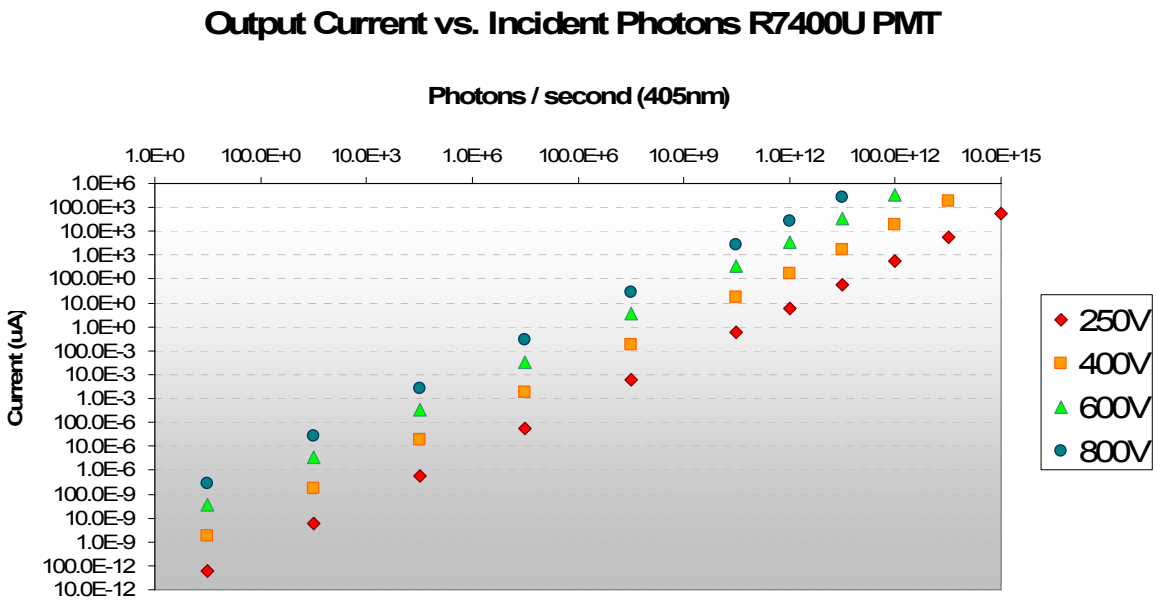

Figure 3-29 – Graph showing output current in µA based on incident photons (405nm), for different supply voltages

As shown in Figure 3-29, adjusting the supply voltage has a profound effect on the sensitivity of the PMT. By changing the supply voltage from 250v to 800v, the output current changes by almost 5 orders of magnitude. The graph also shows that by adjusting the supply voltage, the PMT can sense a huge range of values. If the output current were to be kept constant, and the supply voltage adjusted, the PMT would be able to observe a four order of magnitude range of photons.

In order to calculate the minimum and maximum observable number of photons, 405nm light is first assumed. The energy of one photon is given by

$$E = \frac{h \cdot c}{\lambda} = 4.90480299 \times 10\text{-}19 \text{ joules} \qquad \textbf{Equation 3-1}$$

where h is Planck's Constant, c is the speed of light in a vacuum, and λ is the wavelength of light. At the rate of one photon per second, the power is

$$1\frac{photon}{\text{sec}} = 4.90480299 \times 10\text{-}19 \text{ Watts} \qquad \textbf{Equation 3-2}$$

From the R7400U datasheet, the photocathode has a sensitivity of 0.6 Amps/Watt. Also from the datasheet, an equation can be derived to express the gain of the tube based on supply voltage. This relationship is shown by

$$Gain = 7\text{E}^{-16} \cdot V_s^{\,7.2783} \qquad \textbf{Equation 3-3}$$

where V_s is the supply voltage. The maximum average current for the PMT is given as 0.1mA in the R7400U datasheet. Using this data and the above equations, the following equation for the maximum number of photons is derived.

$$\#Photons_{\max} = \frac{\frac{1}{0.6}\frac{W}{A}\cdot\frac{1}{Gain}\cdot I_{\max}}{1\frac{photon}{\sec}}$$ **Equation 3-4**

#Photons$_{max}$ is then a function of supply voltage. This is assuming the photons have a wavelength of 405nm.

The minimum number of detectable photons by the PMT, when using the PMT as a current source, is determined by the dark current. If the number of incident photons on the PMT produces a current less than the dark current, then their arrival will be unobservable. Based on the R7400U datasheet, an equation was derived to express the dark current as a function of supply voltage.

$$I_{dark} = 1\mathrm{E}^{-4}\cdot e^{0.0091\cdot Vs}$$ **Equation 3-5**

In Equation 3-5, *Vs* is the supply voltage. Based on the previous equations, an equation to express the minimum number of incident photons to be observable is shown below.

$$\#Photons_{\min} = \frac{\frac{1}{0.6}\frac{W}{A}\cdot\frac{1}{Gain}\cdot I_{dark}}{1\frac{photon}{\sec}}$$ **Equation 3-6**

Plotting Equation 3-4 and Equation 3-6 as a function of supply voltage yields the graph shown in Figure 3-30. For convenience, the same data is presented in Figure 3-31 with the y-axis units in Watts instead of photons.

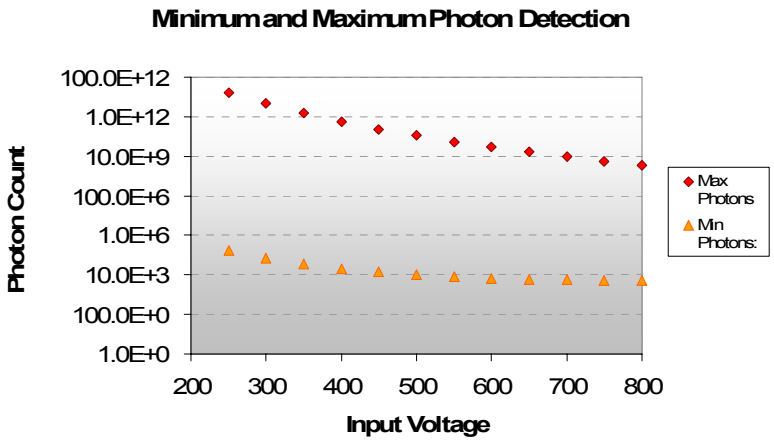

Figure 3-30 – Graph showing minimum photon detection based on dark current noise floor, and maximum photon detection based on absolute maximum average current. Photon energy based on 405nm light.

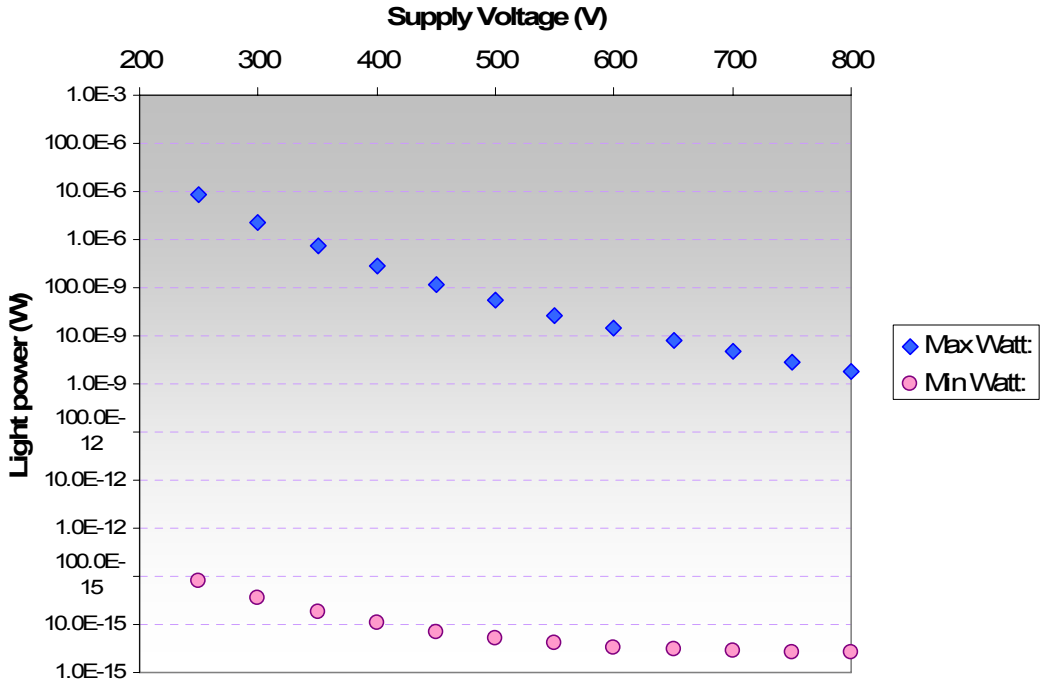

Figure 3-31 – Minimum and maximum detectable amounts of light in watts. Maximum is based on the maximum average current at the anode, and minimum is based on the dark current noise floor.

As is clear in Figure 3-30 and Figure 3-31, as the PMT's supply voltage, and therefore the gain, is increased the maximum amount of observable light decreases in order to keep the total output current below a certain level.

The following circuit was constructed to convert the output current from the PMT to a useful voltage signal which could then be digitized and stored for later processing.

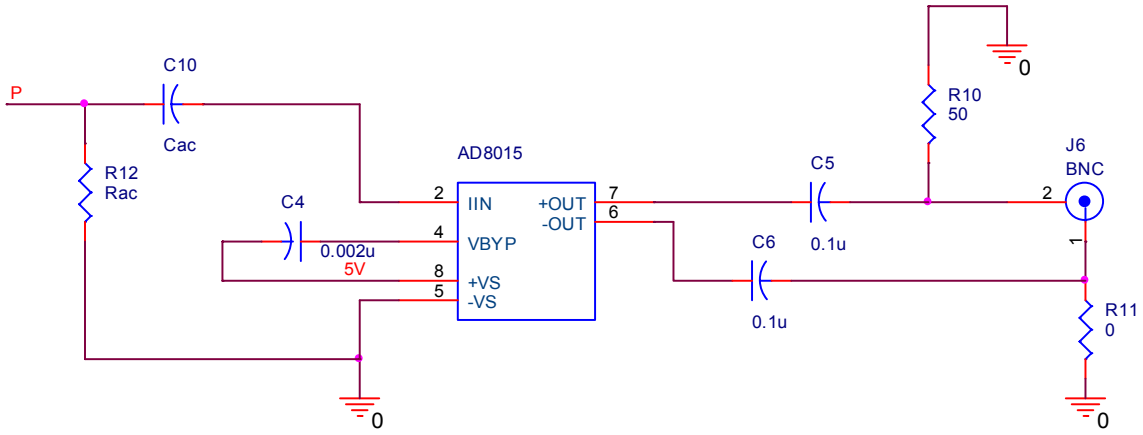

3-32 - Schematic of PMT transimpedance amplifier circuit

The output current from the PMT is connected to node "P". C10 and R12 could be use to form a low-pass filter on the input for better noise immunity, or a high-pass filter to give better ambient light immunity. The amplifier output, J6, can either be AC or DC coupled using C5 and C6, or loaded using R11 and R10. These components can also be used to place a filter on the output of the transimpedance amplifier.

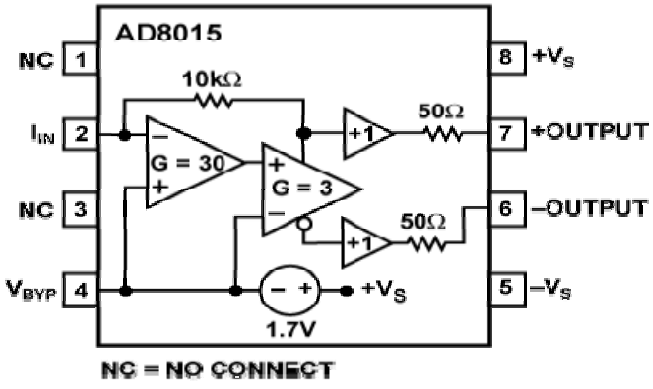

Figure 3-33 – Analog Devices AD8015 Wideband/Differential Output Transimpedance Amplifier

The amplifier chosen for this application is the Analog Devices AD8015 transimpedance amplifier. This amplifier was chosen for several reasons:

- Wideband operation up to 240MHz
- Differential and single-ended outputs
- Single voltage supply operation
- 50Ω output impedance

These features made using the AD8015 amplifier a sensible choice over designing a custom amplifier for this application. The AD8015 also has a linear differential output response for currents ranging from -35µA to 35µA, with a maximum input current from ±300µA, which is well above the maximum average output current of the PMT [7].

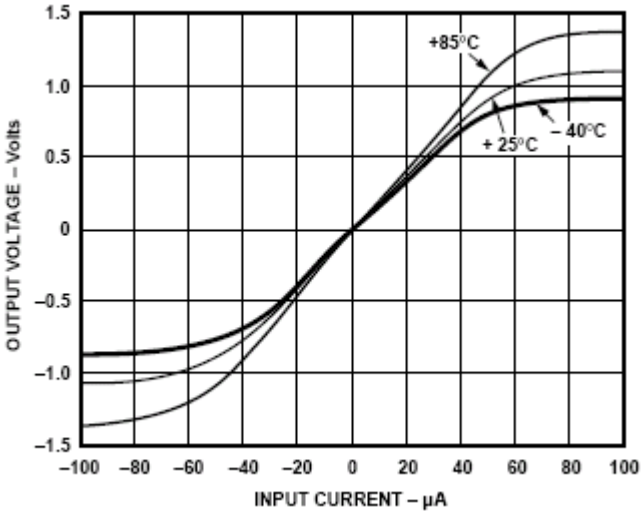

Figure 3-34 – Differential Output vs. Input Current for AD8015

Figure 3-35 shows the populated PCB with PMT, AD8015 and high voltage power supply. The bias voltage output is set by a potentiometer.

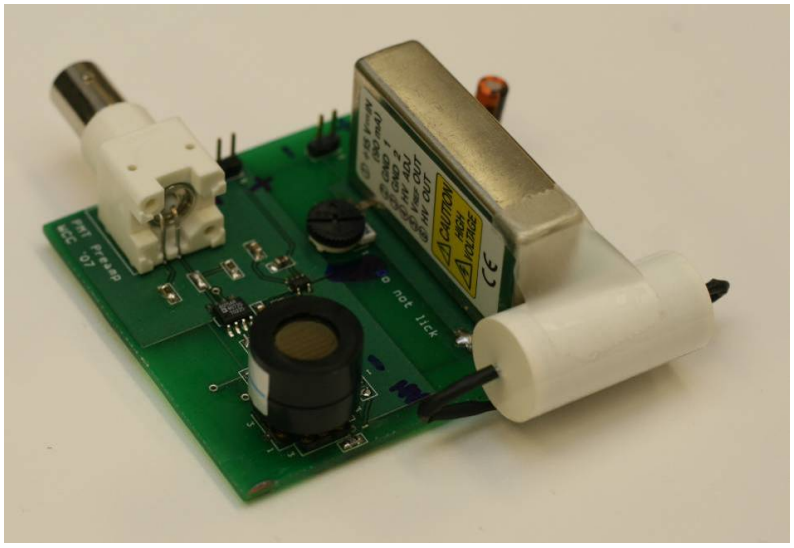

Figure 3-35 – PMT receiver, amplifier, and power supply.

Testing

Initial results show that the AD8015 has a higher amount of noise than anticipated, with a value of about 23mV$_{rms}$ which is primarily comprised of a very strong 90MHz RF noise that couples to all of the traces on the board. Tests show that this is not noise caused by the board, but instead generated by the environment. Placing the board into a shielded metal box improves the SNR slightly. Figure 3-36 shows data received by the PMT board at 1Mbps.

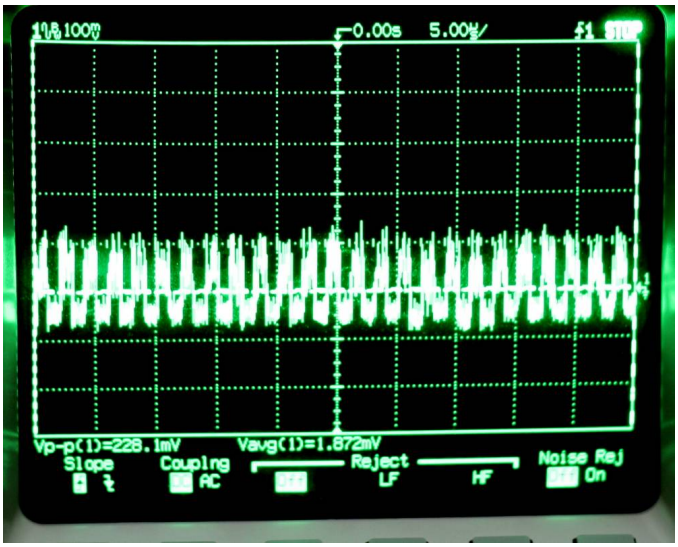

Figure 3-36 – 1MBps data received by PMT receiver board

Experimental Apparatus Conclusion

In conclusion, this chapter has detailed the design and construction of the following:

1) A water tank for testing underwater communication
2) A transmitter system for transmitting data using a 405nm blue laser diode.
3) A PMT based optical receiver

These systems can be used to experimentally test the feasibility of underwater optical communications.

Future work will include improvements to the water tank, such as a flat black coating to the inside to prevent excessive reflection off the walls and the addition of a larger window in place of the current 8" port-hole. Also, improvements to the transmitter system will include water tight packaging, additional code to allow for user specified modulation schemes like non-return-to-zero or pulse-position modulation, and active feedback to maintain a constant output from the laser diode for long periods of operation. Finally, improvements to the receiver board will include a second board revision that will improve the noise characteristics of the receiver, a better system for actively controlling the supply voltage for the PMT, and a lens assembly to collect more light to focus on the PMT face. Of these improvements, automatic gain control of the PMT is the most important in terms of making the system robust for operation in realistic environments.

Chapter 4 will discuss various experiments conducted to validate the above designs and the feasibility of underwater optical communication.

References

[1] B. Johnson, D. Scroggins, B. Kamgar-Parsi, D. Folds and E. Belcher, "3-D acoustic imaging with a thin lens," in *OCEANS '93. 'Engineering in Harmony with Ocean'. Proceedings,* 1993, pp. III444-III449 vol.3.

[2] Melles Griot. Introduction to laser technology. Available: http://www.mellesgriot.com/pdf/CatalogX/X_36_16-27.pdf

[3] K. J. Kaufmann. (2000, 7/2000). Light levels and noise guide detector Choices . *Photonics Spectra*

[4] Maxim IC, "MAX3701 - 2x Blue Laser Driver with Sample and Hold," 2003.

[5] Anonymous Hamamatsu corp. website. *2007(10/26),* Available: http://sales.hamamatsu.com/

[6] T. Hakamata and etc. (2006, *Photomultiplier Tubes: Basics and Applications.* (3rd ed.) Available: http://sales.hamamatsu.com/en/support/technical-notes.php

[7] Analog Devices, "AD8015 Datasheet," 1996.

4. Experiments

Several experiments were conducted in order to validate the work done in Chapters 2 and 3. This involved validation of the tank design, validation of the blue laser diode driver design, validation of the PMT receiver design, and validation of the overall system for underwater optical communication systems.

Several experiments were performed using a red (635nm) laser diode that was capable of signaling upwards of 10Mbps. This allowed various designs to be validated while the blue laser diode driver was still being constructed. While red light isn't the ideal method of underwater optical communication, for all intents and purposes, the use of a red laser could be treated the same as using any type of light source that experiences high attenuation due to the medium.

As discussed in Chapter 3, an FPGA was used to drive the input of a diode driver – whether red or blue – to produce a digital on-off-keying waveform to communicate data. This data was then sent through the tank to a receiver.

Experiments were conducted with both red and blue lasers, along with the PMT receiver.

Communication Using a Red Laser Diode

Unamplified Detector Signal

An initial test was to try and relate bit-error-rates (BER) to the attenuation of light in water. The BER was calculated by transmitting a randomly generated bitstream of equal probability of 1 or 0. This bit stream was sent through the transmitter to the receiver, which was sampled using an ADC (Flashy-D, purchased from KNJN.com). The sampled data was transferred to the "receiver" PC where the data was saved to a file for later processing.

Beam attenuation could be achieved by either varying the amount of scattering and absorption of the channel, through the addition of Maalox to the water, or reducing

the transmitter power. The simplest method of doing this was to put a linear polarizer in front of the transmitter which would attenuate the laser beam before entering the tank.

A Thorlabs PDA100A amplified photo detector was used to detect the red laser light. This receiver has an output from 0v to 10v, when terminated into a high impedance load, such as an ADC or oscilloscope. Since the bandwidth of the detector was a maximum of only 1.5MHz, the detector was always run in the lowest gain, "0dB", setting. At this level the detector has a transimpedance of approximately 1.51 x 10^3 V/A.

Figure 4-1 shows a high SNR (signal to noise ratio) data file sent at 500kbps using the red laser, detected with the PDA100A, and sampled with the 8bit Flashy-D ADC at 10Msamples/second, for a 20-times over-sampling. Return-to-zero encoding was used for its self-clocking benefits, which was useful when post-processing the data to arrive at a BER. Figure 4-1 shows 800 samples, which is equivalent to 40 transmitted bits shown in Table 4-1.

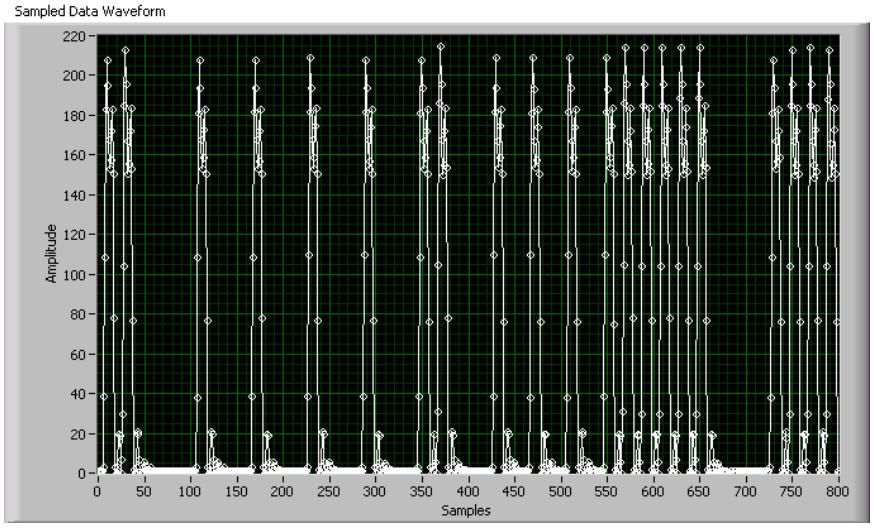

Figure 4-1 – Sampled waveform using red laser diode, PDA100A detector and Flashy ADC.

Table 4-1 – First 40 transmitted bits.

11000100	10010010	01100101	01011111	10001111	…

Figure 4-2 and Figure 4-3 show a picture of the red laser propagating through clear water. The secondary beam above the beam in the middle is the reflection off the surface of the tank. For clear water there is some scattering, but it isn't pronounced.

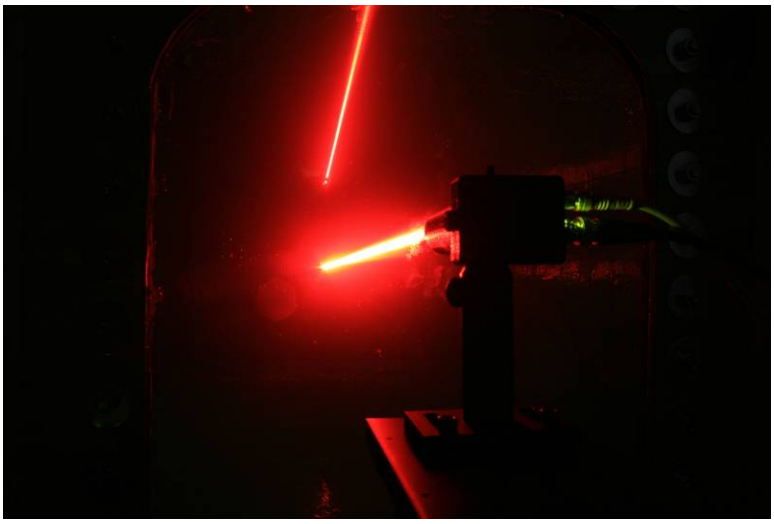

Figure 4-2 – Red laser beam from transmitter to receiver in clear water, no room lights

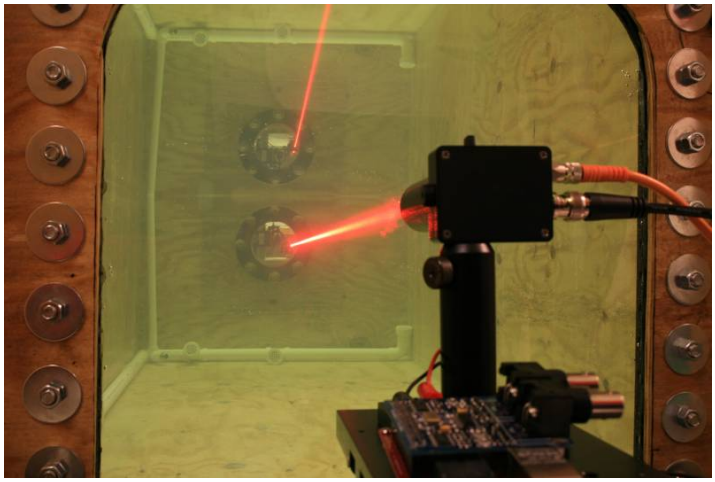

Figure 4-3 - Red laser beam from transmitter to receiver in clear water, with room lights

After the addition of Maalox to the water, the beam begins to be absorbed and scattered, which reduces the amount of light that is incident on the detector. Since the Flashy-D ADC has a fixed input range of 1v, the attenuation of the beam, and the

corresponding reduction in the receiver's signal, produces a quantization error. At 1v, the Flashy-D has a minimum resolution of 3.9mV.

Figure 4-4, as compared to Figure 4-1 shows the different in signal strength after the addition of Maalox. The data in Figure 4-4 is after the addition of 54mL of Maalox to the tank (approximately 900 gallons of water), or approximately 16 ppm (parts per million).

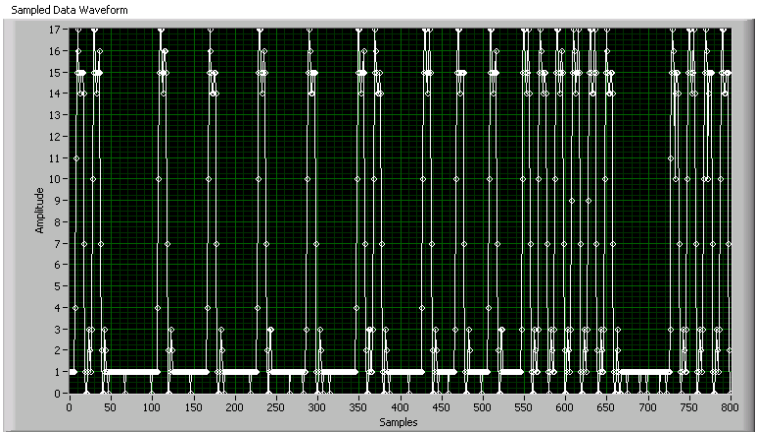

Figure 4-4 – Sampled waveform using PDA100A and red laser. The total signal range only covers 0 – 17 (out of 256).

Figure 4-5 and Figure 4-6 shows the red laser propagating through turbid water. Compare the visibility in Figure 4-3 (greater than 12ft) to Figure 4-5 (less than 12 feet). Also compare the beam spread to previous images.

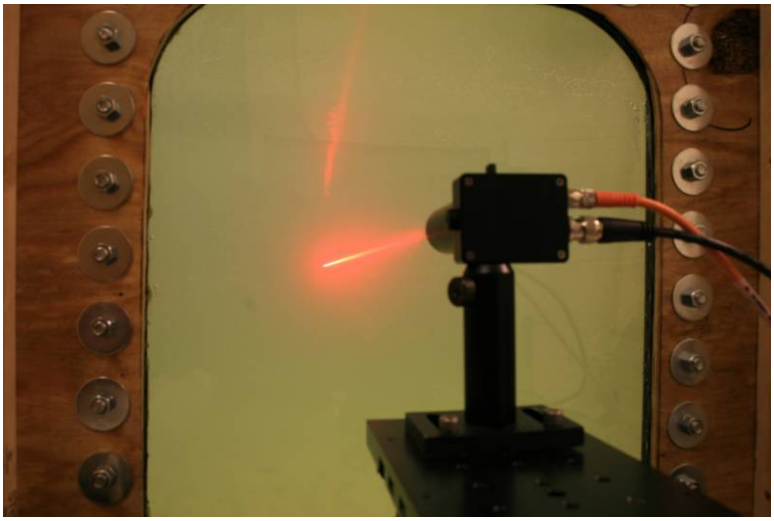

Figure 4-5 – Red laser from transmitter to receiver in turbid water. Room lights on.

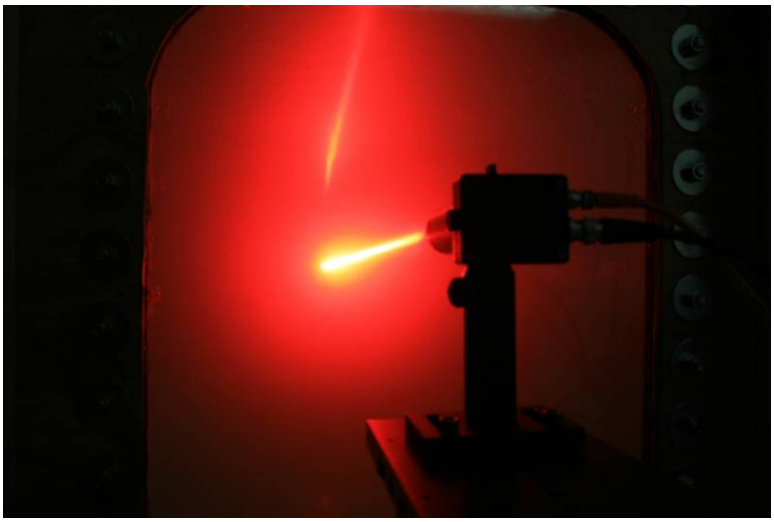

Figure 4-6 – Red laser propagating through turbid water. Room lights off.

A set of data was collected using thirty-four data points, where the amount of Maalox in the tank was varied. For each concentration of Maalox, a transmission was recorded while the tank was calm, and while the pump was circulating the water and particulate. Figure 4-7 shows a plot of average waveform intensities over these thirty-four sets. The received intensity drops off exponentially.

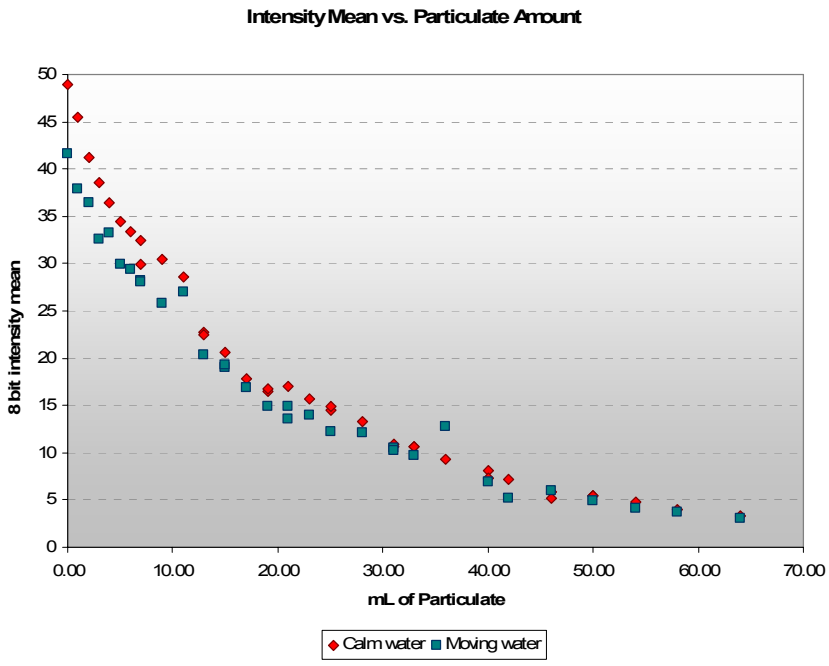

Figure 4-7 – Average intensity of received signal vs. particulate amount and moving vs. calm water

An eye diagram of the received signal can also be generated using Labview™. Figure 4-8 and Figure 4-9 show an eye diagram of the signal shown in Figure 4-4. Even with the severe signal quantization, there is a well defined "eye".

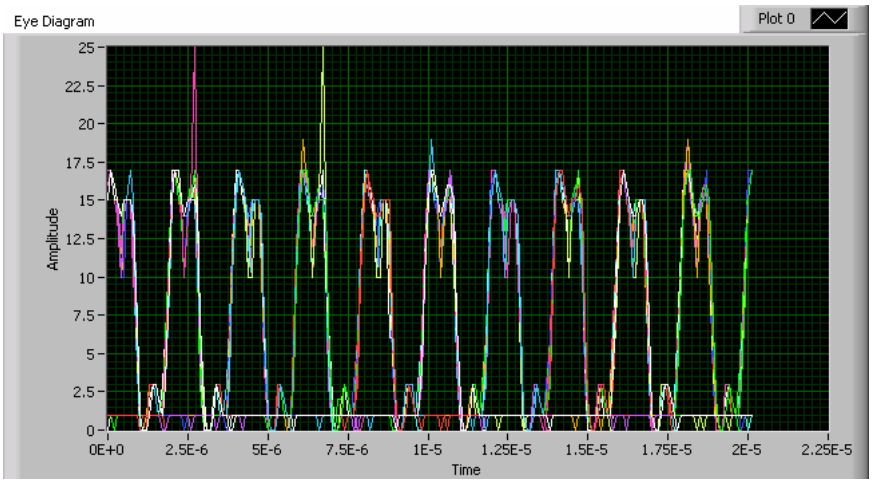

Figure 4-8 – An eye diagram of the received signal showing 10 bits positions, average over 1000 bits. Return-to-zero coding results in the lack of a well-defined "eye".

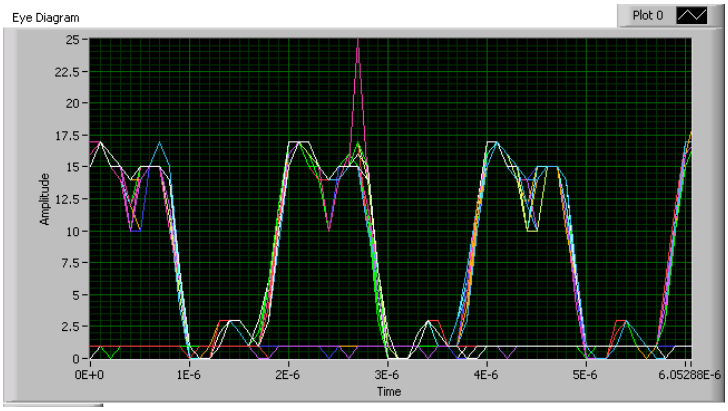

Figure 4-9 – Eye diagram showing 3 bit positions averaged over 1000 bits.

A FFT (Fast Fourier Transform) was taken of the transmission to show the signal strength vs. the noise strength. Comparing Figure 4-10, which is an FFT taken of a data transmission through clear water using the red laser, to Figure 4-11, which is an FFT of the data shown in Figure 4-4, it is clear that the increased quantization error of the signal increases the noise floor at higher frequencies.

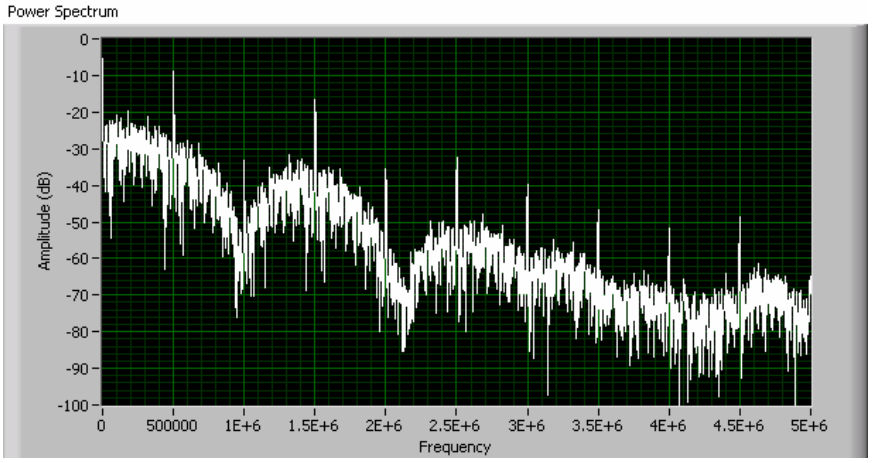

Figure 4-10 – FFT of high SNR (lower particulate) transmission. Amplitude is in dB.

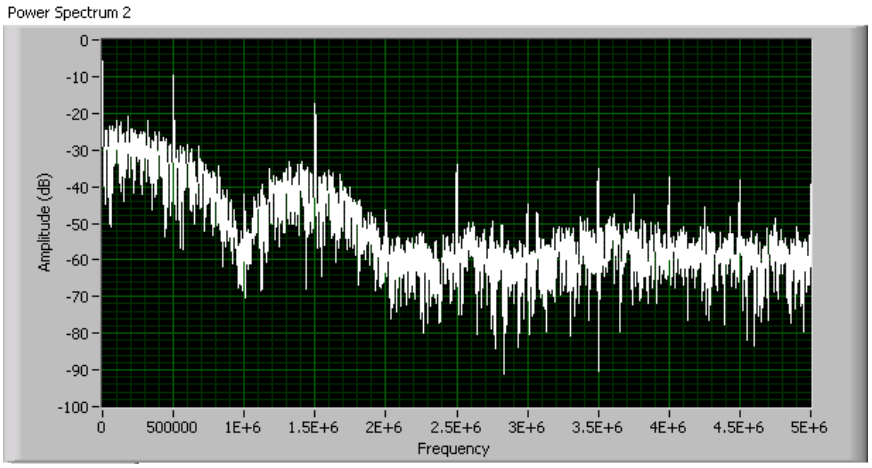

Figure 4-11 – FFT of lower SNR (more particulate) transmission.

Amplified Detector Signal

In order to overcome the 3.9mV quantization limit that the Flashy-D ADC imposed, a new ADC and an AD8369 VGA (Variable Gain Amplifier) were used to create a receiver amplifier and digital sampler board. This work was done by Jim Simpson. The new VGA setup allows for signal amplification up to 40 dB, which brings a 100-fold increase in the minimum observable voltage level.

The downside to this configuration is that it requires that the detector signal be A/C coupled to the VGA. This produces a DC-wander in the sampled waveform. Further work will investigate correcting this, or reducing it to lower levels.

Using PDA100A detector hooked to the VGA board, and sampled at 20Msamples/sec using an 8 bit AD9283 ADC, several transmissions were conducted using various transmitter powers. The transmitter power was adjusted by rotating a linear polarizer in front of the beam. This method provides a simple predictable way of adjusting the transmission power through the tank.

Figure 4-12 through Figure 4-19 show the exponential signal loss, and amplification with the VGA. Each Figure shows an increase of 3dB in amplification.

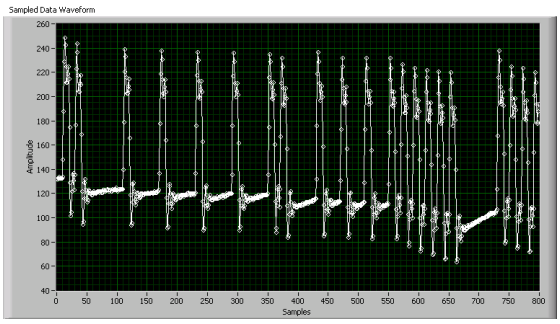

Figure 4-12 – No polarizer. Gain of 5dB

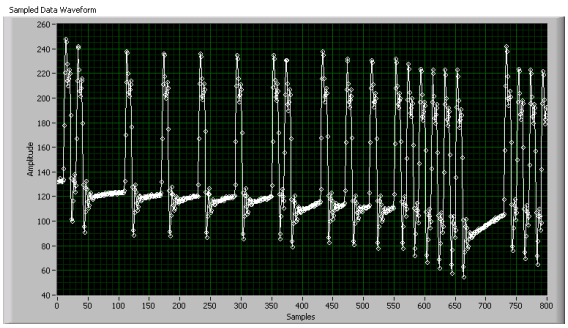

Figure 4-13 – Polarizer at 180º. Gain of 8dB

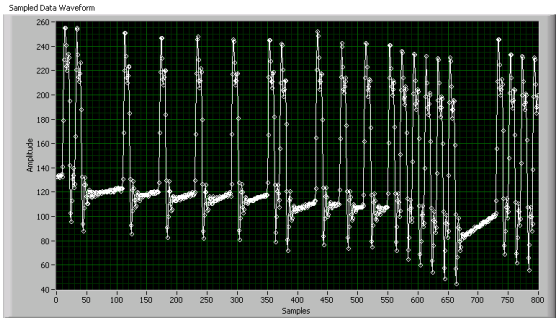

Figure 4-14 - Polarizer at 160º. Gain of 11dB

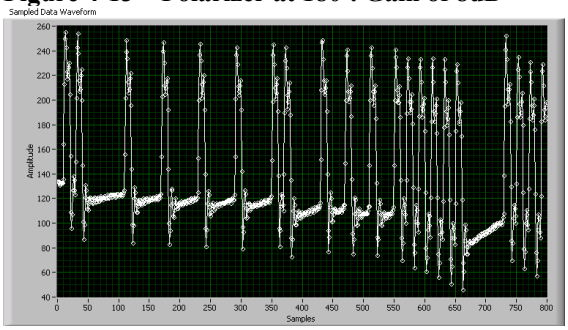

Figure 4-15 - Polarizer at 140º. Gain of 14dB

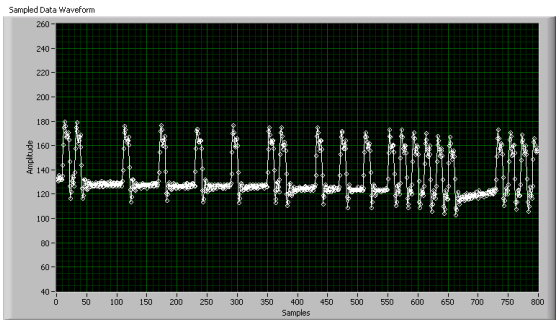

Figure 4-16 - Polarizer at 120º. Gain of 17dB

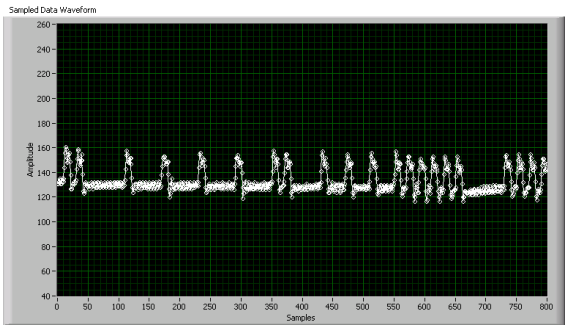

Figure 4-17 - Polarizer at 110º. Gain of 20dB

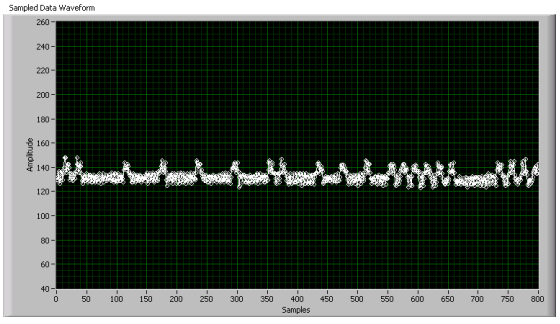

Figure 4-18 - Polarizer at 100º. Gain of 23dB

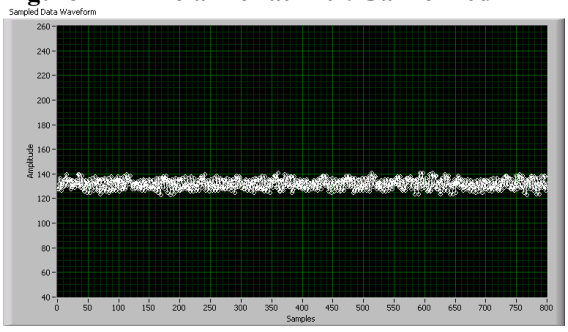

Figure 4-19 - Polarizer at 90º. Gain of 26dB

Figure 4-20 through Figure 4-22 show eye diagrams for the last two images shown above. It is clear from Figure 4-22 that signal processing or analog filtering is required to differentiate the bits.

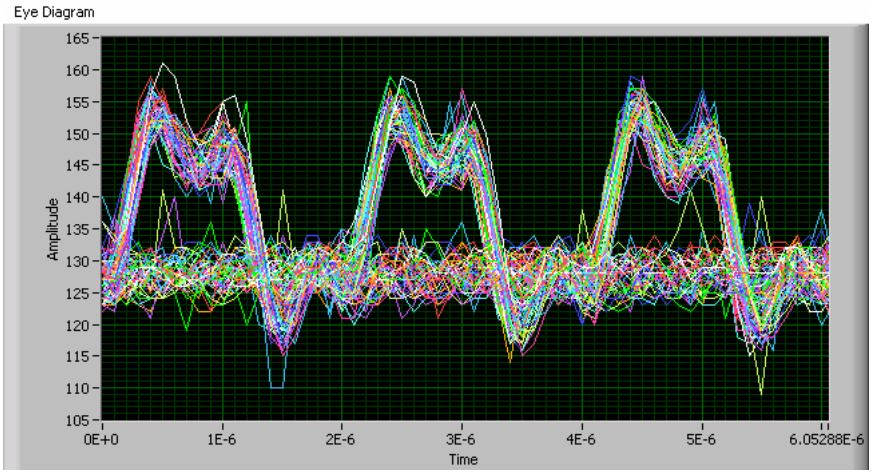

Figure 4-20 - Eye diagram of data shown in Figure 4-17. 3 bit periods shown. Average of 1000 transmitted bits.

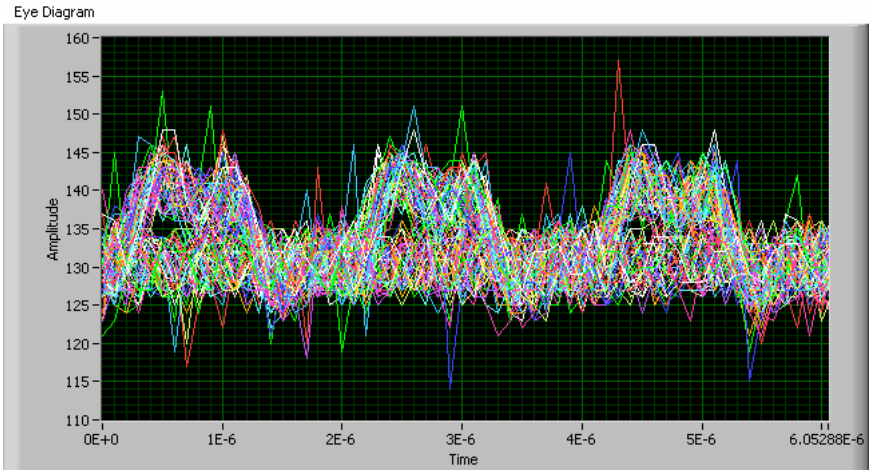

Figure 4-21 – Eye diagram of data shown in Figure 4-18. 3 bit periods shown. Average of 1000 transmitted bits.

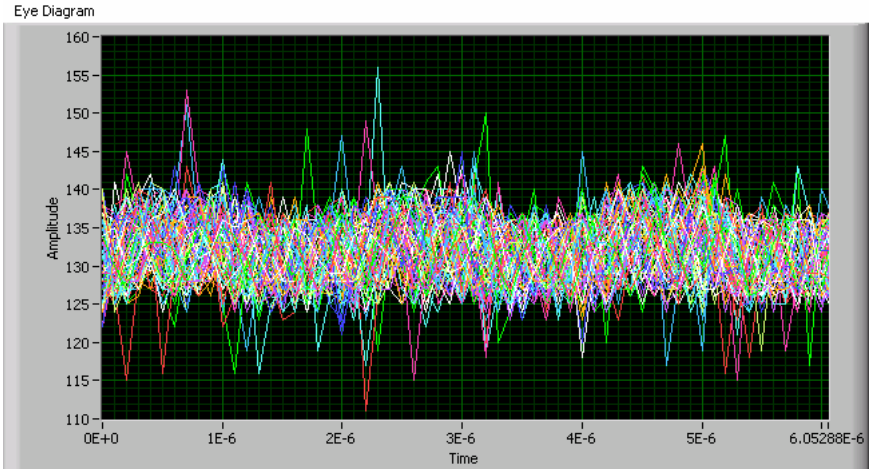

Figure 4-22 – Eye diagram of data shown in Figure 4-19. 3 bit periods shown. Average of 1000 transmitted bits.

Experiments Using Hamamatsu S5973-2 Photodiode Receiver and Red Laser

In addition to the PDA100A, a receiver board designed by Jim Simpson was used to receive a signal from the red laser diode. The board uses the Hamamatsu S5973-2 photodiode, an AD8015 transimpedance amplifier, and the VGA mentioned above to receive and amplify the signal. This was sampled in the same manner as the data in the previous two sections. Other data received using this receiver is shown in the subsequent section.

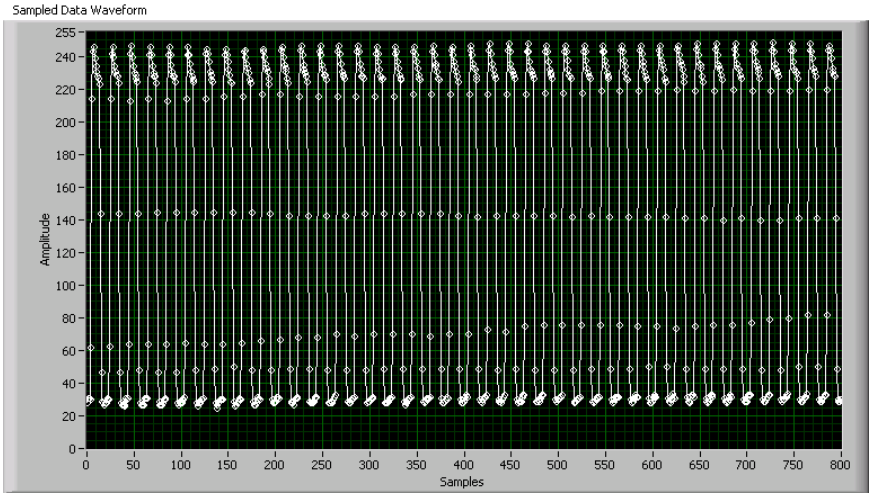

Figure 4-23 – Sampled waveform of red laser diode transmitter sending constant 1's in RZ format. The VGA is amplifying this signal with a gain of 8dB.

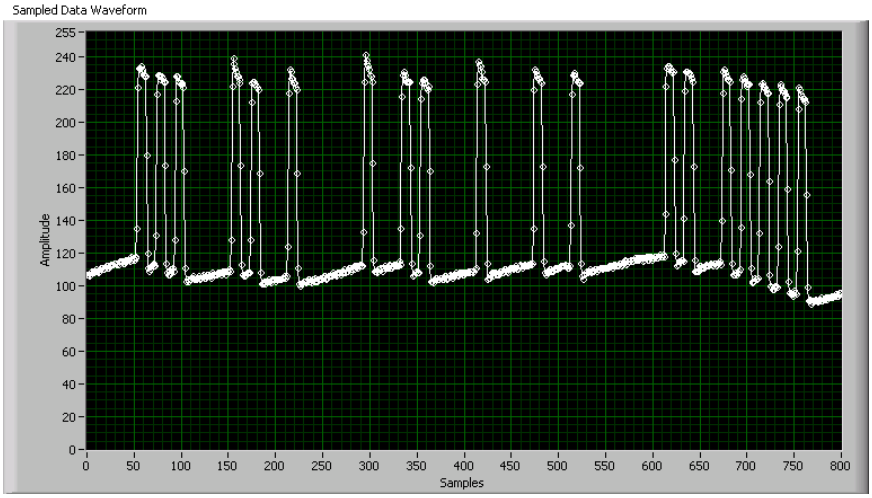

Figure 4-24 – Actual transmitted data from red laser diode, received by the S5973-2 photodiode receiver board. The VGA is amplifying the signal with a gain of 5dB.

Shown in Figure 4-24, the output from the photodiode preamplifier is AC coupled to the input of the VGA, which produces a noticeable DC-wander in the sampled waveform. The corresponding power spectrum to Figure 4-23 and Figure 4-24 is shown in Figure 4-25 and Figure 4-26, respectively.

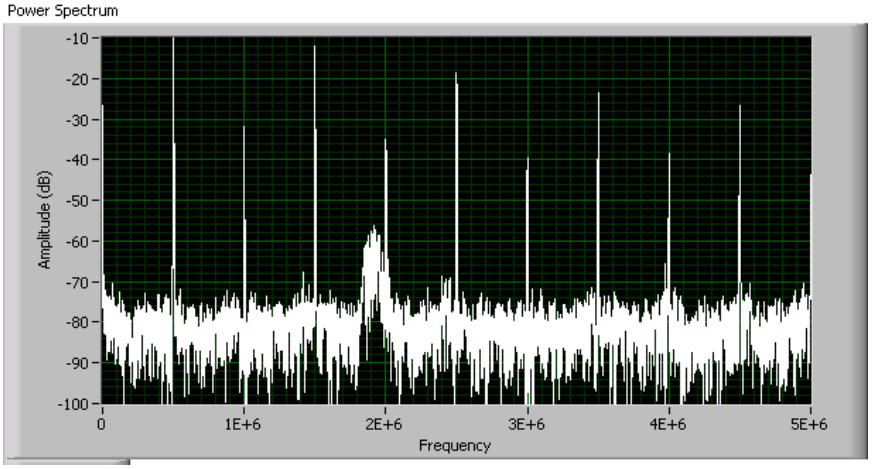

Figure 4-25 – Power spectrum of waveform shown in Figure 4-23. The red laser diode transmitter is sending a constant stream of 1's using RZ encoding, at 500kpbs.

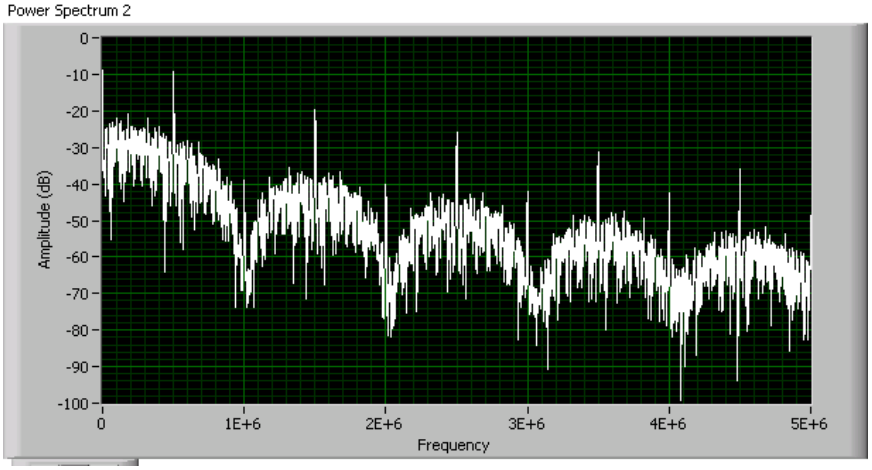

Figure 4-26 – Power spectrum of waveform shown in Figure 4-24. Thirty thousand bits sent via RZ encoding at 500kbps to the S5973-2 photodiode receiver board.

Results of Red Laser Transmission Experiments

The three types of experiments described above help to validate the work done in Chapters 2 and 3. The red (635nm) laser diode was successfully used to communicate in an underwater environment at speeds of 500kbps. This validated the use of a laser for communicating in an underwater environment. It also showed that the tank design discussed in Chapter 3 is adequate for allowing testing of optical communication through water. If non-return-to-zero encoding were used instead of return-to-zero, the effective transmission bandwidth would be doubled to 1Mbps.

Figure 4-2 and Figure 4-3 show 635nm laser light propagating through clear water. The visibility is greater than 12 feet and the beam is relatively well collimated. Figure 4-1 shows the received and sampled signal, which is well defined and free of noise. Figure 4-5 and Figure 4-6 show the same laser beam propagating through water with 16ppm of scattering particulate. This amount of particulate may be roughly equivalent to some coastal waters. The laser beam in these figures is clearly much more scattered, but there is still a well defined beam and spot at the end of the tank and on the detector. The visibility in these figures is clearly less than 12 feet, as the opposite end of the water tank is not visible. The exponential falloff of light intensity vs. concentration of particulate matter is plotted in Figure 4-7. In that experiment, the output from the photodetector was not amplified and sampled signal intensity was ultimately limited by the quantization error in the ADC – or approximately 3.9mV. Even in this example, where the laser is scattered due to the particulate, the eye diagram of the received signal, shown in Figure 4-9, is very well defined. Initial BER calculations for all the data in the plot shown in Figure 4-7 show little, if any, bits in error. These numbers were not included due to the need to perform further testing to assure the software is performing correctly.

The experiments for the amplified detector signal further demonstrate the feasibility of using the work done Chapter 2, and by other members of our lab, for underwater optical communication. By amplifying the signal from the detector using a variable gain amplifier, the lower limit of detectable signal is drastically reduced, perhaps by as much as 30dB. While this number is ultimately limited by the noise characteristics of the detector and VGA, it is clear that effective transmission can be tested for lengths much greater than 12 feet, or for larger amounts of particulate. Using a different wavelength of transmission, like 405nm, will also allow for longer transmission lengths due to the smaller attenuation that the signal receives as it propagates through the water.

Finally, experiments using the S5973 photodiode receiver board further show examples of using laser communication in an underwater environment. The higher blue/green sensitivity of the S5973-2 photodiode allows for more effective detection of light signals.

Blue Laser Communication Through Water

Experiment

A communication test was conducted using the 405nm blue laser diode driver and the Thorlabs PDA100A photodetector. The PDA100A has a weak response, around 0.11 A/W, for 405nm light, so the experiment was conducted using clear water only.

Thirty thousand randomly generated bits, with an equal probability of a "0" or a "1", were transmitted at 500kbps in return-to-zero format. Figure 4-27 shows an output capture from an oscilloscope hooked to the output of the PDA100A photodetector. The 21 mV_{pp} signal is clearly visible, with little noise. The ringing on the rising and falling edge of the signals is due to the limited bandwidth of the detector and overshoot on the laser diode (see figure in Chapter 3).

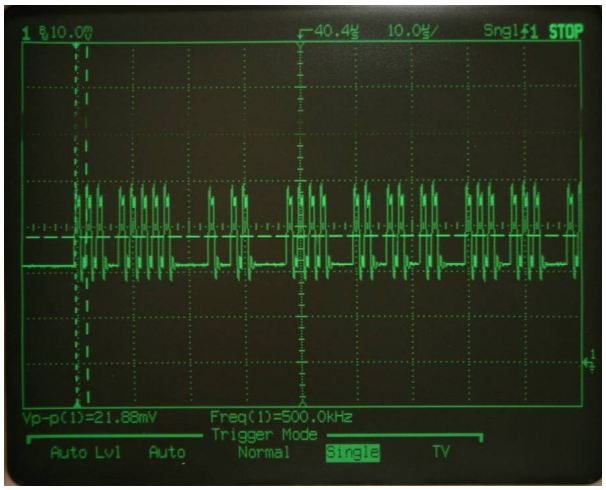

Figure 4-27 – Transmission from 405nm blue laser diode driver board to PDA100A photodetector

The 405nm laser diode driver and transmitter were also tested using a photodiode receiver and preamp. This was designed by Jim Simpson. The photodiode, the Hamamatsu S5973-2, has much larger response to the blue green wavelengths than the PDA100A, with 405nm response of approximately 0.3 A/W. The output from the photodiode preamp was then fed into the VGA mentioned previously and sampled at 20Msamples/sec using an 8 bit AD9283 ADC. This data was then transferred to a PC for post-processing.

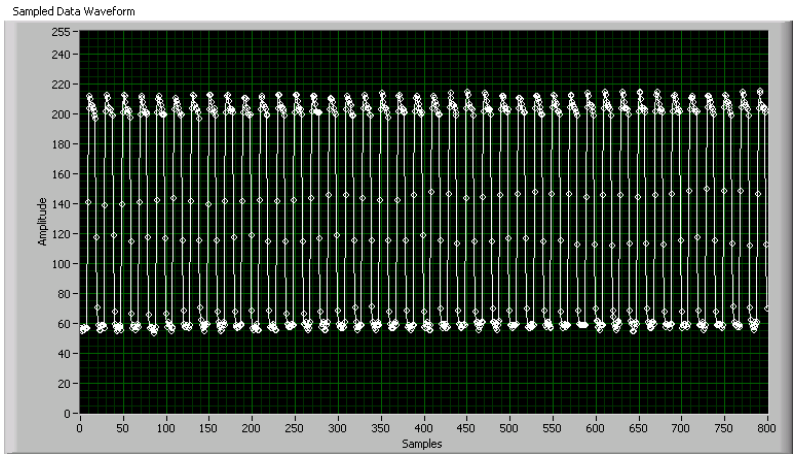

Figure 4-28 – Constant stream of 1's sent via RZ encoding from the 405nm laser diode drive board. The signal is received using a Hamamatsu S5973-2 photodiode and an AD8015 transimpedance amplifier. The resulting signal was amplified using the AD8369 variable gain amplifier with a gain of approximately 11dB.

A FFT was taken of the waveform shown in Figure 4-28. This is shown in Figure 4-29. There is a strong peak of noise at 1.9MHz from unknown origin. The SNR for frequencies below 1.5MHz is around 60dB.

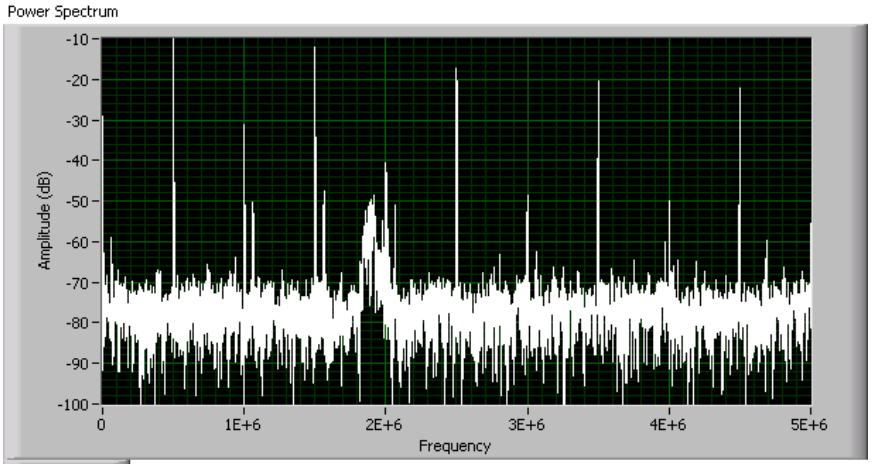

Figure 4-29 – Frequency spectrum of a 500kbps RZ transmitter. Waveform in time is shown in Figure 4-28

Using the same setup as described above, actual data was transmitted via the 405nm laser diode driver and transmitter to the S5973-2 photodiode receiver board. The partial setup for this transmission is show in Figure 4-30 and Figure 4-31.

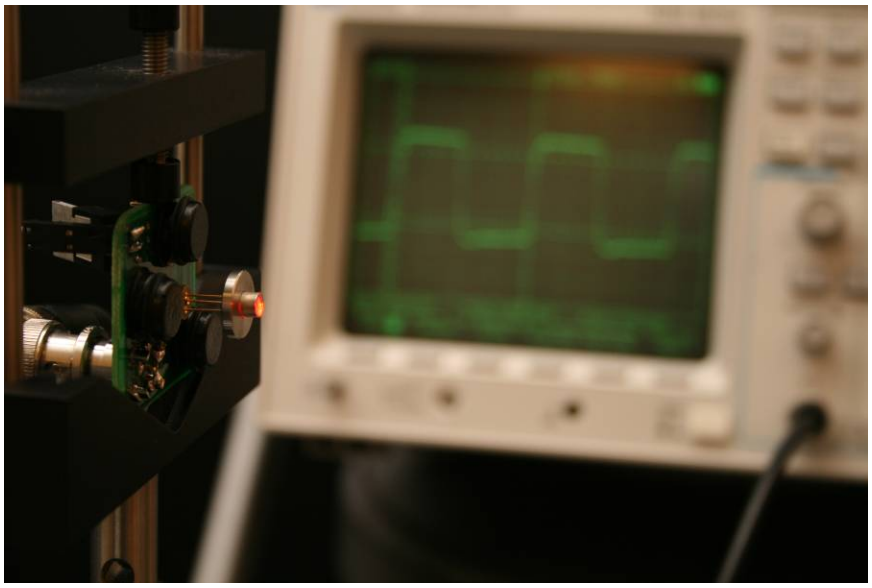

Figure 4-30 – Photo showing setup for receiving a transmission from the 405nm blue laser. Pictured is the receiver board receiving light from a red laser.

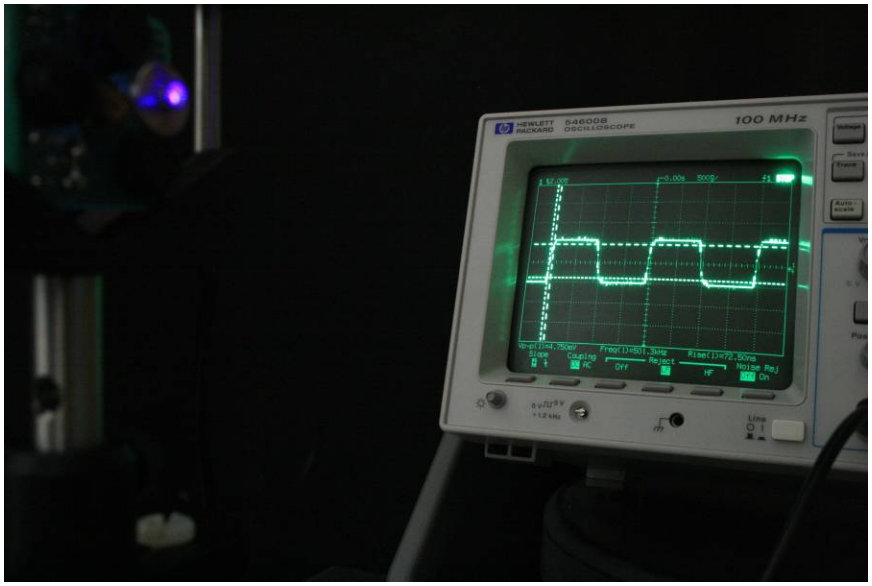

Figure 4-31 – Photo showing photodiode receiver at left, with 405nm laser focused on it, and the received waveform at right. In this image, the receiver board does not have any focusing optics.

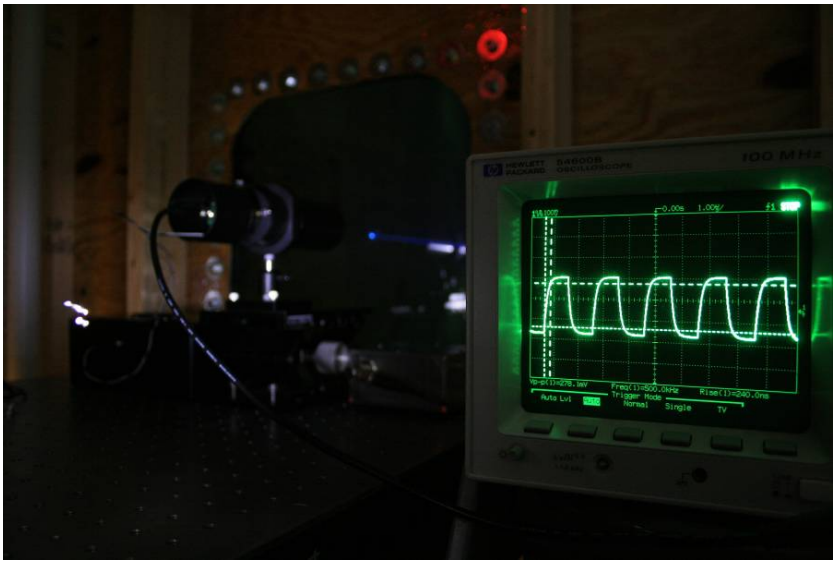

Figure 4-32 – Photo showing photodiode receiver board with focusing optics, receiving data from a 405nm blue laser diode. The laser light can be seen passing through the water in the tank, into the receiver. The waveform on the oscilloscope has a slower response than in Figure 4-31, because the signal was not terminated with a 50Ω impedance.

A FFT of the incoming signal, which is partially shown in Figure 4-33, produces the spectral plot shown in Figure 4-34. An eye diagram of the received signal is shown in Figure 4-35. It is clear from this image that the DC-wander of the signal, which is caused by AC coupling the receiver to the VGA, causes the "eye" to decrease in size.

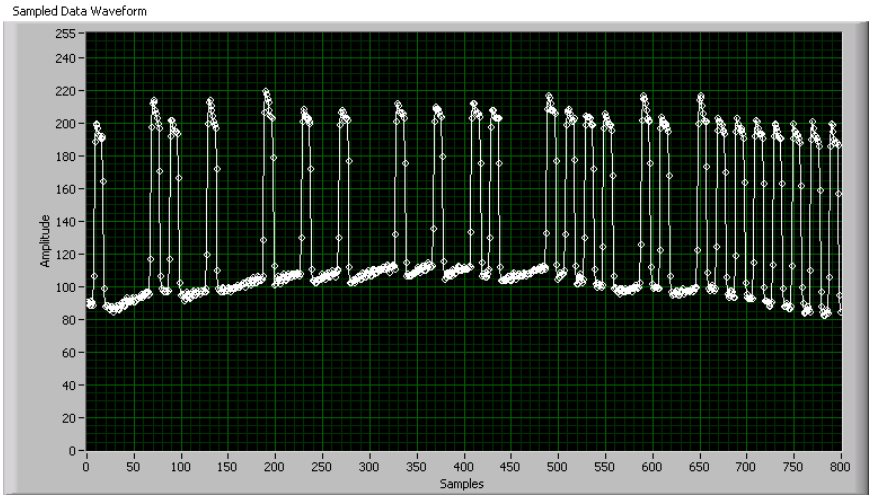

Figure 4-33 – Partial image of sampled waveform. The signal is received using a Hamamatsu S5973-2 photodiode and an AD8015 transimpedance amplifier. The resulting signal was amplified using the AD8369 variable gain amplifier with a gain of approximately 8dB. There is a noticeable DC-wander on the signal, which is caused by A/C coupling the signal.

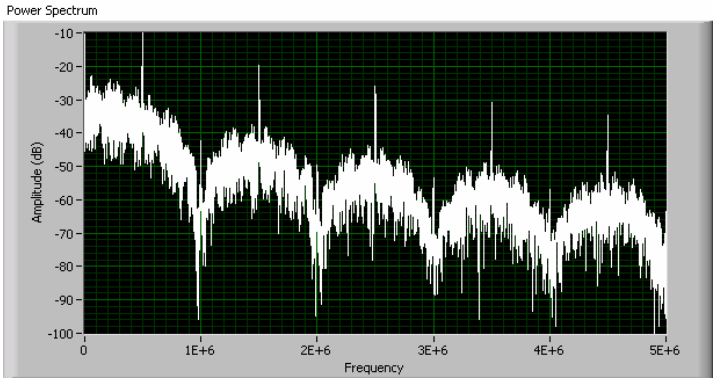

Figure 4-34 – Frequency spectrum of transmission between 405nm laser diode and S5973-2 photodiode receiver.

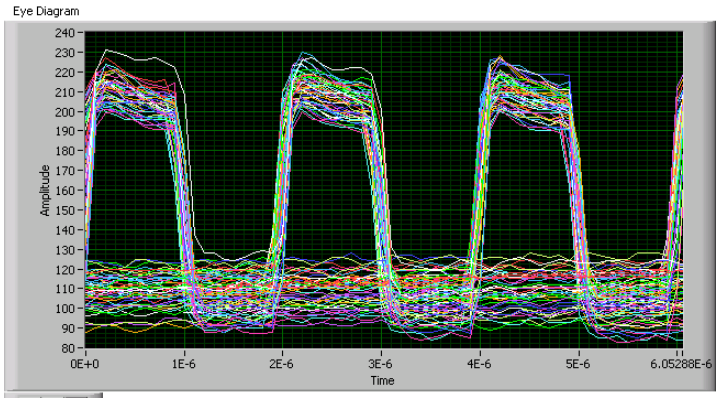

Figure 4-35 – Eye diagram of signal transmitted using 405nm blue laser diode to S5973-2 photodiode receiver.

Results of Blue Laser Transmission Experiments

The experiments in the section above were used to validate the design of the 405nm blue laser diode driver board, and feasibility of using this design to transmit optical communication signals in an underwater environment.

Due to the cost of the diodes, a low output power was used with the diodes in order to prevent any damage. The 405nm laser diode driver board has circuitry for optical feedback to control the diode power, but that feature has yet to be implemented. Instead, the diode was mounted to a heat sink and was driven at a low power. Because of this, initial experiments were conducted in clear water. Further experimentation will involve increasing the output power and adding particulate to the water to get a better picture of scattering and attenuation.

PMT Receiver Test Through Water

Transmission Experiment Before Adding Low Pass Filter to Output

Preliminary testing of the PMT involved using the red laser diode transmitter. The reason for this was due to the extremely high gain and responsivity that the PMT has to 405nm light. In the clear water of the tank the signal would have easily saturated. Therefore, red light was used in order to get a better understanding of the performance of the system. Further testing will involve 405nm blue light.

The experimental setup is shown in Figure 4-36 and Figure 4-37. An adjustable power supply is used to adjust the bias voltage, and thereby the gain, of the PMT. For the experiment, a 1" plano-convex lens was mounted in front of the PMT to collect more light. To decrease the chance of accidentally damaging the PMT, a polarizer was used in front of the laser diode to further reduce the amount of light entering the tank. For comparison, the same amount of light was used in this experiment as in the experiment results shown in Figure 4-19.

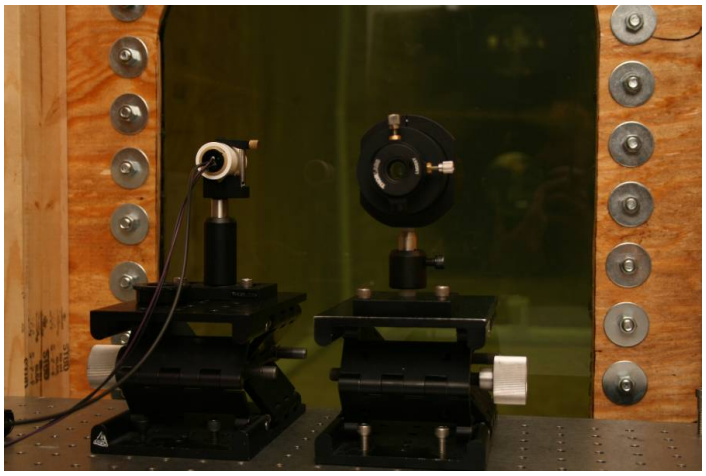

Figure 4-36 – The PMT holder is shown on the left. The PMT socket is isolated from the metal of the optical assembly by a rubber ring and a PVC aperture.

Figure 4-37 – Setup showing PMT and receiver. The metal box in the foreground contains the AD8015 transimpedance amplifier for the PMT's output.

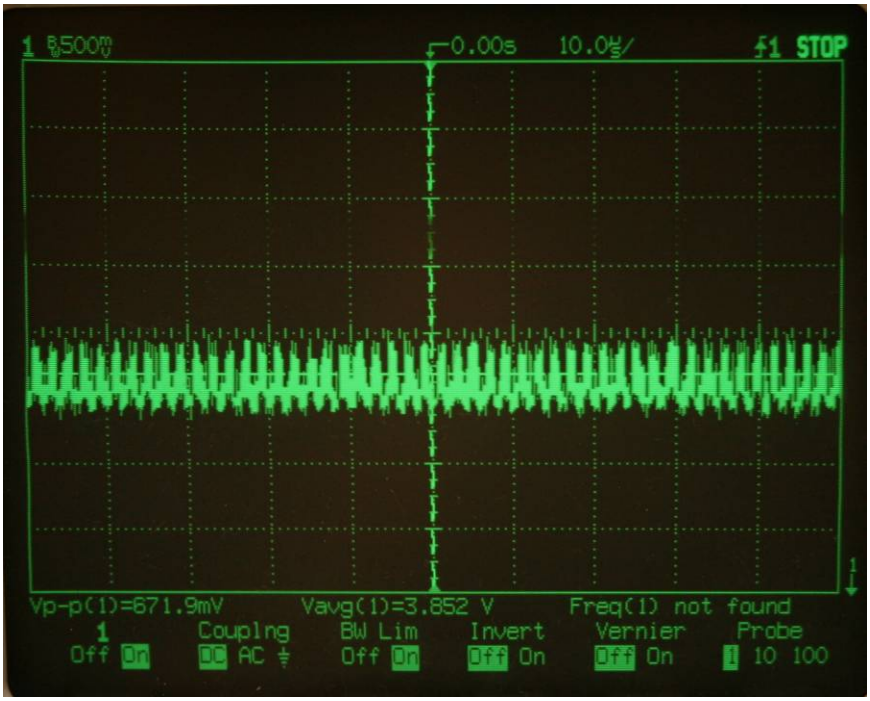

Figure 4-38 – Received signal from red laser diode using PMT. Red transmitter is sending a constant stream of 1's in RZ format at 500kbps. PMT bias voltage set at -400v.

A set of data matching the data in Figure 4-38 was transmitted using the red laser and received using the PMT. The PMT was set at a bias voltage of -275v. A 1" plano-convex lens was placed in front of the PMT to collect more light. The output from the AD8015 transimpedance amplifier was amplified by the VGA with a gain of 14dB. The sampled waveform is shown in Figure 4-39.

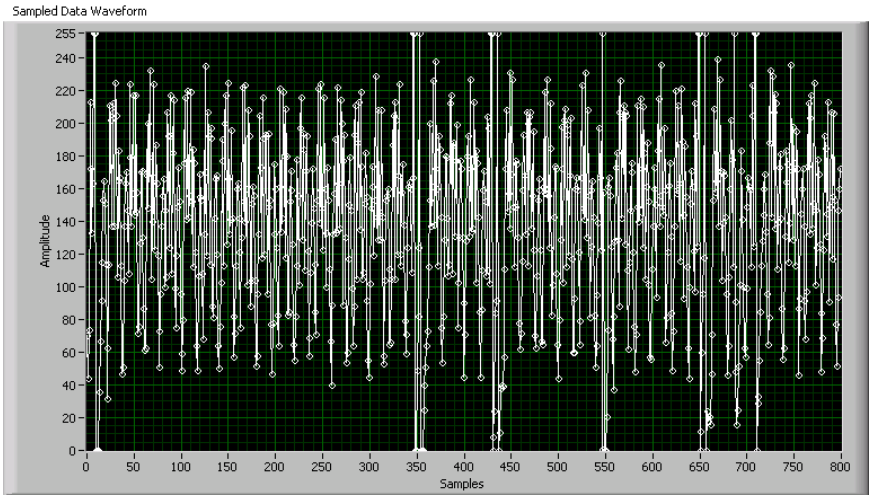

Figure 4-39 – Waveform showing section of received signal from PMT. Bias voltage is -275v. VGA gain set to 14dB.

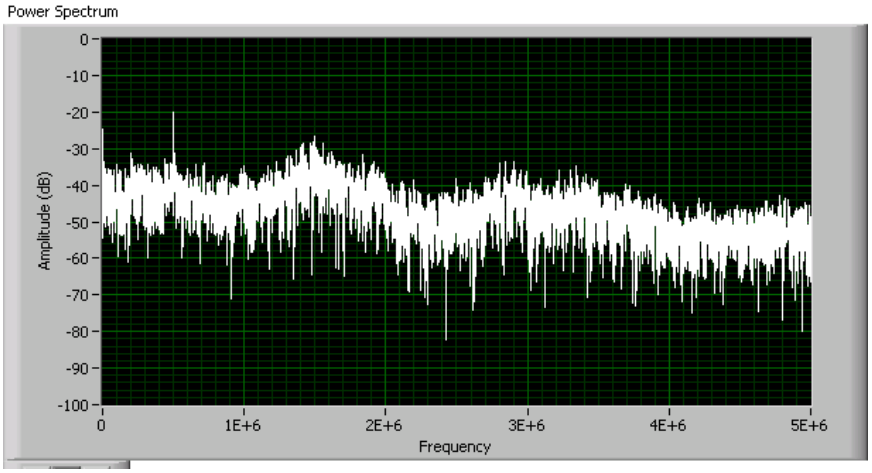

Figure 4-40 – The power spectrum for the data shown in Figure 4-39

Using the same setup, 30k bits were transmitted and received by the PMT. The output signal was amplified by the VGA with a gain of 14dB. The sampled signal is shown in Figure 4-41, and the corresponding power spectrum is shown in Figure 4-42.

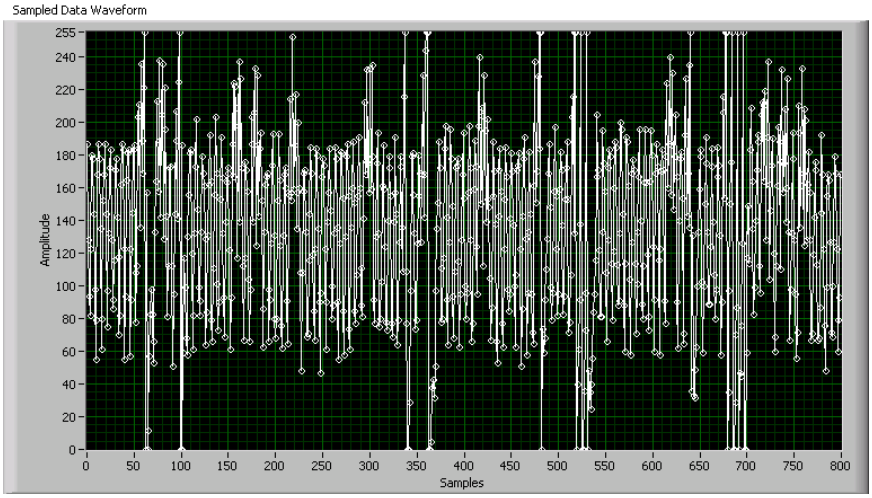

Figure 4-41 – Sampled output of PMT receiving data from red laser transmitter. Data is sampled at 20Msamples/second.

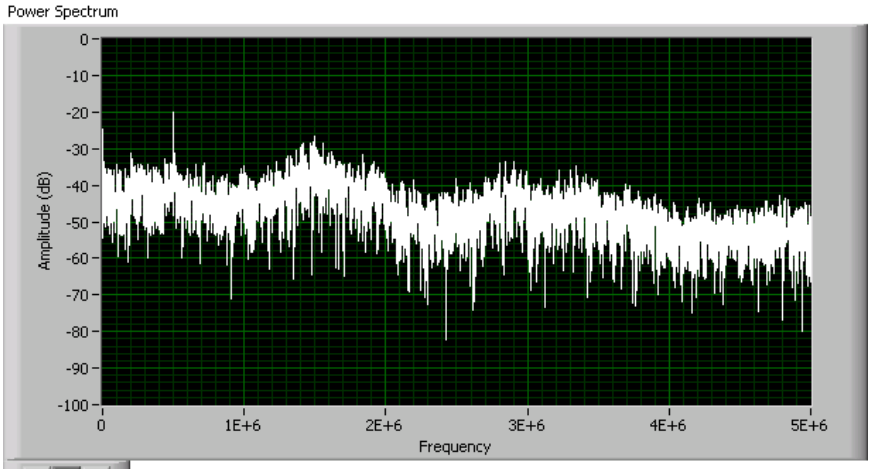

Figure 4-42 – Power spectrum of received signal shown in Figure 4-41

Transmission Experiment After Adding Low Pass Filter to Output

When viewing the output signal on an oscilloscope, there was a significant amount of 13MHz and 90MHz noise on the output signal. Both of these frequencies are not visible on the power spectrum due to the limitations of calculating the FFT. In order to reduce this noise, a 3MHz low-pass-filter (LPF) was added to the output of the AD8015 transimpedance amplifier, before being amplified by the VGA. Compare **Figure 4-38** to **Figure 4-43**. The noise is significantly reduced, but the rise and fall times have been increased.

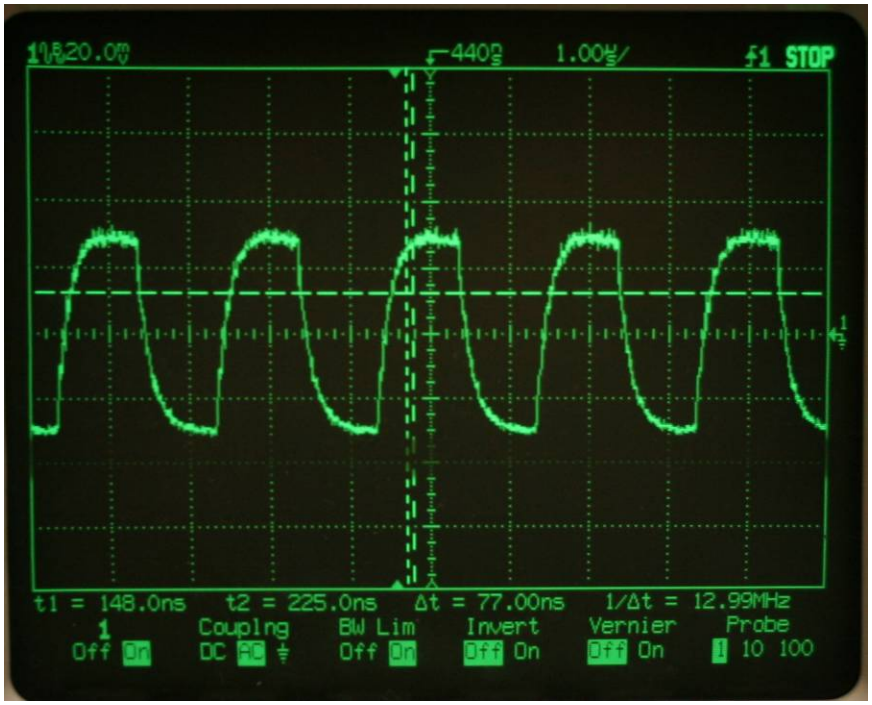

Figure 4-43 – Received waveform from red laser after addition of 3MHz LPF. PMT bias voltage is -275v

The sampled waveform for Figure 4-43 is shown in Figure 4-44. This is compared to the sampled data in Figure 4-39. The power spectrum for the signal after the 3MHz LPF is shown in Figure 4-45. When comparing Figure 4-45 to Figure 4-40, the overall noise floor has dropped, but a noise spike at 1.9MHz has appeared.

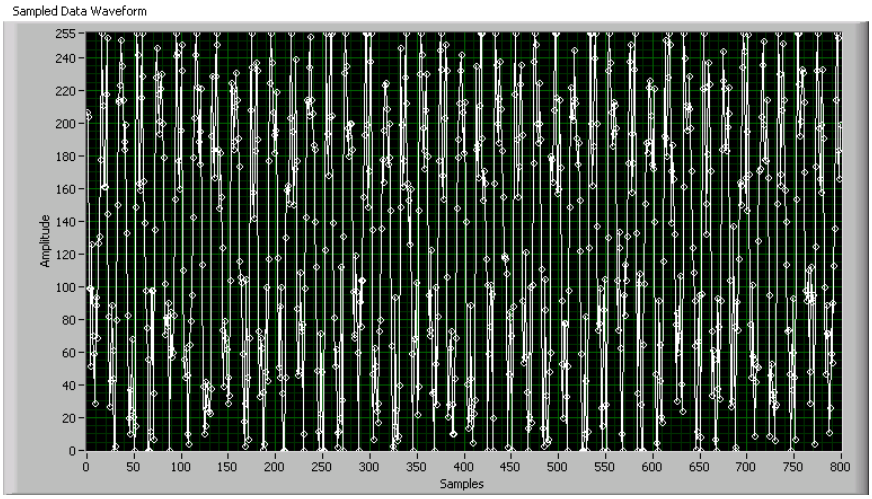

Figure 4-44 – Sampled waveform after addition of 3MHz LPF to output of transimpedance amplifier

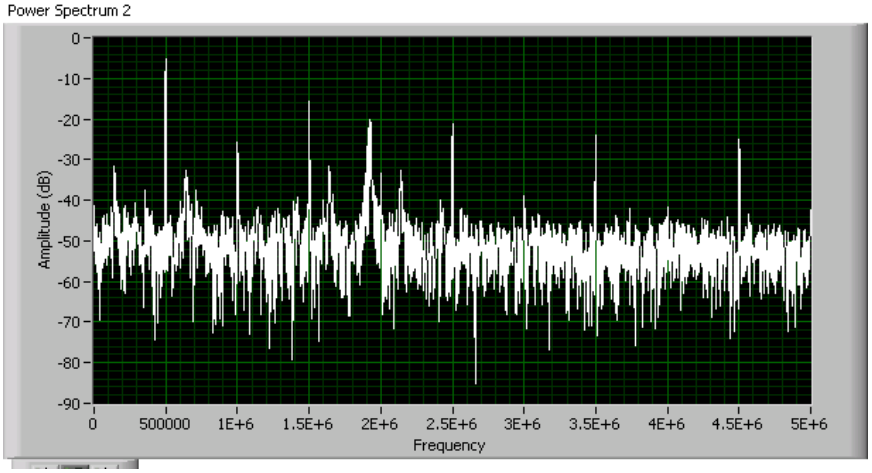

Figure 4-45 – Power spectrum of sampled data shown partially in Figure 4-44

A set of thirty-thousand bits was also transmitted using the red laser transmitter and received using the PMT. An excerpt from the received waveform is shown in Figure 4-46. The corresponding power spectrum is shown in Figure 4-47. Comparing Figure 4-42 to Figure 4-47 shows a significant drop in noise, especially above 1MHz.

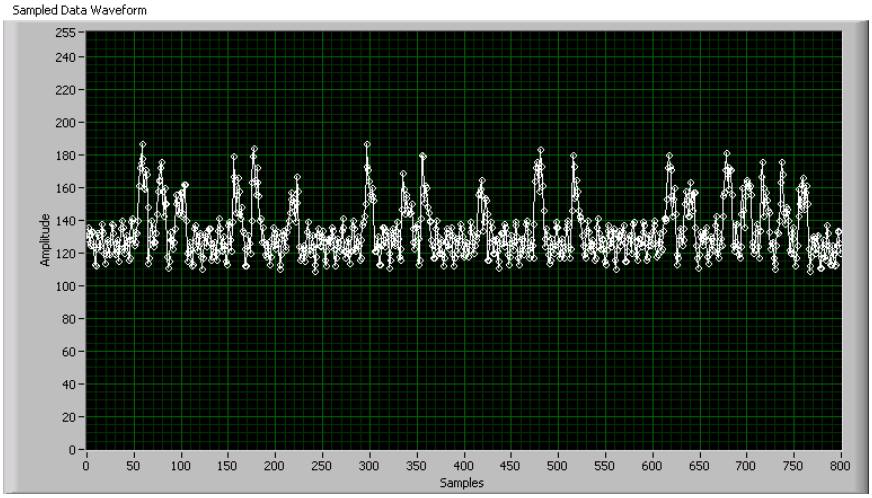

Figure 4-46 – Sampled transmission waveform from red laser transmitter. PMT gain is -275v. VGA gain is 14dB.

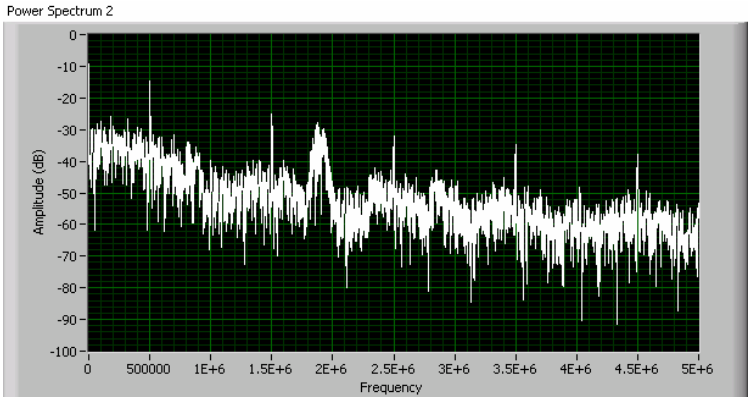

Figure 4-47 – Power spectrum of received data from red laser transmitter through PMT. Transimpedance amplifier has a 3MHz LPF on output. VGA gain is 14dB.

Results of PMT Receiver Experiments

The experiments in the section above validate the design of a photomultiplier tube based receiver for optical communication. A PMT based receiver is extremely useful for observing very low levels of light, and is applicable to long distance communication or communication in very turbid medium.

Figure 4-38 shows a signal received on the PMT. The rise and fall times on the signal are adequate for increasing transmission speeds by at least ten times. A downside to the receiver, shown in Figure 4-40 is a large amount of noise, and a SNR of approximately 10dB. Compared with power spectrum plots from several photodiode receivers, it's clear that further work will need to be done in order to improve the noise filtering of the receiver. Improved electrical enclosures and signal filtering should be explored.

A simple fix for increasing the SNR of the output signal was to include a 3MHz LPF on the output of the transimpedance amplifier. Doing so limits the available detection bandwidth, shown in Figure 4-43, but reduces the total amount of system noise (compare Figure 4-43 to Figure 4-40).

Further experimentation using different transmission wavelengths will give a better picture of the performance of the PMT based receiver system. For the experiments above, a 635nm laser was used due to convenience and concern over damaging the PMT with too large a signal, but large improvements in system responsivity should be gained from a move to a blue/green transmission source.

5. Conclusion

Reliable communication methods for underwater systems are needed to further expand the field of ocean exploration and defense. Current methods, such as acoustic communication, are limited in bandwidth, and the use of cables, such as fiber optic, are not applicable to autonomous vehicles. Tethered communication systems are also very costly to repair if damaged. The field of underwater optical communication systems is a largely unexplored topic of research and offer promising advantages over current methods of aquatic communication.

Applications benefiting from a reliable, high bandwidth, communication systems underwater would include:

- Underwater observatories
- Underwater vehicle to surface ship links
- UAV to moored or floating buoys equipped with RF links.
- AUV to AUV communications
- Diver to diver or diver to ship communications.

A freespace optical communication link is especially beneficial to mobile platforms, like AUVs and divers. However, these applications are also constrained by size, power, and weight restrictions. Because of this, one of the goals of this research was to consider a compact and low power system for underwater communication.

In addition, the goal of this Masters thesis was to build sufficient infrastructure to experimentally validate the performance of underwater optical communication systems under laboratory, but hopefully realistic, water conditions. This required three major objectives to be met:

1. Construction of optical transmitters and receivers
    a. Transmitter based on blue laser diodes.
    b. Receiver based on a photomultiplier tube.

2. Construction of a water tank where the water conditions can be appropriately controlled. e.g. changing the amount of scattering by addition of particulate.
3. Measurement of communications performance in a simulated aquatic environment.

The design and construction of these systems was discussed in Chapter 2, and experimental results were gathered in Chapter 4.

A laser transmitter using 405nm blue laser diode was created. The transmitter is capable of driving a blue laser diode as high as 400MHz, given adequate impedance matching and cabling, and is capable of supplying a 200mA drive current. Several transmitters could be used in parallel and driven from the same controller, to achieve higher output power. Initial testing showed the transmitter driving a blue laser diode at 10MHz, with rise and fall times of approximately 4 ns. This transmitter meets the goal of a blue laser diode based transmitter.

A photomultiplier tube (PMT) based receiver was also constructed to receive low light level transmissions in highly attenuating water conditions. The receiver uses an AD8015 transimpedance amplifier to convert the anode current of the PMT into a useful voltage signal. By adjusting the bias voltage across the PMT, a gain of up to $7x10^5$ can be achieved. Another benefit to the chosen PMT over a photodiode based device is its high photocathode gain at 405nm. This is in contrast to the much higher response of photodiodes to longer wavelengths. The PMT receiver was demonstrated receiving an optical transmission both in the blue and the red. The received signal from the red laser transmission was recorded and digitized. Power spectrum analysis of the signal showed a large amount noise on the signal. The addition of a low-pass-filter, close to the maximum transmission bandwidth, improved the noise performance. Additional work will need to be performed in order to increase the SNR and to validate the PMT receiver at higher datarates. This receiver meets the goal of creating a PMT based receiver circuit.

Finally, in order to experimentally test underwater optical communication systems, a water tank was constructed to provide a testing platform for this, and future, work. The tank is 12’ long and 4’ wide and can hold over 1,200 gallons of water. The water can be filtered and recirculated at 80 gallons-per-minute in order to simulate

various water conditions. Sight windows on either end of the tank allow for optical communication to take place through the full length of the tank. The experiments in Chapter 4 were performed using this tank.

Experiments were conducted in Chapter 4 to validate the various aspects of an underwater communication system. Using a red (635nm) laser diode transmitter, initial data was collected showing the attenuation of light underwater as the amount of particulate was increased. This showed, as expected, an exponential falloff in received power as the beam became more scattered. Data was transmitted using the 635nm laser and received using both a commercial photodetector and custom built detector. Differences in power spectrum were shown between the two, in addition to the use of a variable gain amplifier to further increase the signal strength. A simple method for decreasing the transmitted optical power was to place a linear polarizer in front of the laser beam. Even with the laser at a minimum transmission power (several μW), using the VGA to amplify the signal would provide a useable waveform with an SNR close to 10dB.

Data transmission using the 405nm blue laser diode drive board was also accomplished. The experiment involved transmitting thirty-thousand bits at 500kbps with return-to-zero encoding. The data was transmitted to both a commercial photo detector, and the output viewed on an oscilloscope, and to a photoreceiver which uses a Hamamatsu S5973-2 photodiode with enhanced blue/green response. The sampled waveform was clear and well above the noise floor. A power spectrum plot showed an approximate SNR of over 20dB.

Finally, the PMT receiver was used to receive a data transmission of thirty thousand bits at 500kpbs with return-to-zero formatting. The transmitting source was a 635nm red laser diode, which was used in order to prevent any accidental damage to the PMT, due to its greatly reduced responsivity to red light over blue. Even at this lowered responsivity, the PMT was able to receive the signal, and a power spectrum plot of the sampled waveform shows a SNR of approximately 15 dB, given appropriate filtering on the output of the transimpedance amplifier.

Overall, both transmission and reception of optical signals appropriate for underwater environments was demonstrated. Initial testing demonstrated a reliable channel at 500kpbs, with no expected difficulty in increasing that number from 1MHz to 10MHz. The feasibility of using a PMT as a receiver was demonstrated, along with the feasibility of using a 405nm laser source as a transmitter.

Further work will focus on increasing the transmitted power from the 405nm laser, along with increasing the transmitter bandwidth to slow Ethernet speeds. Data will be collected on various water conditions and their affect on the bit-error-rate of the data and received optical power. Work on the receiver will focus on creating an optical assembly to focus and filter the incoming light as to make the PMT receive more immune to ambient light. Additionally, work will be done to improve the noise characteristics of the PMT receiver to increase the signal-to-noise ratio.

While the use of standard underwater communication systems, like acoustic communications, may persist, the field of underwater optical communications will continue to grow. The benefits of this type of communication – high bandwidth, reliable, and mobile links – are not met by any one other method. Future systems for aquatic optical communications will enable new work and discoveries in our planet's oceans.

Appendices

Water Tank

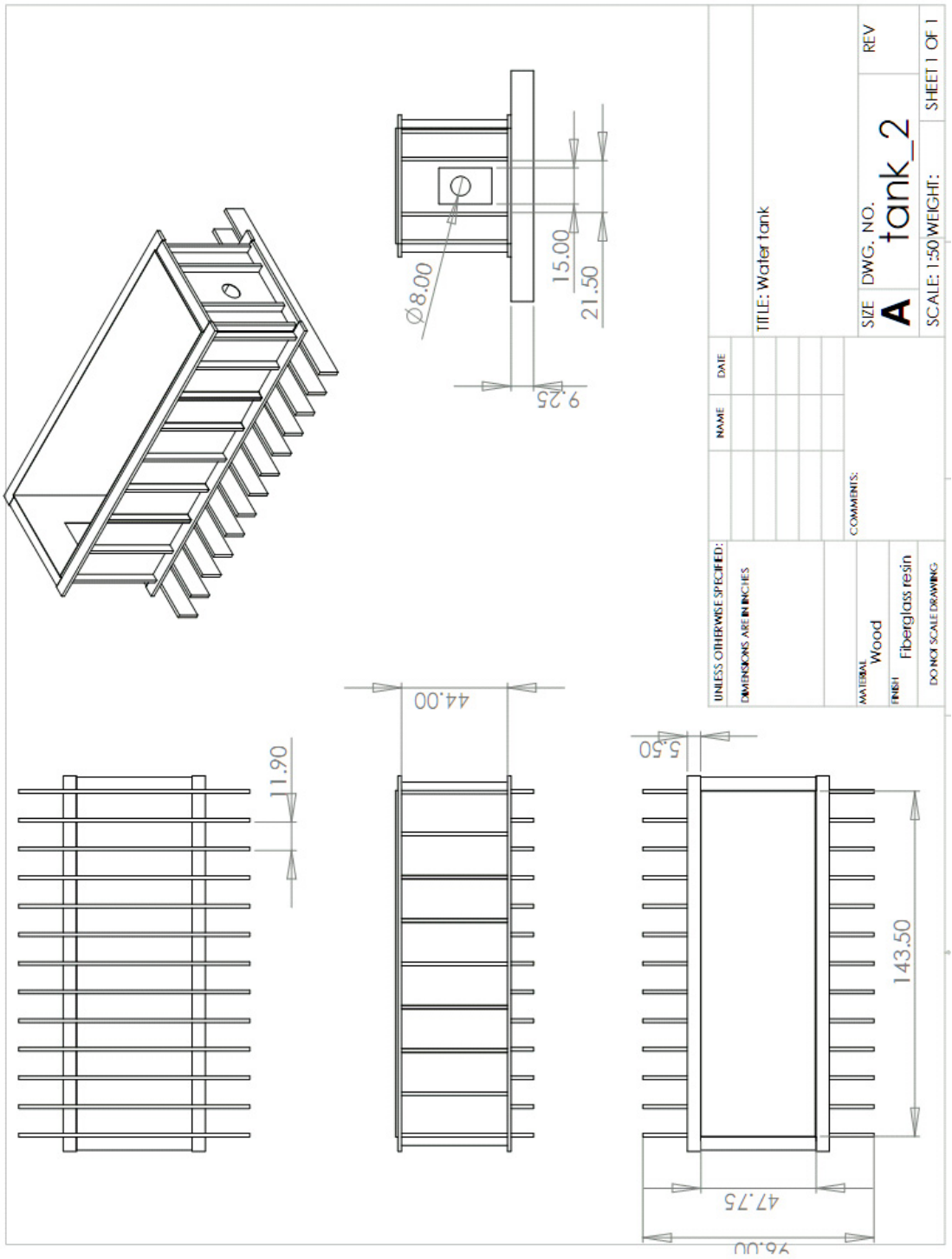
Ø8.00
15.00
21.50
9.25
44.00
11.90
5.50
143.50
47.75
96.00
TITLE: Water tank
SIZE A
DWG. NO. tank_2
REV
SCALE: 1:50 WEIGHT:
SHEET 1 OF 1
UNLESS OTHERWISE SPECIFIED:
DIMENSIONS ARE IN INCHES
NAME
DATE
COMMENTS:
MATERIAL Wood
FINISH Fiberglass resin
DO NOT SCALE DRAWING

Laser Transmitter

Schematic

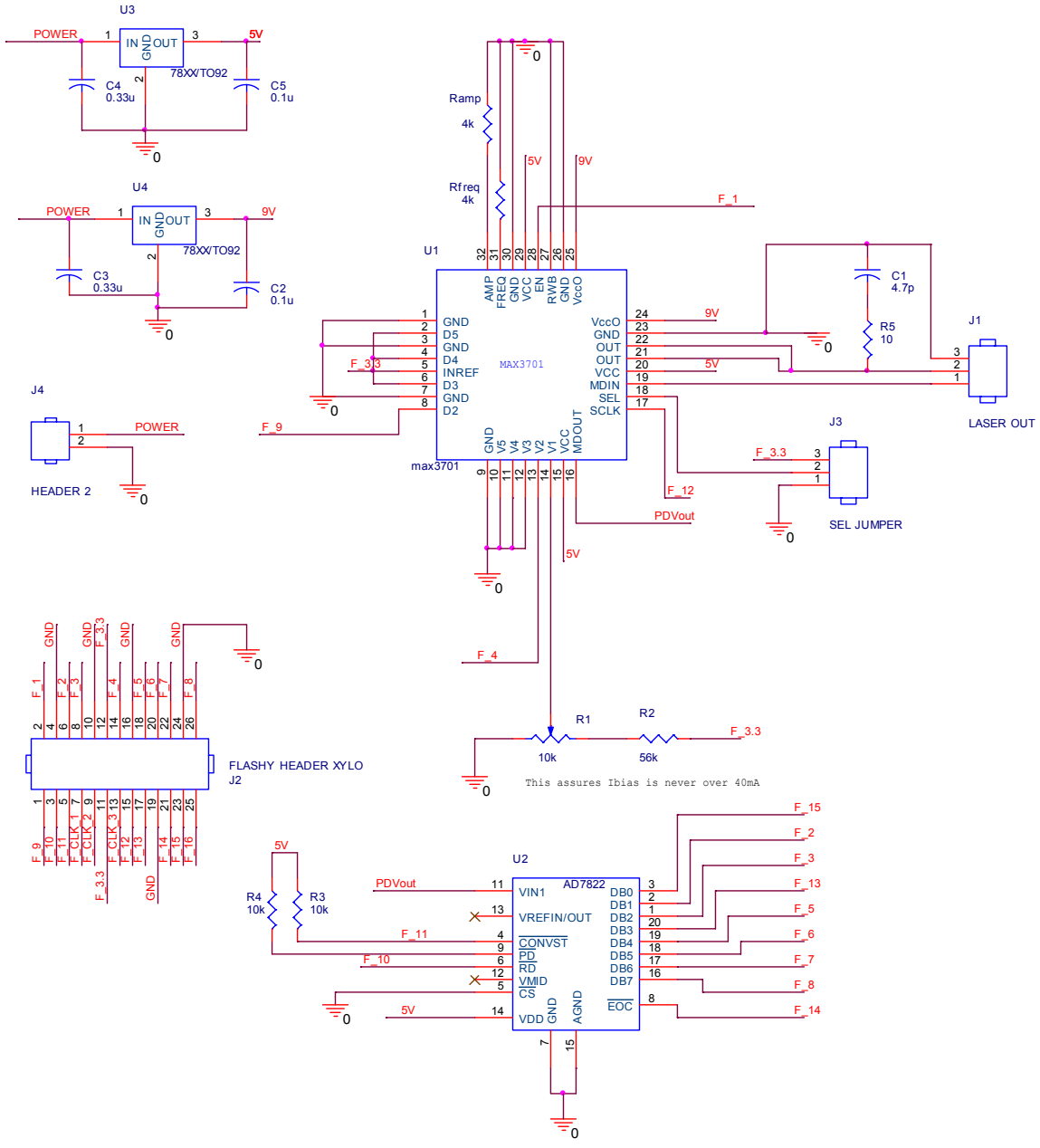

Bill of Materials

Bill Of Materials November 16,2007 11:32:05 Page1			
Item	Quantity	Reference	Part
1	1	C1	4.7p
2	2	C2,C5	0.1u
3	2	C3,C4	0.33u
4	1	J1	LASER OUT
5	1	J2	FLASHY HEADER XYLO
6	1	J3	SEL JUMPER
7	1	J4	HEADER 2
8	2	Rfreq,Ramp	4k
9	3	R1,R3,R4	10k
10	1	R2	56k
11	1	R5	10
12	1	U1	max3701
13	1	U2	AD7822
14	2	U3,U4	78XX/TO92

Board Layout

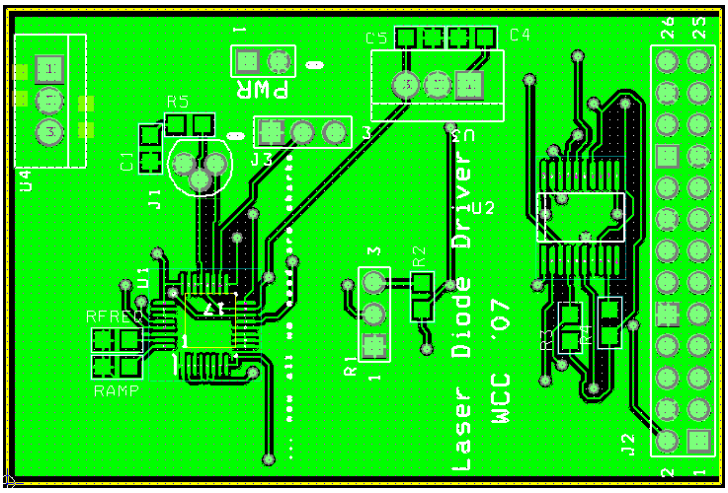

Laser transmitted board - Top layer

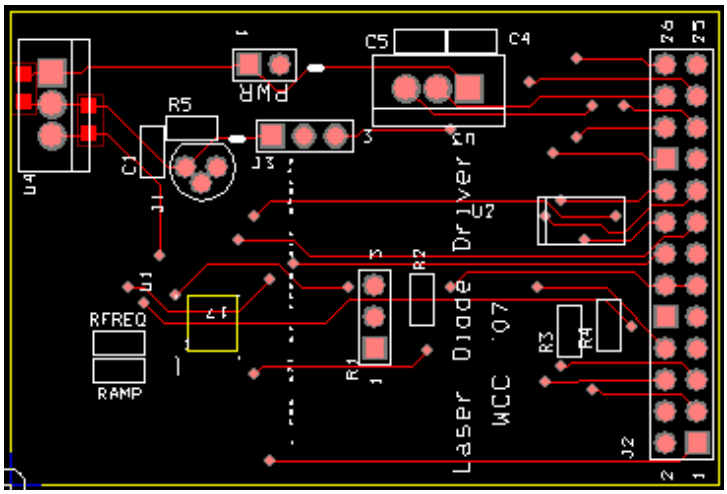

Laser transmitted board - Bottom layer

19-3008; Rev 0; 10/03

MAXIM

2x Blue Laser Driver with Sample and Hold

General Description

The MAX3701 is a laser driver designed to drive a common-cathode laser for the next generation of high-capacity blue DVD applications. It includes a programmable current source for generating a laser bias current, and four programmable data channels for programming the write current levels. The MAX3701 also includes an RF current source with programmable frequency and amplitude control. The RF source, together with the bias generator, provides a disc read waveform. All programmable currents are internally summed together, and can be disabled from a single enable pin. A transimpedance amplifier and a sample-and-hold circuit are available to be used with a monitor photodiode as part of an optical power-control (OPC) loop.

Each of the four programmable inputs can contribute up to 200mA$_{P-P}$ current with a total output current limit of 200mA into a blue laser diode. The four fast-switching channels accept single-ended CMOS, and can write at speeds as high as 400Mbps. The RF circuit delivers an output signal between 200MHz and 600MHz.

The MAX3701 is available in a 5mm x 5mm^2 32-pin thin QFN package.

Applications

2x High-Capacity Blue DVDs

Blue Lasers

1x High-Capacity Blue DVDs

High-Density Optical Drives

Typical Application Circuit appears at end of data sheet.

Features

- For Read/Write Operation of Common-Cathode Blue Lasers
- 0.9ns Rise-Fall-Time
- Low-Noise Oscillator Output (1nA/√Hz)
- 200mA Maximum Output Drive Current
- No Active External Device Required
- Five-Level Output Programmability
- On-Chip Oscillator from 200MHz to 600MHz
- Single-Ended CMOS High-Speed Inputs
- Preamp and Sample and Hold for Optical Power Control
- CMOS/TTL Control Interface
- Low Supply Current
- Enable Control

Ordering Information

PART	TEMP RANGE	PIN-PACKAGE
MAX3701CTJ	0°C to +70°C	32 Thin QFN

Pin Configuration

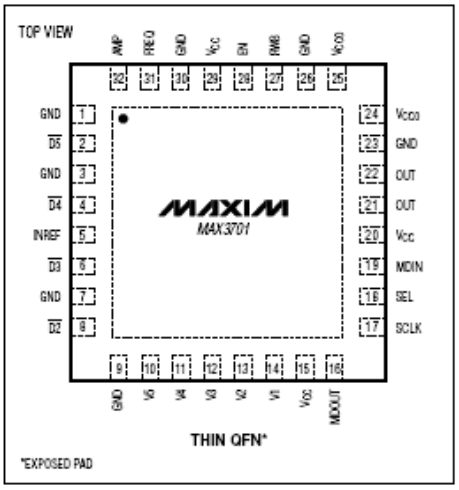

AD8015 Transimpedance Amplifier

ANALOG DEVICES

Wideband/Differential Output Transimpedance Amplifier

AD8015

FEATURES
Low Cost, Wide Bandwidth, Low Noise
Bandwidth: 240 MHz
Pulse Width Modulation: 500 ps
Rise Time/Fall Time: 1.5 ns
Input Current Noise: 3.0 pA/√Hz @ 100 MHz
Total Input RMS Noise: 26.5 nA to 100 MHz
Wide Dynamic Range
Optical Sensitivity: –36 dBm @ 155.52 Mbps
Peak Input Current: ±350 μA
Differential Outputs
Low Power: 5 V @ 25 mA
Wide Operating Temperature Range: –40°C to +85°C

APPLICATIONS
Fiber Optic Receivers: SONET/SDH, FDDI, Fibre Channel
Stable Operation with High Capacitance Detectors
Low Noise Preamplifiers
Single-Ended to Differential Conversion
I-to-V Converters

FUNCTIONAL BLOCK DIAGRAM

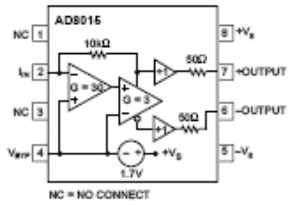

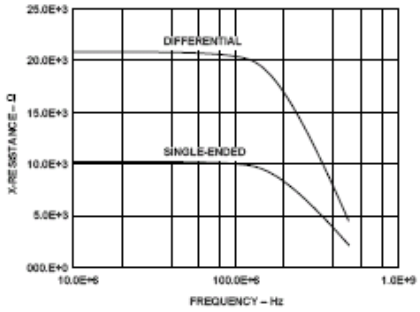

Figure 1. Differential/Single-Ended Transimpedance vs. Frequency

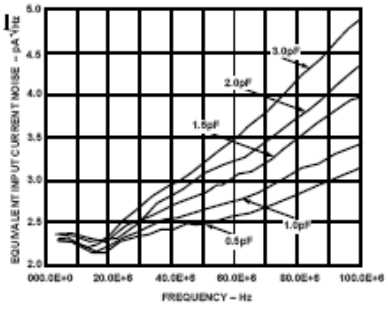

Figure 2. Noise vs. Frequency (SO-8 Package with Added Capacitance)

PRODUCT DESCRIPTION

The AD8015 is a wide bandwidth, single supply transimpedance amplifier optimized for use in a fiber optic receiver circuit. It is a complete, single chip solution for converting photodiode current into a differential voltage output. The 240 MHz bandwidth enables AD8015 application in FDDI receivers and SONET/SDH receivers with data rates up to 155 Mbps. This high bandwidth supports data rates beyond 300 Mbps. The differential outputs drive ECL directly, or can drive a comparator/ fiber optic post amplifier.

In addition to fiber optic applications, this low cost, silicon alternative to GaAs-based transimpedance amplifiers is ideal for systems requiring a wide dynamic range preamplifier or single-ended to differential conversion. The IC can be used with a standard ECL power supply (–5.2 V) or a PECL (+5 V) power supply; the common mode at the output is ECL compatible. The AD8015 is available in die form, or in an 8-pin SOIC package.

REV. A

One Technology Way, P.O. Box 9106, Norwood, 02062-9106, U.S.A.
Tel: 617/329-4700 Fax: 617/326-8703

PMT Receiver

Schematic

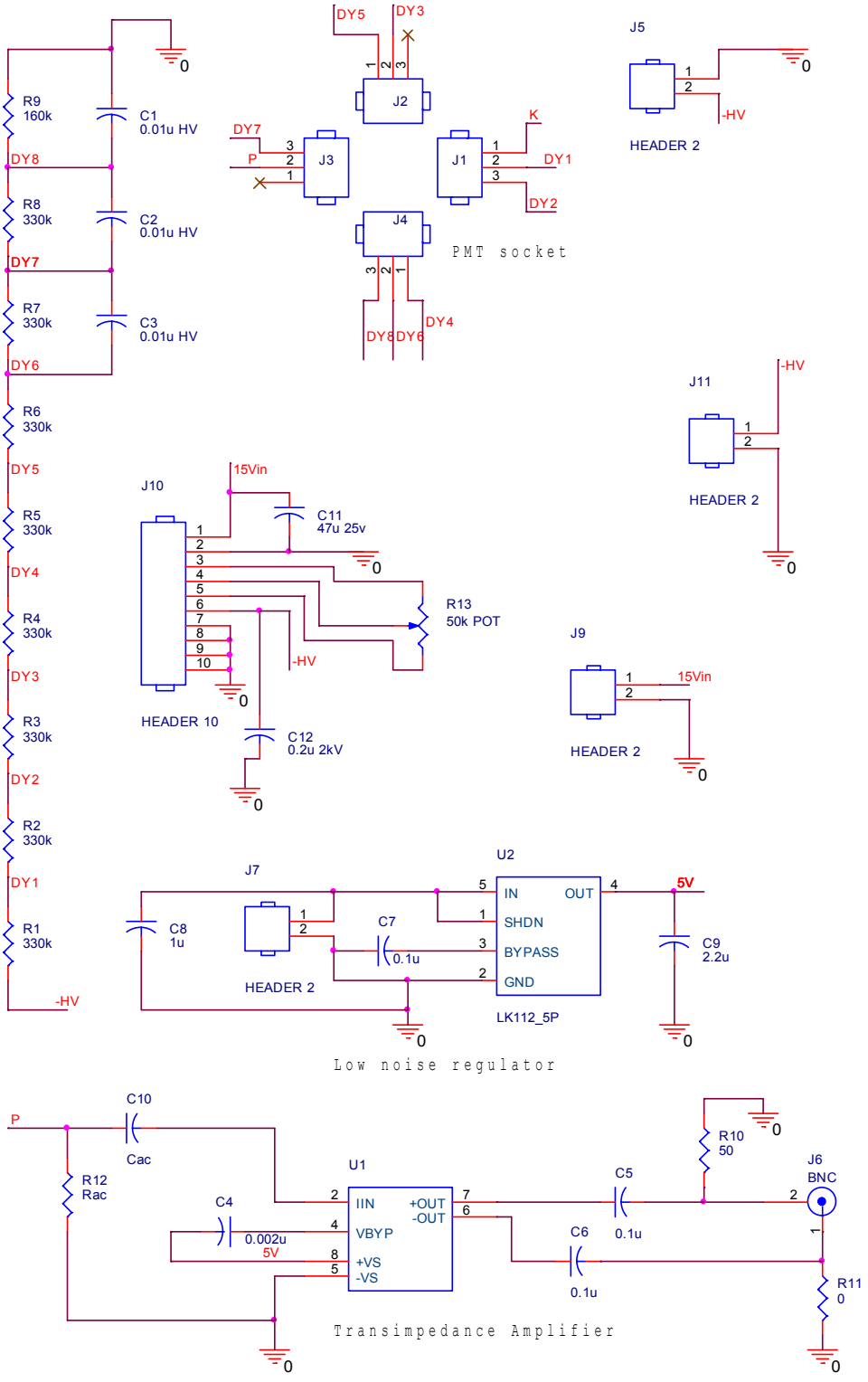

Bill of Materials

Bill Of Materials November 16,2007 11:49:56
Page1

Item	Quantity	Reference	Part	
1	3	C1,C2,C3	0.01u HV	
2	1	C4	0.002u	
3	3	C5,C6,C7	0.1u	
4	1	C8	1u	
5	1	C9	2.2u	
6	1	C10	Cac	
7	1	C11	47u 25v	
8	1	C12	0.2u 2kV ROUND	
9	4	J1,J2,J3,J4	HEADER 3	
10	4	J5,J7,J9,J11	HEADER 2	
11	1	J6	BNC	
12	1	J10	HEADER 10	
13	8	R1,R2,R3,R4,R5,R6,R7,R8	330k	
14	1	R9	160k	
15	1	R10		50
16	1	R11		0
17	1	R12	Rac	
18	1	R13	50k POT	
19	1	U1	AD8015_SO	
20	1	U2	LK112_5P	

Board Layout

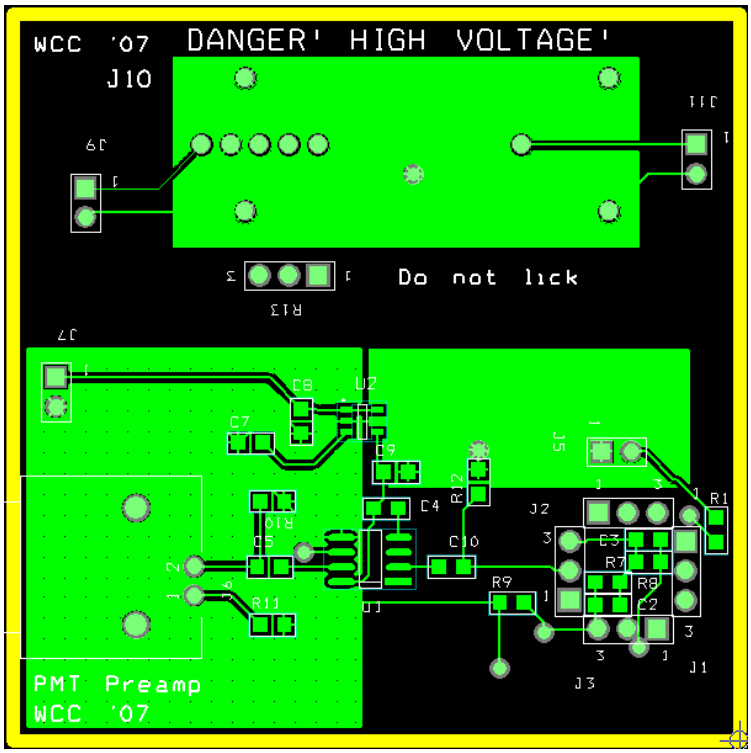

PMT Receiver board – top layer

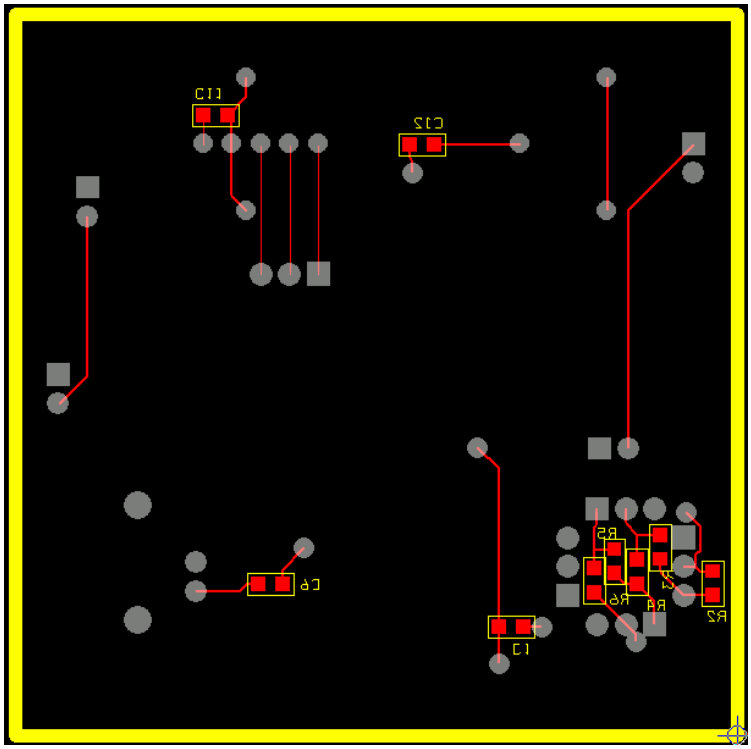

PMT Receiver board – bottom layer

Hamamatsu R7400U PMT Datasheet

HAMAMATSU

METAL PACKAGE PHOTOMULTIPLIER TUBE R7400U SERIES

Compact size (16 mm diameter, 12 mm seated length), Fast Time response (rise time 0.78 ns)

The R7400U series is a subminiature photomultiplier tube with a 16 mm diameter and 12 mm seated length. A precision engineered 8-stage electron multiplier (composed of metal channel dynodes) is incorporated in the TO-8 package to produce a noise free gain of 700,000 times (R7400U). The R7400U series also features excellent response time with a rise time of 0.78 ns. Various types of the R7400U series are available with different spectral response and gain ranges, including those selected specifically for photon counting applications. Hamamatsu also provides a hemispherical lens input option to the series (R7401 and R7402), effectively doubling the active area.

Left: R7400U Right: R7401/R7402

FEATURES

- World's smallest photomultiplier tubes assembled in a TO-8 metal package (1/7th of the Hamamatsu R647). The necessary components are built into a TO-8 package while retaining full photomultiplier tube performance to create a new generation of photosensors.
- Photon counting type: R7400P. The R7400P is specially selected on account of low noise and high gain for use in photon counting applications.
- Hemispherical lens window types: R7401 (bialkali), R7402 (multialkali). The hemispherical lens window doubles the effective input area to 12 mm in diameter.

SERIES

	Solar Blind	UV to Visible Range	UV to Near IR Range	Insulation Cover
Standard	R7400U-09	R7400U/R7400U-03/R7400U-06	R7400U-01/R7400U-02/R7400U-04/R7400U-20	Yes
For Photon Counting	—	R7400P	—	Yes
With Lens	—	R7401 (Visible Range)	R7402 (Visible to Near IR Range)	Yes

GENERAL

Parameter		Description/Value	Unit
Minimum Effective Area		8	mmφ
Dynode	Structure	Metal Channel	—
	Number of Stage	8	
Weight	R7400U Series/R7400P	Approx. 5.3	g
	R7401/R7402/R7401P	Approx. 6.3	
Ambient Temperature	R7400U Series/R7400P	-80 to +50	°C
	R7401/R7402/R7401P	-30 to +50	

VOLTAGE DISTRIBUTION RATIO

Electrodes	K	Dy1	Dy2	Dy3	Dy4	Dy5	Dy6	Dy7	Dy8	P
Ratio	1	1	1	1	1	1	1	1	1	0.5

Supply Voltage: 800 V K: Cathode Dy: Dynode P: Anode

METAL PACKAGE PHOTOMULTIPLIER TUBE R7400U SERIES

CHARACTERISTICS (at 25 °C)

Type No.	Remarks	Spectral Response		Photo-cathode Material	Window Material	Out-line No.	Maximum Ratings		Cathode Sensitivity				
		Range (nm)	Peak Wave-length (nm)				Anode to Cathode Voltage (V dc)	Average Anode Current (mA)	Luminous Min. (μA/lm)	Luminous Typ. (μA/lm)	Blue(5-58) Typ. (μA/lm-b)	Red/White Ratio Typ. x10⁻²	Radiant Typ. (mA/W)
R7400U-09	Solar Blind	160 to 320	240	Cs-Te	Synthetic silica	②	1000(d)	0.1(e)	—	—	—	—	22(a)
R7400U	Visible	300 to 650	420	Bialkali	Borosilicate glass	①			40	70	8	—	62
R7400U-03	UV to Visible	185 to 650			UV glass								
R7400U-06		160 to 650			Synthetic silica	②							
R7400U-01	Visible	300 to 850	400	Multialkali	Borosilicate glass	①			80	150	—	200	60
R7400U-02	UV to Near IR	300 to 880	500						200	250		250	58
R7400U-20		300 to 900	630						350	500		450	78 (at 630 nm)
R7400U-04		185 to 850	400		UV glass				80	150		200	60
R7401	With Lens	300 to 650	420	Bialkali	Borosilicate glass	③			40	70	8	—	62
R7402		300 to 850	400	Multialkali					80	150	—	200	60

(a): Measured at 254 nm.
(b): Measured after a 30-minute storage in darkness.
(c): Measured at a gain of 10^6
(d): Do not apply the maximum supply voltage for more than 30 seconds continuously.

Figure 1: Typical Spectral Response (Solar Blind)

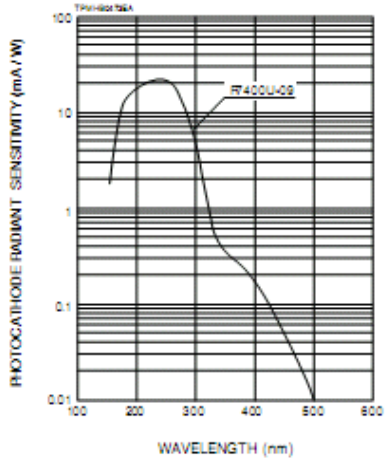

Figure 2: Typical Spectral Response (Bialkali)

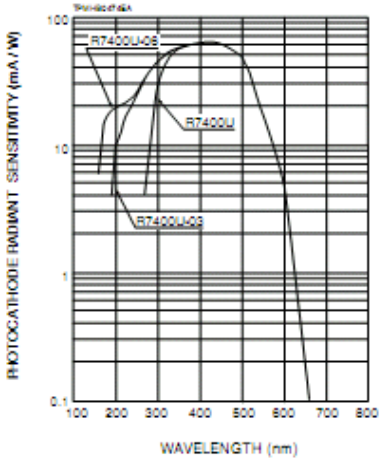

Figure 3: Typical Spectral Response (Multialkali)

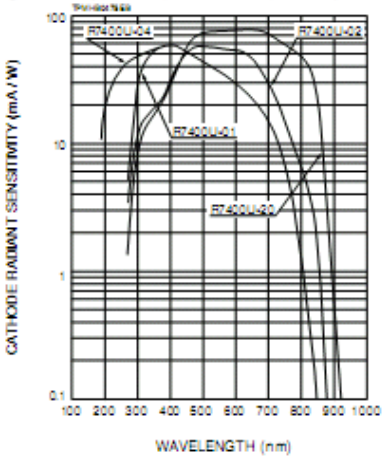

Figure 4: Typical Gain Characteristics

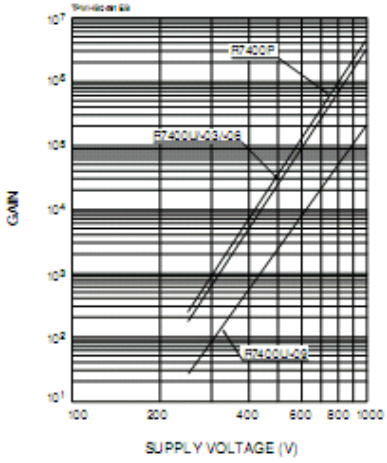

Anode to Cathode Supply Voltage (V dc)	Anode Characteristics								Type No.
	Anode Sensitivity			Gain Typ.	Anode Dark(b) Current		Time Response		
	Luminous		Radiant Typ. (A/W)		Typ. (nA)	Max. (nA)	Rise Time Typ. (ns)	Electron Transit Time Typ. (ns)	
	Min. (A/lm)	Typ. (A/lm)							
800	—	—	1100(a)	5×10^4	0.025	0.5	0.78	5.4	R7400U-09
	10	50	4.3×10^4	7×10^5	0.2	2			R7400U
									R7400U-03
									R7400U-06
	15	75	3.0×10^4	5×10^5	0.4	4			R7400U-01
	25	125	2.9×10^4		2	20			R7400U-02
	35	250	3.9×10^4						R7400U-20
	15	75	3.0×10^4		0.4	4			R7400U-04
	10	50	4.3×10^4	7×10^5	0.2	2			R7401
	15	75	3.0×10^4	5×10^5	0.4	4			R7402

(a): The output current averaged over 30 seconds should not exceed 0.1 mA.

For Photon Counting (P Type)				
Type No.	Gain		Dark Count (c) (s^{-1})	
	Min.	Typ.	Typ.	Max.
R7400P	7.5×10^5	1×10^6	80	400
R7401P				

Figure 5: Typical Gain Characteristics

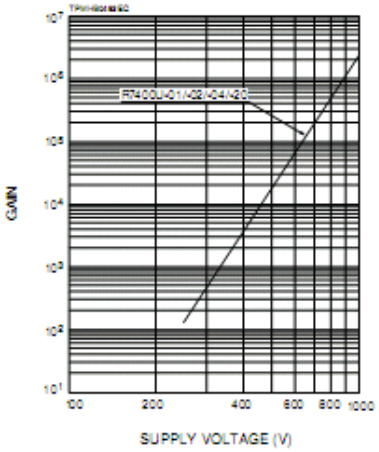

Figure 6: Anode Dark Current (v.s. Supply Voltage)

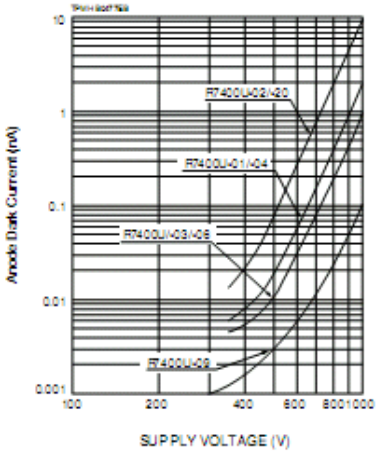

Figure 7: Anode Dark Current (v.s. Temperature)

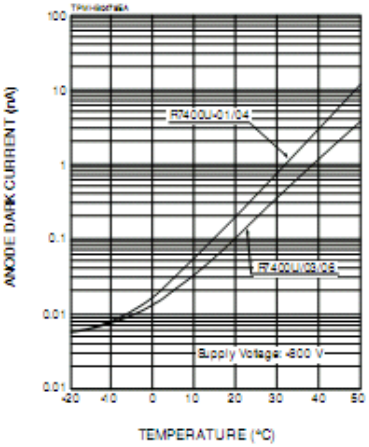

Figure 11: Dimensional Outline and Basing Diagram (Unit: mm)

①R7400U, -01, -02, -03, -04, -20, R7400P

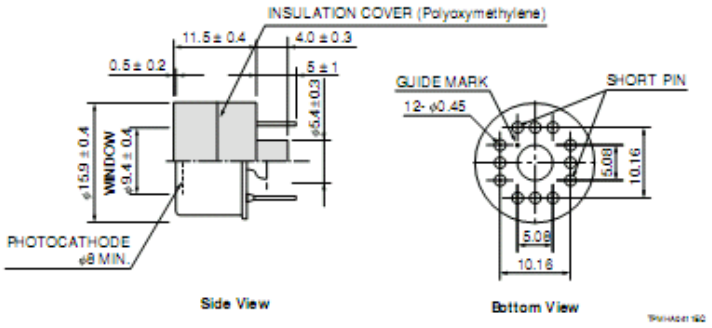

②R7400U-06,-09

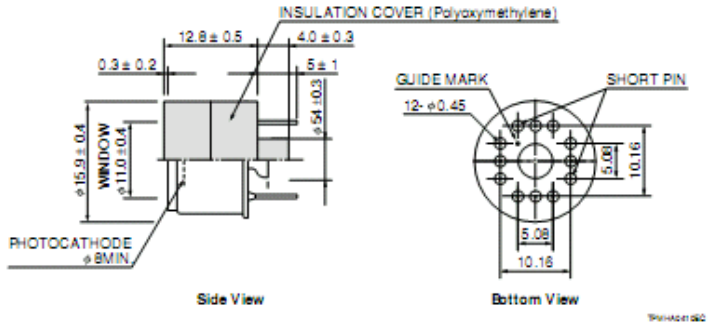

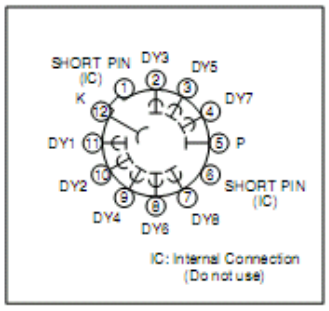

③R7401, R7402, R7401P

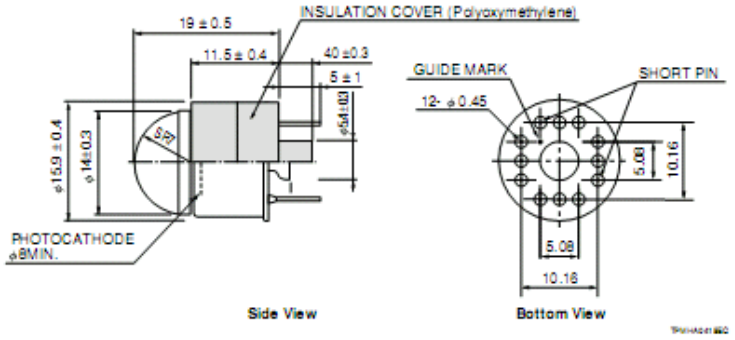

Hamamatsu C4900 Power Supply Datasheet

HAMAMATSU

HIGH VOLTAGE POWER SUPPLY UNIT C4900 SERIES

PATENT

The C4900 series are compact PC–board mountable high voltage power supplies, especially designed for photomultiplier tubes. The design offers better performance and improved fail–safe protection.
The C4900 and–01 output negative polarity and the C4900–50 and –51 output positive polarity high voltages.

FEATURES

- Compact and Lightweight
- High stability
- Low Power Consumption
- Fast Response
- Wide Variable Output Range
- Ample Protective and Fail–safe Functions

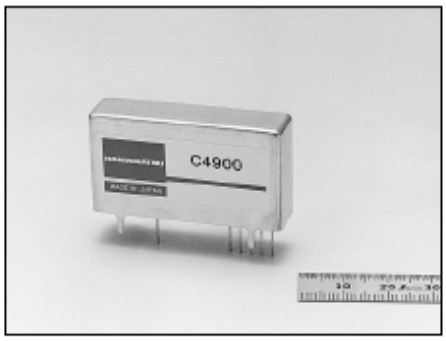

SPECIFICATIONS

Parameter		C4900	C4900-01	C4900-50	C4900-51	Unit
Input Voltage Range		+15 ± 1	+12 ± 0.5	+15 ± 1	+12 ± 0.5	V
Input Current ⑧	with no load	14	15	14	15	mA (Typ.)
	with full load	90	95	90	95	
Variable Output Range		0 to –1250		0 to +1250		V
Specification Guaranteed Output Voltage Range		–200 to –1250		+200 to +1250		V
Output Current ⑮		0.6	0.5	0.6	0.5	mA (Max.)
Line Regulation against ±1 V or 0.5 V Change ⑮		± 0.01				% (Typ.)
Load Regulation against 0 % to 100 % Load Change ⑧		± 0.01				% (Typ.)
Ripple / Noise (p-p) ⑮		0.007				% (Typ.)
Output Voltage Controlling Modes		By external controlling voltage (0 V to +5 V) or external potentiometer (50 kΩ ± 2.5 kΩ)				–
Controlling Voltage Input Impedance		80				kΩ (Typ.)
Reference Voltage Output		+5.13 (with 50 kΩ external potetiometer)				V (Typ.)
Output Voltage Setting (Absolute value)		(Controlling voltage × 250) ± 0.5 %				V (Typ.)
Output Voltage Rise Time (0 % → 99 %) ⑮		50				ms (Typ.)
Temperature Coefficient ⑮		± 0.01				%/°C (Typ.)
Operating Temperature Range ⑮		0 to +50				°C
Storage Temperature Range		-20 to +70				°C
Dimensions (W × H × D)		46 × 24 × 12				mm
Weight		31				g
Protective Functions		Units protected against reversed power input, reversed/excessive controlling voltage input, continuous overloading/short circuit in output				–

⑧ At Maximum Output Voltage. ⑮ At Maximum Output Voltage and Current.

HIGH VOLTAGE POWER SUPPLY UNIT C4900 SERIES

Figure 1: Output Voltage Controlling

BY EXTERNAL VOLTAGE

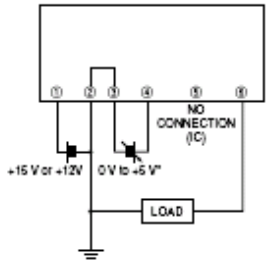

*The instability in the external controlling voltage should be minimized as it directly affects the output voltage quality.

● BY EXTERNAL POTENTIOMETER

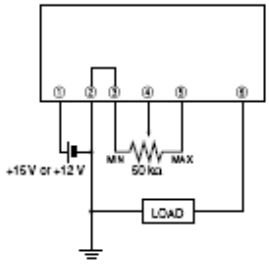

PIN ASSIGNMENT
① +15 V or +12 V IN
② GND 1 (Input/Output GND)
③ GND 2 (Controlling Voltage GND)
④ HV ADJ (Controlling Voltage Input)
⑤ Vref OUT (Reference Voltage Output : 5.19V Typ.)
⑥ HV OUT
- The housing is internally connected to pin ②.
- Pins ② and ③ are internally connected.

TACCfcona02

Figure 2: Output Voltage Controlling Characteristic

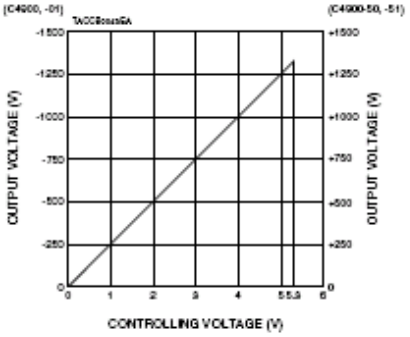

Figure 3: Example of Ripple/Noise Reduction Circuit

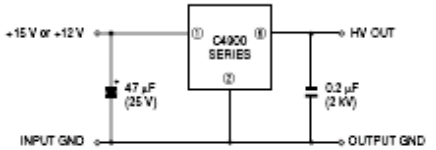

*The ripple/noise can be halved by adding capacitors as illustrated above.

TACCfcona03

Figure 4: Dimensional Outline (Unit: mm)

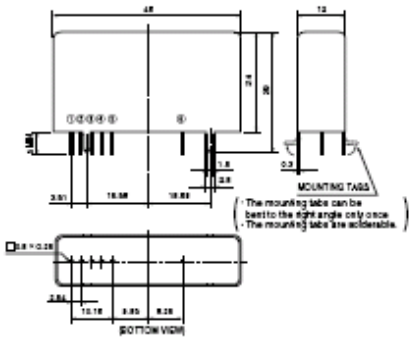

Drilling Data for PC Board (Soldering Face)

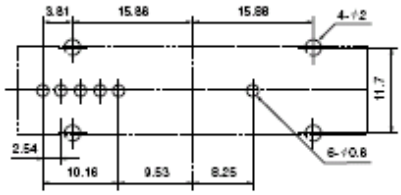

*PATENT: USA No.5548502, 5568343 JAPAN: No.2758552, 2784136 EUROPE: No.641066, 649222

HAMAMATSU HOMEPAGE URL http://www.hamamatsu.com

HAMAMATSU PHOTONICS K.K., Electron Tube Center
314-5, Shimokanzo, Toyooka-village, Iwata-gun, Shizuoka-ken, 438-0193, Japan, Telephone: (81)539/62-5248, Fax: (81)539/62-2205

U.S.A.: Hamamatsu Corporation: 360 Foothill Road, P.O.Box 6910, Bridgewater, N.J. 08807-0910, U.S.A., Telephone: (1)908-231-0960, Fax: (1)908-231-1218 E-mail: usa@hamamatsu.com
Germany: Hamamatsu Photonics Deutschland GmbH: Arzbergerstr. 10, D-82211 Herrsching am Ammersee, Germany, Telephone: (49)8152-375-0, Fax: (49)8152-2658 E-mail: info@hamamatsu.de
France: Hamamatsu Photonics France S.A.R.L.: 9, Rue du Saule Trapu, Parc du Moulin de Massy, 91882 Massy Cedex, France, Telephone: (33)1 69 53 71 00, Fax: (33)1 69 53 71 10 E-mail: infos@hamamatsu.fr
United Kingdom: Hamamatsu Photonics U.K. Limited: 2 Howard Court, 10 Tewin Road Welwyn Garden City Hertfordshire AL7 1BW, United Kingdom, Telephone: 44-(0)1707-294888, Fax: 44-(0)1707-325777 E-mail: info@hamamatsu.co.uk
North Europe: Hamamatsu Photonics Norden AB: Smidesvägen 12, SE-171 41 SOLNA, Sweden, Telephone: (46)8-509-031-00, Fax: (46)8-509-031-01 E-mail: info@hamamatsu.se
Italy: Hamamatsu Photonics Italia: S.R.L.: Strada della Moia, 1/E, 20020 Arese, (Milano), Italy, Telephone: (39)02-935 81 733, Fax: (39)02-935 81 741 E-mail: info@hamamatsu.it

TACC1013E02
MAY. 2001 IP
Printed in Japan (500)